Orally Bioavailable Cyclin A/B RxL Inhibitors: optimization of a novel class of macrocyclic peptides to target E2F high and G1–S-checkpoint compromised cancers

Justin A. Shapiro,‡ Nathan J. Dupper,‡ Breena Fraga-Walton, Andrew T. Bockus, Siegfried S.F. Leung, Kai Yang, Chinmay Bhatt, Megan K. DeMart, Miguel P. Baldomero, Luis Hernandez, Gabriel Fung, Sammy Metobo, Steven Xie, Bryan M. Lent, David C. Spellmeyer, Joshua Luna, Dalena Hoang, Manesh Chand, Yuliana Gritsenko, Catherine E. Gleason, Frances Hamkins-Indik, Jie Zheng, Ranya Odeh, Meisam Nosrati, Daphne He, Ramesh Bambal, Peadar Cremin, Jinshu Fang, Bernard Levin, Evelyn W. Wang, Marie Evangelista, David J. Earp, Constantine Kreatsoulas, Rajinder Singh, Pablo D. Garcia, James B. Aggen*

Circle Pharma, 169 Harbor Way, South San Francisco, CA 94080

KEYWORDS: *Cyclin, Cell-permeable cyclic peptides, Macrocycles, beyond the rule of five, Protein-protein interaction inhibitors, Cancer therapeutics, CDK2*

ABSTRACT: Cyclins A and B bind and activate their cognate cyclin-dependent kinase (CDK) to regulate progression through S and G2/M phases of the cell cycle. These complexes orchestrate multiple activities within their cell cycle phase, the orderly transition between phases, and the regulation of critical cell cycle checkpoints. Cyclins recruit substrates and regulators through the interaction of an RxL-motif with a Hydrophobic Patch (HP) on the Cyclin surface. We recently disclosed the first class of passively permeable macrocyclic peptides that bind to the HP of both Cyclin A and B to induce potent and selective apoptosis of cancer cells with high levels of E2F activity. While these macrocycles demonstrated *in vivo* tumor regression in cell-line derived xenograft models of small-cell lung cancer via intraperitoneal dosing, their oral bioavailability was insufficient to progress pre-clinical development. Here we describe the optimization of this series for drug-like properties and oral bioavailability. We leveraged computationally guided designs and SAR data to direct focus onto high-value optimization sites. This effort resulted in a new macrocyclic scaffold with improved physiochemical and ADME properties. Further optimization resulted in the discovery of a lead compound which demonstrates tumor regression in CDX models of small-cell lung cancer via oral dosing. We are currently evaluating Cyclin A/B inhibition in a Ph.1 clinical trial.

INTRODUCTION

Oral Peptide Drug-Discovery for Intracellular PPIs

The inhibition of protein-protein interactions (PPIs) have seen increased focus in therapeutic discovery and development campaigns in recent years.[1] Despite increased interest, many PPIs have historically been considered undruggable by small molecules due to the nature of their binding surfaces. Traditional drug targets typically consist of pockets that are small, three-dimensional, partially or completely buried inside a protein, and/or have catalytic activity. These targets are readily occupied by small molecules that follow Lipinski's rules of drug likeness, such as low molecular weight and rotatable bond count. By contrast, small drug-like molecules are ill-suited to disrupt the large, flat, non-polar surfaces through which proteins associate to form complexes.[2] Many PPIs are critical to the maintenance of biological functions and are at the heart of many disease pathologies, and so medicinal chemists increasingly search the beyond the rule of five (bRo5) chemical space for molecules that can "drug the undruggable" to modulate these sites.

A modality that has shown great promise in PPI inhibitor development has been macrocyclic peptides.[3-4] Because they share intrinsic structural and architectural features with larger proteins (both being polymers of amino acids linked through amide backbones) they can more readily mimic the geometric arrangements of target's natural substrates.[4] They are more resistant to enzymatic degradation than their linear peptide counterparts[5] while also having fewer degrees of freedom, which can allow for potency enhancements by biasing them towards an active conformation.[6] Because they tend to rely on a diffuse array of weak binding interactions as opposed to just a few extremely strong binding interactions, they are highly target specific and generally well tolerated.[4] Due to their modular nature, they are readily optimized and amenable to high-throughput synthetic techniques and library generation platforms.[7]

Despite these advantages, many challenges remain with the development of macrocyclic peptide therapeutics.

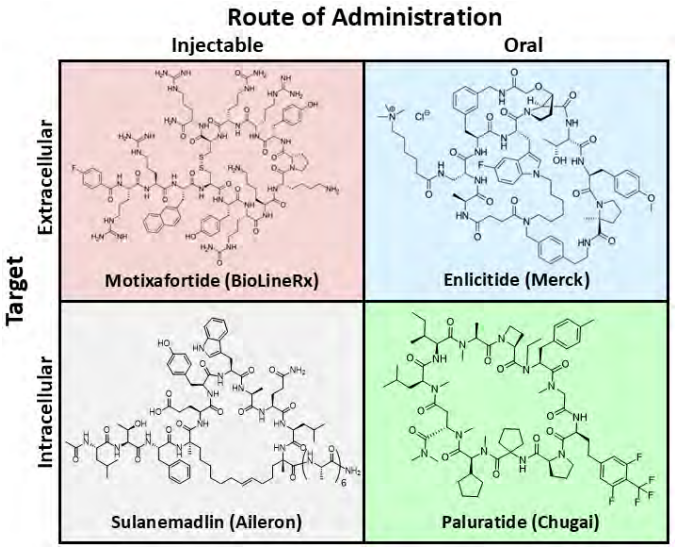

Figure 1. Representative macrocyclic peptide therapeutics organized by route of administration and location of molecular target. (top left) Motixafortide, an injectable drug with an extracellular target. (bottom left) Sulanemadlin, an injectable drug with an intracellular target. (top right) Enclicitide, and oral drug with an extracellular target. (bottom right) Paluratide, and oral drug with an intracellular target.

Macrocyclic peptide PPI inhibitors fall into four categories; injectables targeting extracellular proteins, injectables targeting intracellular proteins, orally delivered compounds targeting extracellular proteins, and orally delivered compounds targeting intracellular proteins[8] (**Figure 1**). Many such compounds are highly polar and can neither cross the cell membrane nor the gut wall and thus fall into the first category (e.g. Motixafortide).[9] Macrocycles that can cross the cell membrane to reach their target, either by passive permeation or by active transport, but are not absorbed into systemic circulation from the gut can be administered by injection (e.g. Sulanemadlin).[10] Inhibitors of proteins on the cell-surface do not require intrinsic permeability and can therefore be administered orally with the help of enabling formulations containing permeation enhancers and picomolar affinity (e.g. Enlicitide).[11] Reported examples of macrocyclic peptides that inhibit intracellular PPIs and can be administered orally are few and largely limited to previously drugged targets (e.g. Paluratide).[12]

Recent publications on passively permeable and orally bioavailable peptide macrocycles emphasize the importance of property-based drug design principles.[12-13] Removal of all charged or highly polar residues, biasing towards lipophilic character and a high proportion of backbone N-alkylation are all correlated with higher drug-likeness. Critically, peptides that are too large are unlikely to be permeable/oral, but reducing size too much is also detrimental, presumably due to a loss of conformational flexibility (i.e. "chameleonicity").[14] Total polar surface area (TPSA), H-bond donor/acceptor count (HBD/HBA), and number of rotatable bonds (#RotB) have also been identified as important properties to track in the bRo5 space.[15-19] These lessons provide powerful examples to extend the principles of oral peptide drug discovery to previously undrugged intracellular mechanisms.

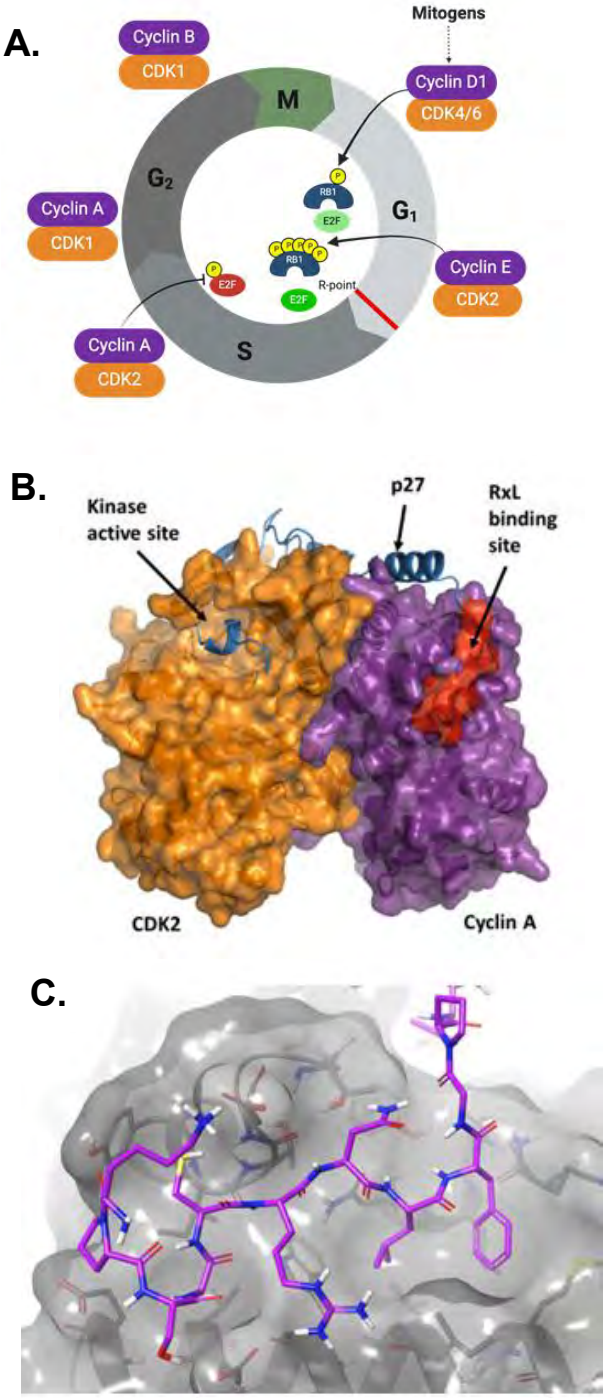

Figure 2. (A) Representation of the cell cycle as regulated by phosphorylation of retinoblastoma (Rb) and early region 2 binding factor (E2F) by CDK/Cyclin complexes. (B) Crystal structure of regulatory peptide p27 bound to the CDK2/Cyclin A complex (PDB: 1JSU). RxL motif of substrate bound to hydrophobic patch highlighted in red. (C) Crystal structure of cyclin A RxL binding site with endogenous ligand p27 shown in purple (PDB: 1JSU)

Cyclins as a Drug Target

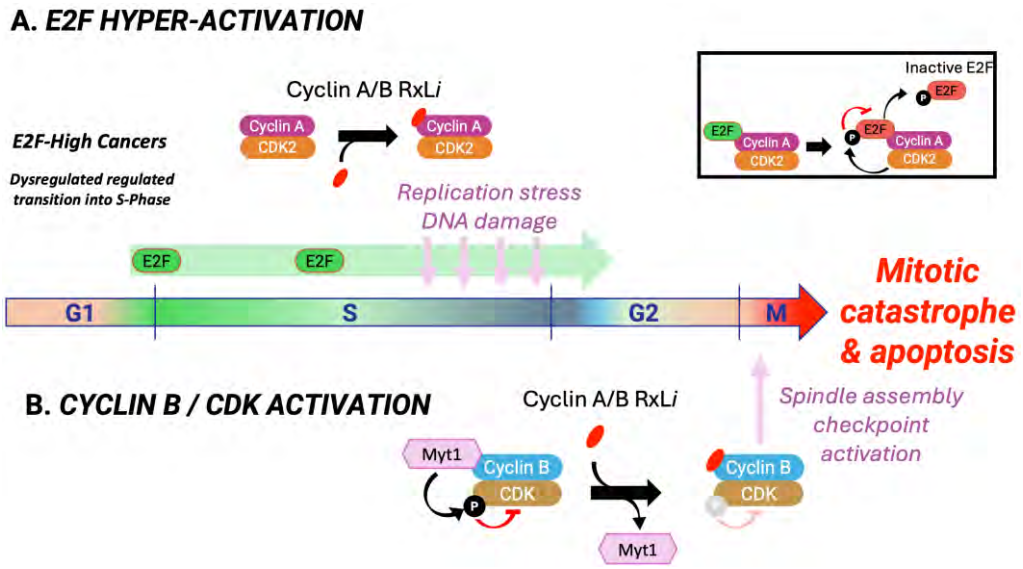

Figure 3. **Model for the mechanism of action of Cyclin A/B RxL inhibitors**: Cancers with dysregulated G1/S checkpoints (e.g., Rb loss) have high levels of E2F activity, which leads to replication stress and DNA damage during S-phase, making them dependent on latter checkpoints of the cell cycle to proliferate. For example, the S/G2 transition requires attenuation of E2F activity for cells to complete S-phase. This process depends on the RxL-motif of E2F interacting with Cyclin A, for CDK2 to phosphorylate and inactivate E2F (**insert top right**). Cyclin A/B RxL inhibitors block this interaction leading to hyperactivity of E2F throughout S-phase and into G2, thus further increasing replication stress, DNA damage and dysregulated S/G2 transition (**Panel A**). In G2/M, the Cyclin A/B RxL inhibitor blocks the kinase Myt1 RxL-dependent interaction with the Cyclin B / CDK complex. Myt1 phosphorylates CDK, which results in CDK kinase activity inhibition. Thus, blocking the Myt1 interaction results in activation of the Cyclin B / CDK complex (**Panel B**). The combination of hyperactive E2F, replication stress, DNA damage and activation of Cyclin B / CDK leads to persistent spindle assemble checkpoint activity, blocks progression at G2/M and ultimately results in mitotic catastrophe and cell death by apoptosis in E2F high cancers.

The process by which a cell grows, duplicates DNA, and divides in two (hereafter the cell-cycle) is divided into different phases (G1, S, G2, M) during which different critical activities are orchestrated by distinct Cyclin/CDK complexes at each phase (**Figure 2A**).[20] In a healthy cell, the orderly transition between these phases, activities within each phase, and critical checkpoints are tightly regulated by phosphorylation events catalyzed by cyclin-dependent kinases (CDKs) which are themselves activated by their cognate cyclins.[21-24] While the cyclin family is diverse in structure and function,[25] in the context of the cell-cycle they serve two key roles: (1) Binding to the CDK causes a conformational change in the kinase necessary for its catalytic activity,[26] and (2) The cyclin recruits protein substrates and regulators, such as Rb and E2F (**Figure 2A**), through PPIs between their RxL-motif with the Hydrophobic Patch (HP) on cyclins (**Figure 2B**).[27] Following these two events, the phosphorylation site of such substrates can access the catalytic binding pocket of the CDK enabling phosphorylation to occur. Direct inhibition of the catalytic site of CDKs is a validated strategy for the treatment of various cancers,[28] and small-molecule inhibitors with varying selectivity profiles are in clinical trials.[29-30] Although a valuable approach, high structural homology between kinase binding pockets can lead to off target toxicity,[31] and frequently lead to the development of resistance.[32] For these reasons, alternative mechanisms for modulating the Cyclin/CDK complexes are highly attractive.

Kaelin and coworkers first demonstrated the therapeutic potential of inhibiting the interaction of RxL-containing substrates with the Cyclin A/CDK2 complex (**Figure 2C**), using peptides based on the RxL of p27 conjugated to the cell-penetrating TAT peptide.[33] They showed selective lethality in cells with high levels of E2F activity due to retinoblastoma (Rb) dysregulation, while having minimal effect on non-transformed fibroblasts.[33] Attempts to develop peptides or small molecules inhibiting the RxL binding site have been historically hampered by weak binding and a reliance on conserved positively charged groups to form salt-bridges with the target, thwarting permeability and cellular inhibition.[34-36] Some efforts to design small molecule

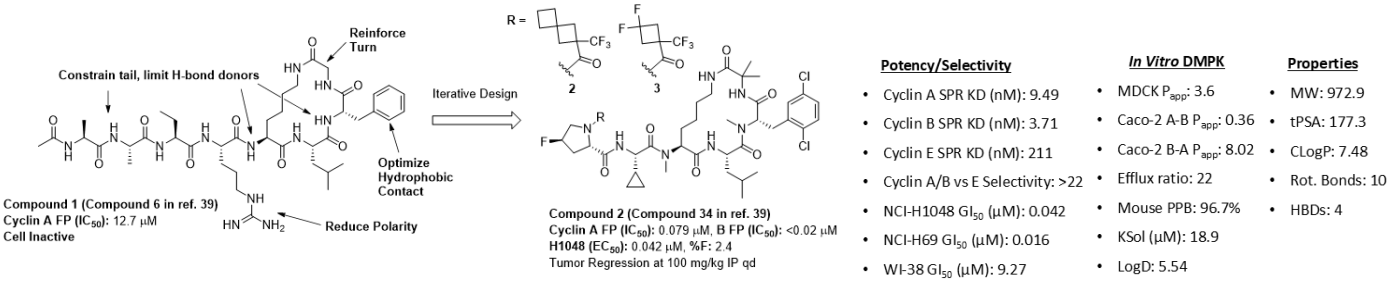

Figure 4. (left) Summary of hit-to-lead campaign, detailed in ref. 39. (right) Profile of biophysical and cellular potency, *in vitro* DMPK parameters, and molecular properties of Compound **2**.

inhibitors of the Cyclin A RxL binding site that adhere to the Lipinski's rules have been described. However, these compounds did not display cellular activity, and no further development of these series has been reported.[37]

We recently disclosed a series of passively permeable macrocyclic peptides which mimic the RxL substrate motif and tightly bind Cyclins A, B, E, or combinations thereof. Using such tool compounds with differential Cyclin selectivity profiles we showed: (1) significant antiproliferative effects with dual Cyclin A/B RxL inhibitors in E2F-high small-cell lung cancer cell lines, (2) activity in Cyclin E was not required and (3) selective Cyclin A or Cyclin B inhibitors had modest effect on proliferation.[38] We developed a mechanistic model for the dual Cyclin A/B RxL inhibition driven effects in E2F-high cancers as represented in **Figure 3**. Briefly, the combined effects from Cyclin A RxL inhibition (replication stress, DNA damage) and Cyclin B RxL inhibition (displacement of Myt1 resulting in Cyclin B/CDK complex activation) triggers hyperactivation of the spindle-assembly checkpoint (SAC) ultimately leading to apoptotic cell death selectively in cancers with G1/S compromised checkpoints and E2F pathway high signatures. These effects are not observed in non-transformed fibroblast or primary human progenitor stem cells,[38] suggesting a large therapeutic window. Indeed, these tool Cyclin A/B RxL inhibitors were well tolerated and efficacious *in vivo* on several cell-line derived xenograft (CDX) mouse models when administered via intraperitoneal[39] or intravenous[38] dosing.

Our larger goal was to identify a compound from this series suitable for advancement into clinical investigation as an orally delivered drug candidate. While the lead Compound **2** (Compound 34 in ref. 39) (**Figure 4**) demonstrated encouraging properties and the first *in vivo* proof of concept efficacy for this mechanism of action, its low oral bioavailability (2%) highlighted a key shortcoming which we aimed to address in the subsequent optimization campaign. Based on our observation that achieving free-drug concentration in plasma above the GI_{50} for a few hours resulted in tumor regressions, we were able to set a benchmark for exposure during our campaign to develop oral inhibitors. In order to provide focus for our optimization efforts, we contrasted the characteristics of Compound **2** to the reported physicochemical property space permissive of oral bioavailability relevant to macrocyclic peptides.[12-13,16-17,19] While some properties of **2** fell within the permissive space, such as TPSA (177) and #RotB (10), some were less optimal, including LogD (5.54) and the HBD count (4), which might be limiting its observed bioavailability.[12-13,16-17,19] With these findings in mind, we began our lead optimization campaign to develop an orally bioavailable peptide macrocycle inhibitor of Cyclin A/B. This required that we first improve oral bioavailability sufficient to achieve efficacy in a relevant tumor model via oral dosing, at reasonable and tolerated dose levels, followed by confirmation of oral absorption across preclinical species. Based on our prior results with the NCI-H69 tumor model we anticipated oral efficacy would require achieving free drug C_{max} levels in excess of the GI_{50}. To meet this goal we focused our optimization on: (i) improving oral bioavailability with a target of $\geq 20\%$ by modulating compound properties such as TPSA, HBD count, and LogD; (ii) Lowering the exposure target by increasing cellular potency, with a target of $GI_{50} < 20$nM vs. our screening SCLC cell line, and by ensuring that plasma protein binding did not increase to the point where the unbound fraction would become limiting.

RESULTS

Identifying Sites for Structural Diversification

While the potential for structural diversity in macrocyclic peptides is very useful during the library generation and hit discovery phases of a campaign, lead optimization can often be a daunting prospect because the number of sites for variation in larger scaffolds multiplies the challenge for optimization relative to typical small molecule scaffolds. Fortunately, the process of discovering Compound **2** provided us with robust historical SAR[39] that we drew on to identify three high-value regions of the scaffold on which to focus (**Figure 5a**).

Phenylalanine residue ortho-position

During the hit-to-lead campaign, we derived significant benefit by first mono-chlorinating the phenylalanine at the meta-position, which provided improved potency by burying a lipophilic substituent into a deep pocket. Later we discovered that further 2,5-dichlorination was also tolerated as the *ortho*-chloro rested in a partially exposed shelf based on molecular modeling (**Figure 5a**, highlighted in red), and conferred improvements in PK parameters. Although not disclosed previously, we discovered that this position was broadly tolerant to a variety of substituents. We hypothesized that the 2-position of the Phe could be a synthetic

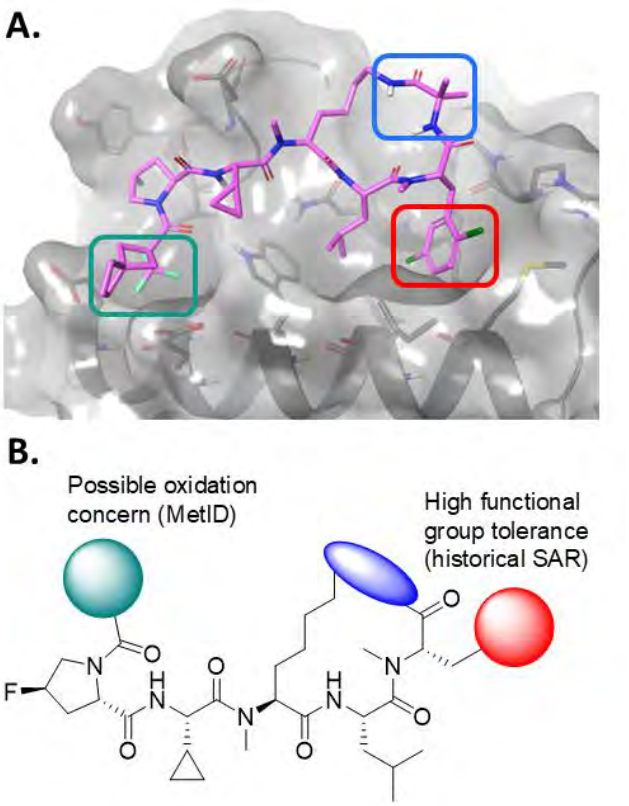

Figure 5. (top) Computational model of Compound **2** in the RxL binding site of Cyclin A, with sites of interest for lead optimization highlighted. (bottom) Summary of lead optimization strategy.

handle by which we could modulate physicochemical properties.

Bridge from Lariat to Phenylalanine residue

We also noted that the residue bridging the Nε-position of the lysine lariat and the C-terminus of the phenylalanine (2-Aminoisobutyric acid in Compound **2**) could be replaced with a variety of residues without significant detrimental effects to biochemical or cellular activity, as long as the residues side-chain was not highly polar and the residue was either a *D*-stereoisomer or alpha-disubstituted. Our docking model indicated that this portion of the lariat was not involved in any key interactions with the Cyclin A binding pocket but was likely involved somehow in the preorganization of the ligand (**Figure 5a**, highlighted in blue).

Interestingly, replacement of this position with *D*-proline counterintuitively reduced passive permeability as measured by MDCK, even though this side chain reduces the HBD count by one (**Supplementary Figure S1**). Because proline enforces conformational rigidity, this may indicate that macrocycle flexibility in this region is important for permeability. In contrast to the proline analog mentioned above, an early matched-pair **4** (Compound 13 in ref. 39) and **6** (**Table 1**) indicated that removal of the Nε-H is beneficial to permeability, and in this case does not negatively impact potency. However, as we highlighted in our prior report,[39] N-methylation at this position was not consistently tolerated from a potency perspective. It is also noteworthy that an ester linkage (**5**) in place of the amide improves permeability to the same degree as N-methylation. Based on the molecular modeling and the encouraging trends in MDCK for this early SAR series, we highlighted the region from Nε-lysine to the N-terminus of the bridging residue as the second major site for diversification (**Figure 5b**, highlighted in blue).

Table 1. Replacement of lariat amide with ester or N-methyl.

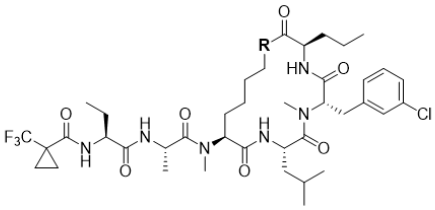

ID	R	Cyclin A FP-2 IC_{50} (μM)	MDCK Papp x10^{-6} cm/s
4	-NH-	2.843	0.5
5	-O-	4.442	6.9
6	-NMe-	1.277	7.2

C-terminal Acid Cap

Finally, while Compound **2** was acceptable for an IP proof-of-concept efficacy demonstration, we wanted to continue addressing potential metabolic liabilities which might limit oral exposure. We noted that the highly lipophilic spirocyclic N-terminal capping portion of the tail was a site of oxidation (see supporting information), and while not an extreme concern we were aware that it could get worse as the overall properties of the scaffold were modified. From the hit-to-lead campaign we identified other capping groups of interest that we could substitute should we encounter unanticipated problems with the spirocycle. Specifically, compound **3** (Compound 32 in ref. 39) (**Figure 4**) showed similar in vivo PK, improved solubility, and would theoretically be more resistant to alkyl oxidation due to the presence of the terminal difluoromethylene group. Knowing that the tail species may need further optimization lead to our choice of this region as our final diversification site (**Figure 5b**, highlighted in green).

With these three high-value regions of the scaffold identified (2-Phe substituent, bridging residue from lariat to Phe, capping group), we proceeded with our structure and property-based lead optimization campaign to generate orally bioavailable macrocyclic inhibitors of the Cyclin A/B RxL binding site for the treatment of E2F-high cancers.

Table 2. Diversification of phenylalanine residue of Compound **2**.

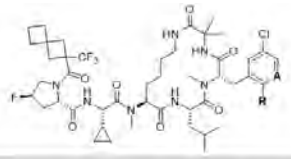

ID	R	A	Cyclin A FP-2 IC_{50} (μM)	H1048 GI_{50} (μM)	MDCK Papp x10^{-6} cm/s
2	Cl	CH	0.079	0.042	3.6
7	Me	CH	0.075	0.028	1.0
8		CH	0.028	0.026	0.9
9		CH	0.034	0.032	0.6
10		CH	0.022	0.039	0.4
11		CH	0.049	0.073	0.3
12		CH	0.073	0.107	1.1
13		N	0.071	0.019	1.9

Diversification of 2-Phe Substituents on Compound 2 Scaffold

Substituents ranging from alkyl groups (**7**), ethers (**8**), hetero-biaryls (**9** and **11**), and amines (**10**) were selected based on predicted tolerability in molecular modeling (**Table 2**). All were generally well tolerated in a biochemical FP assay and in an antiproliferative cellular assay against small-cell lung cancer line NCI-H1048, in line with expectations and historical SAR. While the spread of values is not large enough to draw definitive conclusions, there appears to be a slight trend of smaller volume substituents correlating with more potent cellular activity. Unfortunately, all modifications sampled reduced the MDCK permeability, suggesting they are unlikely to increase oral exposure. Unexpectedly, matched-pairs **12** and **13**, which differ only by a carbon-to-nitrogen substitution at the 3-position of the phenyl ring, are differentiated in cellular activity and permeability despite having equivalent biochemical activity. Despite an increase in TPSA, the pyridone-ether appears to confer a special advantage. Although all modifications in this series showed reduced MDCK values relative to Compound **2**, the broad tolerability was encouraging because it hinted that we could significantly alter the 2-position of the

phenylalanine in the hopes of improving other pharmacokinetic parameters of our inhibitors without loss of biochemical / cellular potency. While none of these compounds themselves were selected for further in vitro or in vivo PK profiling, the structure-activity relationship was noted for future exploration in more advanced iterations of the scaffold.

Table 3. Methylation of the lariat nitrogen.

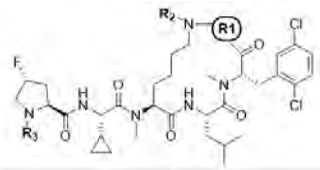

ID	R1	R2	R3	Cyclin A FP-2 IC_{50} (μM)	NCI-H1048 GI_{50} (μM)	MDCK Papp x10^{-6} cm/s
2		H		0.079	0.042	3.6
14		Me		1.020	NC	2.7
15		H		0.117	0.082	2.5
16		Me		0.296	0.160	2.6
17		H		0.065	0.023	1.0
18		Me		0.077	0.031	5.5

Methylation of the Nε-Position of the Lariat Lysine

Based on observations from modeling and early SAR that the Nε-position of the lariat lysine does not appear to participate in an H-bonding interaction with the Cyclin A/B RxL binding sites, we synthesized an N-methyl analog of Compound **2** (**Table 3**). To our surprise, the N-methylated analog **14** lost over 10-fold biochemical potency and showed lower MDCK permeability. To assess if this phenomenon was general or isolated to this compound, we synthesized a closely related matched-pair **15/16**. While the effect was not as stark in this case, there was still a notable 2-fold loss of potency in both biochemical and cellular assays and no improvement in MDCK. Noting that Compound **2** had relatively low KSol and the introduction of this methylation marker has been associated with solubility decreases, we hypothesized that we were hitting a threshold of solubility where compounds were precipitating out of assay media and interfering with accurate evaluation. Given the improved KSol from Compound **2** (18.9 μM) to **3** (109 μM),[39] we decided to synthesize a non-methylated/methylated matched-pair in the context of the difluorocyclobutyl capping-group. Gratifyingly, **18** maintained biochemical and cellular potency and showed 5-fold improvement in MDCK when compared to **17**. Based on these results, we continued to utilize both the spiro-cap and the difluorocyclobutyl-cap as SAR continued.

Scheme 1. Comparison of synthetic strategies for "extended lariat" compounds.

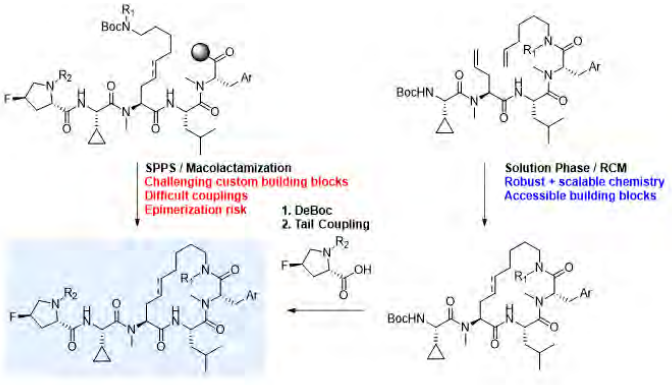

Replacement of Bridging Residue with Extended Alkyl Chain and Methylation of Extended Lariat

Based on encouraging results from Nε-position lysine lariat methylation, we wanted to remove additional heteroatoms from the macrocycle while still maintaining the same macrocyclic ring size. In order to achieve this, we required an alternative synthetic route to our standard SPPS lariat scheme. We conceptualized two potential alternative synthetic routes: (1) Solid-phase peptide synthesis in which custom synthesized extended lysine analogs are cyclized with the C-terminus of the phenylalanine position via lactamization (**Scheme 1**, left), or (2) A solution-phase approach in which a C-terminal olefin is cyclized with a lariat olefin via a ring-closing metathesis reaction (**Scheme 1**, right). While the advantage of SPPS is clear in library synthesis and early discovery, as the lead optimization campaign progressed and increasing quantities of material were required, we were interested in developing robust synthetic methods with lower usage of precious custom building blocks, higher yield, and an improved ability to generate larger quantities of intermediates which could be modified by late-stage derivatization. Furthermore, methods to synthesize extended lysine intermediates were low yielding, cumbersome, and had long lead times. Finally, the phenylalanine derivatives were problematic in terms of resin loading, challenging subsequent couplings/methylations, and epimerization during the final macrocyclization step. For these reasons, we chose to pursue a solution-phase synthetic route based on an RCM macrocyclization followed by late-stage diversification.

Table 4. Initial extended lariat compounds.

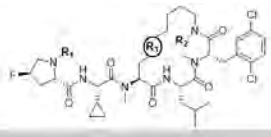

ID	R1	R2	R3	Cyclin A FP-2 IC_{50} (μM)	NCI-H1048 GI_{50} (μM)	MDCK Papp x10^{-6} cm/s
19[a]		H	-CH=CH-	0.740	0.434	NC
20[a]		H	-CH=CH-	0.161	0.046	7.0
21[b]		Me	-CH=CH-	0.276	0.244	2.9
22[b]		Me	-CH=CH-	0.101	0.098	6.5
23		H	-CH2CH2-	0.055	0.016	5.2
24		Me	-CH2CH2-	0.035	0.026	9.0

[a]Compound was tested as mixture of *E/Z* isomers (~9:1), major isomer identity not elucidated. [b]Alkene isomer identity not elucidated.

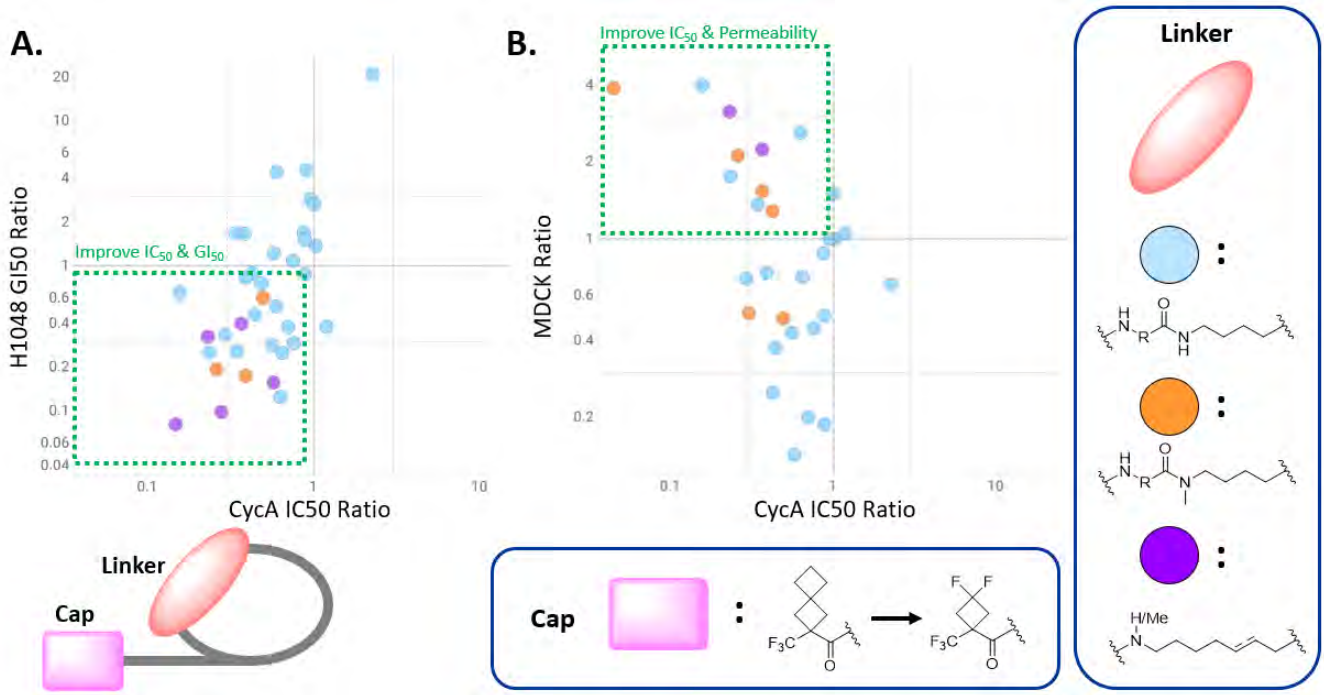

Figure 6. Database-wide matched-pair analysis of the effects of swapping from a spirocyclic-cap to a difluorocyclobutyl-cap. Each point represents one matched-pair. Compounds containing a bridging residue between the lariat and the phenylalanine and not containing a methylation on the lariat amide are represented by blue dots. Compounds containing a bridging residue and a methylation on the lariat amide are represented by orange dots. Compounds containing an extended lariat in place of a bridging residue are represented by purple dots. (A) Correlation plot between ratios of biochemical activity in Cyclin A FP binding assay (y-axis) to ratios of antiproliferative activity in NCI-H1048 cell culture (x-axis). (B) Correlation plot between ratios of biochemical activity in Cyclin A FP binding assay (y-axis) to ratios of permeability as measured by MDCK (x-axis).

Comparison of matched-pairs **19** and **20** show a substantial advantage of the difluorocyclobutyl-cap over the spiro-cap in the context of a fully alkyl replacement for the bridging residue in both biochemical and cellular assays (**Table 4**). This is consistent with **16/18**, in which the lariat was made more lipophilic by the alkylation of the Nε-position of the extended lysine lariat and thus the removal of an H-bond donor. This trend is continued, albeit less dramatically, when the scaffold is further methylated in the case of **21** and **22** where the difluorocyclobutyl-cap is again more active. Furthermore, in this case MDCK is improved more than 2-fold over the spiro-cap. To evaluate the generality of this trend, we conducted a database wide analysis on what effect changing a spiro-cap to a difluorocyclobutyl-cap (**Figure 6**), with all else being equal, has on the binding affinity, cellular inhibition, and MDCK permeability. When a bridging residue is present and the Nε-position of the lariat nitrogen is not methylated, biochemical potency is generally held steady or improved, but no clear relationship is observed for cellular potency or MDCK (blue dots). However, when a bridging residue is present and the Nε-position of the lysine lariat is methylated (orange dots) or when the bridging residue is replaced with an extended alkyl chain (purple dots), a clear advantage across all three parameters can be observed.

Mixtures of E and Z isomeric products were obtained from the RCM reaction, possibly due to the flexibility of the linear starting material. Reaction mixtures showed a ratio of roughly 3:1 for the unmethylated Nε-position lariat (**19** and **20**), which could be further purified to ~9:1. However, the methylated Nε-position lariat (**21** and **22**) was significantly more selective (>10:1). For these early RCM-based alkene containing compounds complete separation proved challenging and they were tested as mixtures. For this reason, assigning E/Z ratios was not undertaken. Thankfully, hydrogenation of this double bond to the saturated alkyl chain from **20** to **23** and **22** to **24** (**Table 4**) provided a potency advantage in biochemical and cellular assays in both cases, as well as avoids the synthetic challenge of selectively synthesizing or separating E/Z isomers. Both compounds display impressive MDCK, with **24** having the best potency/permeability profile that we had seen in our campaign to this point. Encouraged, we decided to profile these compounds further.

Table 5. Comparison of activity and DMPK parameters of extended lariat Compounds **22** and **24** compared to original leads **2** and **3**.

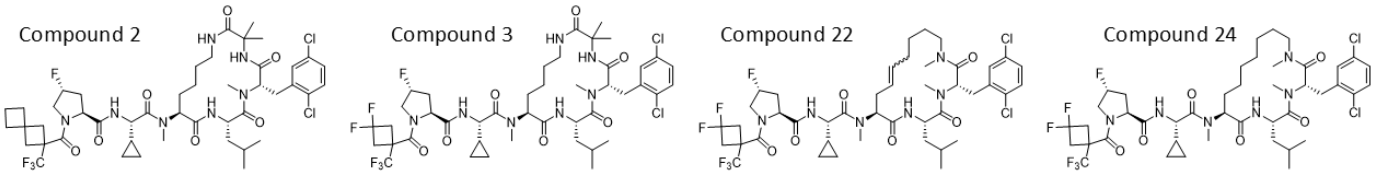

ID	Cyclin A FP-2 IC_{50} (μM)	NCI-H1048 GI_{50} (μM)	MDCK Papp x10^{-6} cm/s	Ksol (μM)	%PPB	tPSA	cLogP	Mouse Cl (mL/min/kg) (2 mpk IV)	%F (PO)
2	0.079	0.042	3.6	18.9	96.7	177.3	7.48	36.3	2 (30 mpk)
3	0.053	0.025	0.7	106.6	96.7	177.33	6.82	31.21	NC
22	0.101	0.098	6.5	NC	99.0	139.4	7.87	36.4	10 (10 mpk)
24	0.035	0.026	9.0	2.8	99.0	139.4	8.36	14.81	NC

PK Profiling of Extended + Methylated Lariat Scaffold

To determine where our compounds stood in comparison to our starting points (Compound **2** and **3**) and determine where we still needed to improve, we evaluated calculated parameters, in vitro ADME properties, and mouse PK readouts (**Table 5).** We have significantly reduced TPSA and increased CLogP in both **22** and **24**. Although this appears to help increase MDCK permeability, it comes at the cost of dramatically reduced solubility. Furthermore, this class of compounds displays high plasma protein binding, which may limit free-drug exposure above GI_{50}. We noted some encouraging signals from in vivo PK; **22** has similar IV clearance and **24** has reduced IV clearance when compared to Compounds **2** and **3**. Furthermore, **22** shows 10% oral bioavailability at 10 mpk, which is a dramatic improvement over 2% at 30 mpk seen in the early lead. While these compounds were not predicted to demonstrate oral efficacy based on free-drug exposure, we determined that this was a much-improved scaffold for optimization and we opted to continue diversification from **24**, given its superior cellular potency and high MDCK permeability.

Revisiting 2-Phe Diversification on 24 Scaffold

Scheme 2. Late-stage diversification strategy for *ortho*-position of phenylalanine on extended lariat scaffolds.

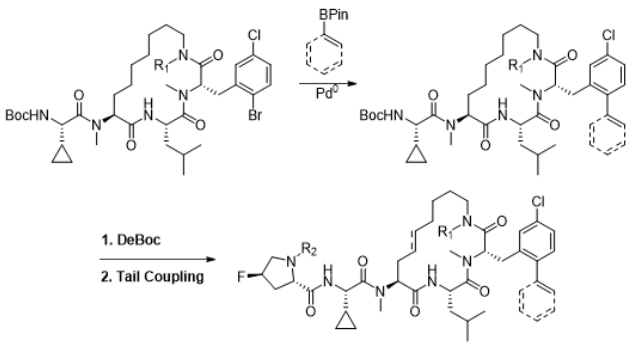

We wished to revisit the 2-substituted phenylalanine derivatives exemplified by **Table 2** in the context of promising, more lipophilic macrocyclic core, to explore these substituents' effects on cellular potency and pk parameters. We utilized an enabling Suzuki reaction (**Scheme 2**) to efficiently diversify a late-stage intermediate. In this way compounds such as **25-28** were synthesized and evaluated (**Table 6**).

Both saturated and unsaturated heterocycles were tolerated in the 2-position of the phenylalanine. There appeared to be a general improvement in both the cellular and biochemical activity in line with our potency goals of compounds substituted with larger groups at this position. In addition to the potency increases, several groups led to improved permeability and increased solubility. However, plasma protein binding generally remained very high which limited free drug exposure. This was true even in cases where %F was improved (e.g. **27**). Modestly increasing the polarity through the introduction of a methylated lactam (**28**) did reduce plasma protein binding, but this was at the expense of any measurable oral exposure (likely due to a dramatic reduction in MDCK).

Looking back to the earlier SAR generated on the ortho position of the Phe for the Compound **2** scaffold, we took inspiration from the matched-pair between **12** and **13** (**Table 2**). In this case, the conversion of an ether to a pyridone-ether resulted in an unexpected improvement (given the increased TPSA) in MDCK and was well tolerated in biochemical and cellular potency. With this in mind, we synthesized **29** and were excited to see not only very potent cellular activity but also exceptional permeability combined with a reduced %PPB and improved solubility. While IV clearance was moderate, the compound still displayed 6.4% oral bioavailability and achieved free-drug exposure above GI_{50}. Encouraged, we proceeded to optimize this series to develop an analog which met our >20% oral bioavailability goal in preparation for PO efficacy.

Optimizing Pyridone-Ether Phe Series and Nomination of 33 for Efficacy

Table 6. Diversification of phenylalanine residue of Compound **24** leads to pyridone-ether **29** with free Cmax above GI_{50}.

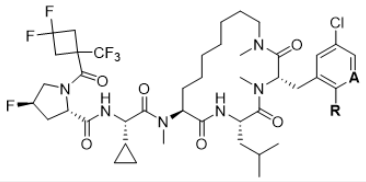

ID	R	A	Cyclin A FP-2 IC_{50} (μM)	NCI-H1048 GI_{50} (μM)	MDCK Papp x10^{-6} cm/s	Ksol (μM)	%PPB	Mouse Cl (mL/min/kg) (2 mpk IV)	%F (30 mpk PO)
24	Cl	CH	0.035	0.026	9.0	2.8	99.0	14.81	NC
25		CH	<0.02	<0.01	2.9	43.1	98.4	36.75	NC
26		CH	<0.02	<0.01	8.2	9.5	98.6	98.37	2.2
27		CH	0.027	0.012	12.0	18.9	98.6	48.72	12.9
28		CH	0.023	0.013	1.4	80.4	95.6	19.04	<0.01
29	OMe	N	0.038	<0.01	14.0	30.2	94.5	60.13	6.4

We hypothesized that increasing the alkyl group size on the pyridone ether could benefit this series in two ways, first by blocking metabolic demethylation and second by increasing lipophilic character to aid in passive crossing of the gut wall. Based on the broad substituent tolerance that we had seen in both the extended lariat series (**Table 6**) and the earlier bridging residue containing series (**Table 2**), we anticipated relatively flat SAR as we increased the size of the alkyl ether portion of **29** (**Table 7**). To our surprise, however, a modest change from methyl to ethyl in **30** reduces the cellular potency even though the biochemical potency remains unchanged. Furthermore, increasing the alkyl character in this way does not improve the MDCK as expected and reduces the KSol, so this compound was not profiled further. Increasing steric bulk and lipophilic character further by introducing the branched isopropyl (**31**) or isobutyl (**32**) also negatively impacted cellular potency to outside our target of < 20 nM and were thus not profiled further. To strike a balance between increased lipophilicity/metabolic stability and retained potency , we replaced the methyl ether with a cyclopropyl ether in **33** (CIRc-014 in ref. 38). Gratifyingly, this compound maintains a cellular potency near the bottom of the assay and is nearly unchanged in MDCK, KSol, or %PPB. While the IV clearance of **33** remains moderate/high, it nevertheless displays an oral bioavailability of 27.2% in mouse at 30 mg/kg and achieves free-drug exposure above the GI_{50}. **33** was selected for further profiling in preparation for an in vivo efficacy study.

Table 7. Alkyl scan of pyridone-ethers leads to Compound **33**, which retains potency and *in vitro* DMPK while boosting oral bioavailability.

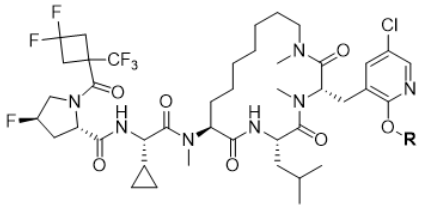

ID	R	Cyclin A FP-2 IC_{50} (μM)	NCI-H1048 GI_{50} (μM)	MDCK Papp x10^{-6} cm/s	Ksol (μM)	%PPB	Mouse Cl (mL/min/kg) (2 mpk IV)	%F (30 mpk PO)
29	-Me	0.038	<0.01	14.0	30.2	94.5	60.13	6.4
30	-Et	0.025	0.20	13.4	11.5	95.3	NC	NC
31	-iPr	0.033	0.100	NC	NC	NC	NC	NC
32	-iBu	0.027	0.057	NC	NC	NC	NC	NC
33	-cyPr	0.050	0.015	13.2	27.3	96.6	68.05	27.2

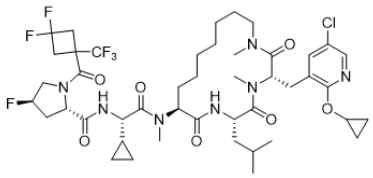

Compound 33

Biochemical
- Cyclin A SPR KD (nM): 2.7
- Cyclin B SPR KD (nM): 1.0
- Cyclin E SPR KD (nM): 33.8
- Cyclin A/B vs E Selectivity: >12

Cellular
- NCI-H1048 GI_{50} (uM): 0.015
- NCI-H446 GI_{50} (uM): 0.042
- NCI-H69 GI_{50} (uM): 0.004
- WI-38 GI_{50} (uM): 19.06

Properties
- MW: 962.5
- tPSA: 161.56
- CLogP: 7.6
- Rot. Bonds: 12
- HBDs: 2

***in vitro* DMPK**
- KSol (μM): 27.3
- LogD: 3.86
- MDCK P_{app}: 13.2
- Mouse PPB: 96.6%

Figure 7. Profile of biophysical and cellular potency, molecular properties, and *in vitro* DMPK parameters of Compound **33.**

Table 8. Dose-escalating pharmacokinetics in mouse for Compound **33**. Oral bioavailability maintained from 30 to 100 mpk.

Route (Mouse)	Dose (mg/kg)	T_{max} (h)	C_{max} Total drug (ng/mL)	C_{max} Free drug (ng/mL)	AUC-inf (ng*h/mL)	$T_{1/2}$ (h)	Cl (mL/min/kg)	%F PO
IV	2	-	-	-	489.86	1.37	68.05	-
PO	30	1.0	1210.00	60.52	2002.23	0.99	-	27.2
PO	100	0.5	2990.00	101.66	8112.69	3.15	-	34.9

A more in-depth analysis of **33** can be seen in **Figure 7**. Compound **33** binds to Cyclins A and B at 2.7 nM and 1.0 nM, respectively, in a surface plasmon resonance (SPR) assay, confirming the highly potent activity measured in our screening FP assay. Furthermore, binding of **33** is >12-fold less potent to Cyclin E, demonstrating selectivity for our desired mechanism of action. At the outset of the lead optimization campaign, we identified HBD count and LogD as properties to monitor and lower to improve oral bioavailability. From Compound **2** to **33**, HBD count was lowered from 4 to 2 and LogD was lowered from 5.54 to 3.86, representing a successful improvement in drug-like character of our macrocyclic peptide series.

33 was modeled in the RxL binding site of Cyclin A (**Figure 8**) and shown to align well with the pharmacophore H-bond network of Compound **2**. The two remaining H-bond donors are involved in polar contacts with Gln254 and Ile281. All amide bonds not directly engaging in productive interaction with the target are alkylated. The replacement of the bridging residue in the macrocycle with an alkyl chain and the methylation of the extended lariat are not predicted to disrupt the ability of the scaffold to adopt an active conformation. The replacement of the spiro-cap with the difluorocyclobutyl-cap does not alter the predicted orientation of the trifluoromethyl group into the S-pocket. The 5-chloro and 2-pyridone cyclopropyl ether substituents do not appear to make any clashes with either the HP or the shallow shelf consisting of Ile231, Met210 and Arg250.

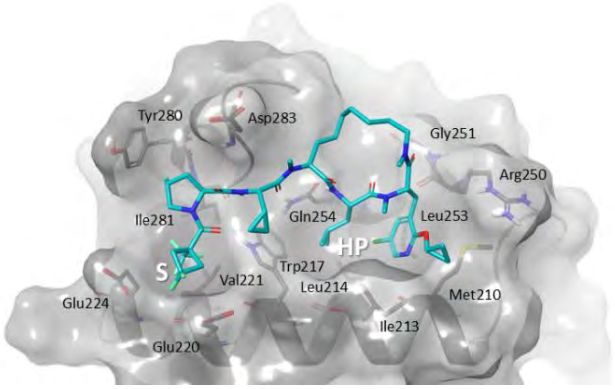

Figure 8. Computational docking model of Compound **33** in the RxL binding site of Cyclin A.

In addition to our general screening anti-proliferation assay against NCI-H1048, two additional SCLC lines were evaluated. Based on efficacy results of Compound **2** against NCI-H69 and NCI-H1048 in vivo[39] we wanted to evaluate **33** in NCI-H69 and a more challenging model (besides NCI-H1048) using a cell line of intermediate-sensitivity to our compounds. We determined that **33** inhibits NCI-H446 with a GI_{50} of 42 nM, compared to a GI_{50} of 4 nM in NCI-H69 and 15 nM in H1048. Therefore, NCI-H69 and NCI-H446 were selected for *in vivo* efficacy studies. To ensure dose-linearity, **33** was administered via PO dosing in mouse at 100 mpk and showed proportional exposure (**Table 8**). With these results in hand, **33** was nominated to progress to PO efficacy evaluation against two CDX mouse models of SCLC.

In Vivo Oral Efficacy of Cyclin A/B RxL Inhibitor 33 in SCLC Tumor Xenograft Mouse Models

We evaluated the in vivo antitumor activity of **33** in two SCLC cell-line derived xenograft (CDX) models, NCI-H69 and NCI-H446 (**Figure 9**). In NCI-H69, **33** was dosed at 25 and 50 mg/kg via oral dosing (PO) twice daily (BID) for 14 days. Treatment with **33** induced substantial dose-dependent tumor growth inhibition (TGI), including regression, in the NCI-H69 model, with a mean % tumor growth inhibition (%TGI) value of 53% at 25 mg/kg PO BID and a mean regression value of 40% at 50 mg/kg PO BID. In the NCI-H446 model, **33** was dosed at 100 mg/kg PO three times daily (TID), 25 mg/kg PO TID, 100 mg/kg PO BID, and 50 mg/kg PO BID for 14 days. Substantial dose-dependent TGI and regression was observed in all dosing groups, with %TGI of 79% and 85% for 25 mg/kg PO TID and 50 mg/kg BID, respectively, and mean regression values of 80% and 44% for 100 mg/kg PO TID and 100 mg/kg PO BID, respectively. Tumors in the NCI-H446 model were monitored for 27 days after the last dose, and a clear dose response in regrowth was observed in order from highest to lowest response as

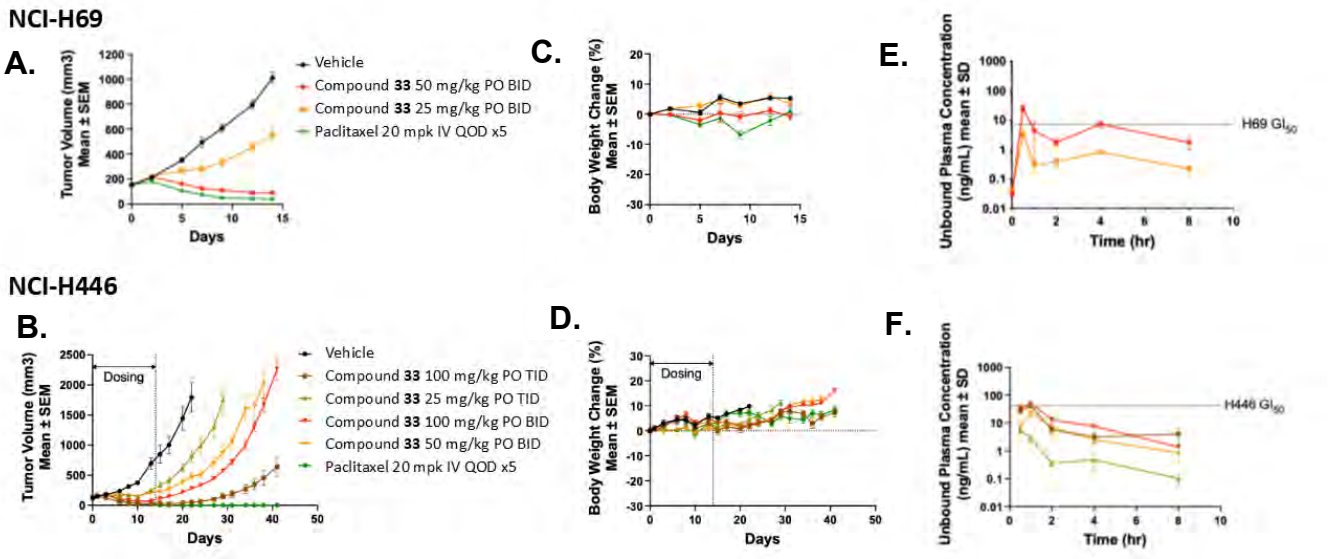

Figure 9. Orally bioavailable Cyclin A/B RxL inhibitor has antitumor activity in the NCI-H69 and NCI-H446 SCLC xenograft models.(A) Tumor volume curves for NCI-H69 xenograft tumors treated with vehicle or Compound 33 at 25 and 50 mg/kg PO BID for 14 days or paclitaxel at 20 mg/kg IV every other day (QOD) x 5 (9 days). (B) Tumor volume curves for NCI-H446 xenograft tumors treated with vehicle or Compound 33 at 50 and 100 mg/kg PO BID or 25 and 100 mg/kg TID for 14 days or paclitaxel at 20 mg/kg IV QOD x 5 (9 days). (C, D) Body weight change for treated animals. (E,F) Unbound plasma concentration of Compound 33 in animals after the final dose. For (A-D), n = 10-11 mice per arm, and data are mean ± SEM.. For (E, F), n = 3-5 mice per timepoint, and data are mean ± 1 SD.

follows: 100 mg/kg PO TID, 100 mg/kg PO BID, 50 mg/kg PO BID, 25 mg/kg PO TID.

In both models, treatment was well tolerated with mean body weight loss not exceeding 10% over the course of the studies. Plasma PK analysis in both studies showed a clear correlation between unbound drug exposure relative to GI_{50}

Table 9. Cross-species pharmacokinetics of Compound **33**.

Parameter	Species	Compound 33
Clearance (mL/min/kg)	Mouse	68
	Rat	46
	Dog	22.4
	Mini-Pig	28
Volume of Distribution (L/kg)	Mouse	1.1
	Rat	3.0
	Dog	2.6
	Mini-Pig	1.8
$t_{1/2}$ (h)	Mouse	1.4
	Rat	1.3
	Dog	4.7
	Mini-Pig	1.5
Oral %F	Mouse	27.2
	Rat	17.4
	Dog	22.6
	Mini-Pig	6.2

and increased anti-tumor activity. These results confirm that orally dosed Cyclin A/B inhibitors may present a new treatment option for patients with SCLC.

Preclinical Pharmacokinetics (PK) of 33

PK of **33** was evaluated in single dose oral (PO) and intravenous (IV) dose studies in the mouse, rat, dog, and minipig. Following a single IV dose of **33**, moderate to high plasma clearance (CL) was observed, ranging from 70% and 74% of total hepatic blood flow rate in the dog and minipig, to 94% and 84% of total hepatic blood flow rate in the mouse and rat, respectively. The values of volume of distribution at steady state (Vss) were slightly greater than their estimated total body water, suggesting minor distribution of **33** into tissues. The mean elimination half-life (t1/2) ranged from 0.7 hours in mouse to 4.7 hours in dog. Following a single PO dose of 33 in the mouse, rat, dog, and minipig, oral bioavailability was found to be greater than 17% in mouse (27%), rat (17%) and dog (23%), and slightly lower at 6.2% in the minipig.

In Vitro Evaluation of Potential Off-Target Toxicity and Drug-Drug Interaction with 33

As with the IP administered Cyclin A/B inhibitor Compound **2**, **33** was evaluated in a panel of 489 kinases at 1 and 10 μM test concentrations and showed a clean profile, as expected given the mechanism of action. **33** also demonstrated no significant off-target activity when tested at up to 10 μM in a safety pharmacology functional panel SAFETY scan47 E/IC50 (Eurofins Discovery) that included cell-based assays to evaluate agonistic and antagonistic activity against GPCR proteins and ion channels, enzyme inhibitors and transporter blockers (see Supporting Information). Compound **33** also showed no off-target activity in KINOMEscan assay (Eurofins Discovery) (see Supporting Information). Finally, **33** showed some levels of reversible inhibition

against human cytochrome P450 (CYP) 3A4 and 2D6, and potential irreversible inhibition against CYP3A4 (see Supporting Information).

CONCLUSIONS

Herein, we report the lead optimization campaign from a proof-of-concept molecule with IP efficacy to a novel class of orally bioavailable Cyclin A/B RxL inhibitors. Advanced lead compound **33** displays potent and selective antiproliferative activity against SCLC tumor cells and in vivo efficacy against CDX mouse models of SCLC when dosed orally. This was achieved by leveraging both computationally guided structure and property-based design, which is part of what we refer to as our MXMO™ platform, and the rich SAR data obtained in the Compound **2** development campaign.[39] In the early stages of the project progress was driven entirely by high-throughput solid-phase peptide synthesis, but as the needs of the project changed and the scaffold design evolved beyond standard SPPS capabilities solution-phase chemistry was required, highlighting successful cross-functional collaboration and the value of adaptability in peptide drug discovery.

During this project, we identified Circle's first clinical candidate, CID-078, which is structurally related but distinct from **33** and has a similar in vitro and in vivo profile. CID-078 is currently being investigated in a Phase 1 clinical trial for patients with SCLC, triple-negative breast cancer, or solid tumors harboring RB1 mutation (NCT06577987). This highlights the power of medicinal chemistry to discover drug-like compounds in the bRo5 peptide space and marks a major milestone for Cyclin A/B inhibition as a clinical-stage target. The structure, pre-clinical profile, and human trial data for CID-078 will be disclosed in future communications.

EXPERIMENTAL SECTION

Synthesis and Characterization

Unless otherwise mentioned, all solvents and chemicals were obtained from commercial sources and used without purification. Compounds **2**-**18** were synthesized using SPPS. Linear sequences were synthesized in parallel on a Biotage eSyro II peptide synthesizer equipped with 48 reaction vials using 2-chlorotrityl chloride resin, Fmoc-protected amino acids, and HATU coupling. Site-specific on-resin methylation was achieved using a modified Fukuyama-Mitsunobu protocol in toluene on the same instrument. Linear peptides were cleaved from the resin with TFA or HFIP, concentrated under reduced pressure, and cyclized using T3P with DIEA in DCM/DMF. Compounds **19**-**33** were synthesized using solution phase chemistry outlined in the supporting information. All products were purified via HPLC. The progress of reactions was typically monitored by LC-MS (Waters UPLC Acquity I-Class equipped with Acquity QDa). Purification of final compounds to > 95% purity was carried out by reverse phase C18 chromatography using Waters HPLC system equipped with the following components: Waters 2767 Sample Manager, Waters 1525 Binary HPLC Pump, Waters 2545 Binary Gradient Module, Waters SFO System Fluidics Organizer, 515 HPLC Pump, Waters Acquity QDA and Waters 2998 Photodiode Array Detector. Proton (1H) and carbon (13C) NMR spectra were recorded on a Bruker Avance 500 (500.13 MHz for 1H; 125.76 MHz for 13C). Chemical shifts are given in parts per million (ppm) (δ relative to residual solvent peak for 1H and 13C).

Calculated and Measured Compound Properties

ClogP and TPSA values were calculated using the Chemdraw model. MDCK monolayer cell permeability, kinetic solubility (Ksol), mouse plasma protein binding via ultracentrifugation (%PPB), and Caco-2 monolayer permeability (A-B and B-A) were generated by Pharmaron using standard experimental conditions (see Supporting information).

Binding model prediction

Binding model of **33** to Cyclin A was generated using the Schrödinger suite 2024-3, following previously reported procedures.[39] In brief, the protein model of Cyclin A was based on the co-crystal structure of Cyclin A and a lariat macrocycle (PDB: 1URC). The protein was prepared using the Protein Preparation Workflow, and the resulting model was used to create the docking grid. The 3D structure of **33** was generated from its SMILES using the LigPrep module. The initial binding pose of **33** was obtained by performing alignment to the previously published binding model of Compound **2**. The Ligand Alignment module was utilized to align common structures by maximum common substructure, with the ligand specified as a macrocycle and the binding site of cyclin A specified as the receptor. The aligned model was subsequently refined by docking using Glide SP with the "Refine only" option.

Molecular matched-pair analysis

A sequence-based matched pair analysis was performed to compare molecules at the residue-level. With compounds represented as linear peptide sequences, a matched pair is defined as 2 aligned sequences with only 1 residue difference. For each molecular pair, property ratios were calculated to examine the effect of the corresponding residue transformation. For compound 1 and compound 2 of a matched pair, the ratio of property A is calculated by the following formula:

$$Ratio_A = \frac{A_{compound\ 2}}{A_{compound\ 1}}$$

Cell Lines and Cell Culture

NCI-H1048, NCI-H446, NCI-H69, and WI-38 cell lines were originally obtained from American Type Culture Collection (ATCC). NCI-H69 and NCI-H446 cells were maintained in RPMI-1640 media supplemented with 10 % fetal bovine serum (FBS), NCI-H1048 cells were maintained in HITES medium (Base medium: DMEM:F12 supplemented with 0.001 mg/ml insulin, 0.01 mg/ml Transferrin, 30 nM selenium, 10 nM hydrocortisone, 10 nM beta-estradiol, and additional 2 mM glutamine to a final concentration of 4.5 mM) supplemented with 5 % fetal bovine serum (FBS). WI-38 cells were maintained in DMEM supplemented with 10% FBS.

Early passage cells of all the cell lines listed above were frozen using Recovery Cell Culture Freezing media (Gibco) and were maintained in culture no more than 4 months where early passage vials were thawed.

MTT Proliferation Assay

NCI-H1048 and WI-38 cell lines were plated in 96-well plates at 5 x 10^3 cells/well with 100 mL media/well. NCI-H69 cells were grown to confluency in a T150 flask. Cells were collected by centrifugation at 1100 r.p.m. and resuspended in 30ml media of which 10ml was used to seed six 96-well plates. The following day, cells were dosed using a Bravo liquid Handler (Agilent Technologies). The plate controls Roscovitine and Staurosporine were used to define the top and bottom of the growth inhibition curves, respectively. Inhibitors were dosed in duplicate in either an 8- (WI-38, NCI-H1048) or 10-point (NCI-H69) 1:3 serial dilution with 10μM maximum concentration. Roscovitine was dosed in singlet in an 8- or 10-point 1:2 serial dilution with 100μM maximum concentration. Staurosporine was dosed in singlet in an 8- or 10-point 1:2 serial dilution with 1μM maximum concentration. After dosing, plates were maintained in tissue culture incubators (37 ^oC; 5 % CO_2) for 3 (WI-38) or 5 days (NCI-H1048, NCI-H69) to allow for at least 2 cell doublings before processing in an MTT proliferation assay (R&D systems, #4890-050-K) performed according to manufacturer instructions. The average absorbance value obtained with the highest two concentrations dosed for roscovitine and staurosporine was used for background subtraction. The top of the assay (100% growth) was determined by normalization with the top of the roscovitine curve. Growth inhibition 50 (GI_{50}) was determined by nonlinear regression analysis using log(inhibitor) vs response -variable slope (four parameters) using GraphPad Prism (10.1.0) software.

Fluorescence Polarization Assay

Binding affinity for the compounds of Formula I were determined by Fluorescence Polarization (FP) competitive assay based on previously established protocols[14,27] with modifications as described below. Cyclin/CDK protein complexes were sourced as follows: CyclinA2/CDK2 (CRELUX Protein Services), CyclinB1/CDK1 (Eurofins, discovery. Cat. No. 14-450) and CyclinE1/CDK2 (Eurofins, discovery. Cat. No. 14-475). FP binding assays were performed in 25 mM HEPES pH 7.5, 100 mM NaCl, 1mM DTT, 0.01% NP-40 and 1 mg/mL BSA for all 3 protein complexes in black 96-well plates. After experimental plates are set, they were equilibrated by gentle mixing by placing them on an orbital shaker at 100 rpm for 2 hours at rt and then read on a SpectraMax i3X Multi-Mode Microplate Detection platform. Affinity of the Cyclin/CDK complexed for the fluorescent labeled probe was determined by adding increasing concentration of each protein complex in buffer containing a carboxyfluorescein labeled probe (FAM probe) at 2 nM. For the 'FP2 Probe' (Supporting Information) we used 8 nM for Cyclin A2/CDK2, and 10 nM for both Cyclin B1/CDK1 and Cyclin E1/CDK2. Methods to prepare the FAM probes are described in the heading below. Under these conditions, the dynamic range was >100 mP between 100% binding of FAM probe and complete inhibition of binding by saturating excess of an unlabeled competitor compound, with all experiments showing a Z' factor > 0.80. IC_{50} for test compounds were determined in eight-point serial dilution dose response curves. Reported IC_{50} are the average of 2-3 independent experiments.

Single Dose Intravenous (IV) and Oral (PO) PK in Mice

All experiments conducted were performed following the guidance of the Association for Assessment and Accreditation of Laboratory Animal Care (AAALAC). Single dose intravenous (IV) and oral (PO) mouse PK was dosed at in male C57/BL6 mouse, respectively. The dosing formulation was prepared by dissolving the test article in 5% DMSO:10% Solutol HS15: 85% DI water to yield concentration of 0.5 mg/mL for IV, and prepared in 30% PEG400: 20% Solutol HS15: 50% Phosal 53 MCT to yield concentration of 3.0 mg/mL for the PO dosing. 3 mice each were dosed at 2 mg/kg via tail vein (IV) and at 30 mg/kg via oral gavage (PO). Approximately 0.05 mL of blood was collected from a tail or facial vein in tubes containing K3 EDTA at 0.083 (IV only), 0.25, 0.5, 1, 2, 4, 8 and 24 h post-IV and post-PO dose. Plasma samples were obtained via centrifugation and sample cleanup was conducted by protein precipitation with acetonitrile that contained an internal standard (IS, Dexamethasone). LC-MS/MS (Shimadzu LCMS-8060 and L-40D) quantitation of test articles and IS were achieved with positive ion MRM transitions. The reversed-phase chromatographic system consisted of a gradient mobile phase at a flow rate of 0.6 mL/min, containing 0.1% formic acid in 5% acetonitrile in water (mobile phase A) and 95% acetonitrile in water (mobile phase B) and an ES-CN column. Analyst version 1.6.2 was used to measure peak areas and peak area ratios of test articles to IS. A calibration curve was constructed from the peak area ratios (Test article to IS) with a weighted (1/x2) linear regression using Watson version 7.5 LIMS and a calibration curve ranging between 0.5 and 1000 ng/mL. Individual test article's plasma concentration vs time profiles were used to calculate the pharmacokinetic parameters by employing a non-compartmental analysis (PhoenixTM WinNonlin 8.3).

Single Dose Intravenous (IV) and Oral (PO) PK in Mouse, Rat, Dog and Minipig of 33

All experiments conducted were performed following the guidance of the Association for Assessment and Accreditation of Laboratory Animal Care (AAALAC). Preclinical single dose IV and PO PK of **33** was performed in male C57/BL6 mice, male Sprague Dawley rats, male beagle dogs, and male Bama minipigs. The dosing formulation was prepared by dissolving **33** in 5% DMSO:10% Solutol HS15: 85% DI water to yield concentration of 2 mg/mL for IV dose in mice and concentration of 1 mg/mL for IV dose in rats, dogs, and minipigs. The dosing formulation was prepared in 30% PEG400: 20% Solutol HS15: 50% Phosal 53 MCT to yield concentration of 6.0 and 3.0 mg/mL for the PO dosing in mice and rats, respectively. Similarly, PO dosing of dogs was prepared by dissolving **33** in the same formulation and yield a final concentration at 41.7 mg/mL. 0.8 mL of the formulation was then filled into a size#00 Gelatin capsule and sealed before dosing. PO dosing minipigs was prepared by dissolving **33** in the same formulation and yield a final concentration at 22.5 mg/mL. 8.0 mL of the formulation was then filled into a size#11 gelatin capsule before dosing. 12 mice were dosed in single dose IV and another 12 mice were dosed in single dose PO, followed by sparse sampling up to 24 hours post dose. Approximately 0.05 mL of blood was collected from a tail or facial vein in tubes containing K3 EDTA. Similarly, rat, dog, and minipig PK were performed

with 3 rats per dose group with serial blood sampling in tubes containing K3-EDTA up to 24 hours post dose. Plasma samples were obtained via centrifugation and stored at -80°C before processing. Protein precipitation with acetonitrile containing internal standard was conducted to process the plasma samples, followed by vortex mixture and centrifugation. Afterwards, clean supernatant was further diluted with water before injected into LC-MS/MS for quantitative analysis. Shimadzu (LC-30AD or LC-40D) HPLC were coupled with triple quadruple tandem mass spectrometers (AB API 5500, 6500+, or Shimadzu LCMS-8060) to quantify **33** and internal standards. The quantitation of **33** was achieved with positive ion MRM transition at 962.2/171.1, 962.3/422.9, or 962.3/373.1. Internal standard Dexamethasone or Tolbutamide was quantified using positive ion MRM transition 393.2/373.1, or 271.1/155.1, respectively. The reversed-phase chromatographic system consisted of a gradient mobile phase at a flow rate of 0.6 mL/min, containing 0.1% formic acid in water (mobile phase A) and acetonitrile (mobile phase B) and an ES-CN column (for rat and mouse), a Raptor Biphenyl column (for dog), or a Waters xbridge® C18 column. Analyst version 1.6.2 was used to measure peak areas and peak area ratios of 33 to IS. A calibration curve was constructed from the peak area ratios (**33** to IS) with a weighted (1/x2) linear regression using Watson version 7.5 LIMS and a calibration curve ranging between 0.5 and 1000 ng/mL. **33** plasma concentration vs time profiles were used to calculate the pharmacokinetic parameters by employing a non-compartmental analysis (PhoenixTM WinNonlin 8.3).

SCLC Cell Line Xenograft Studies

All experiments conducted were performed following the guidance of the Association for Assessment and Accreditation of Laboratory Animal Care (AAALAC). The NCI-H69 and NCI-H446 xenograft studies were approved by the Institutional Animal Care and Use Committee (IACUC) and performed at Labcorp Early Development Laboratories, Inc. (Animal Use Protocol Number: VUF 05).

NCI-H69 and NCI-H446 human small-cell lung cancer cells were obtained from ATCC. Tumor volume (TV) was determined by measuring the length (L) and perpendicular width (W) with calipers and calculated using the formula

$$TV = 0.5 \times L \times W^2$$

As a measure of efficacy, the % tumor growth inhibition (%TGI) is calculated at the end of treatment using the following formula

$$mean\ \%TGI = 100 - \left(\frac{\Delta T_{mean}}{\Delta C_{mean}}\right) \times 100$$

ΔT_{mean} and ΔC_{mean} represent the mean volume on the day of evaluation minus the tumor volume at the start of dosing for the treatment and control groups, respectively. In cases where the mean tumor volume in treatment groups is smaller at the end of the study in comparison to the start of dosing, regression values are calculated instead using the formula

$$\text{mean \% Regression} = -\left(\frac{\Delta \mathrm{T}_{\mathrm{mean}}}{\mathrm{T}_{0,\mathrm{mean}}}\right) \times 100$$

$\Delta T_{0,mean}$ represents the mean tumor volume at the start of dosing for the treatment groups.

For the NCI-H69 model, 5×10^6 NCI-H69 cells were suspended in serum-free RPMI-1640 medium, combined with an equal volume of ECM gel (Sigma-Aldrich, #E1270), and implanted subcutaneously into the flanks of 6-7 week old female Nude mice (Envigo, Hsd:Athymic Nude-Foxn1^{nu}). When tumors were 100–200 mm^3 in size, 13 days after implantation, the mice were randomized and put into treatment groups. Mice were treated twice daily (BID) with oral (PO) doses of **33** at 50 or 25 mg/kg or vehicle (30% PEG400, 20% Solutol HS15, 50% Phosal 53 MCT) for 14 days or with intravenous (IV) injections of 20 mg/mkg paclitaxel every other day (QOD) for 5 doses. Tumors and body weight were measured three times per week for the duration of the study. Plasma samples were collected for PK analysis by LCMS/MS at multiple time points shown on day 14.

For the NCI-H446 model, 5×10^6 NCI-H446 cells were suspended in serum-free RPMI-1640 medium, combined with an equal volume of ECM gel (Sigma-Aldrich, #E1270), and implanted subcutaneously into the flanks of 7-8 week old female Nude mice (Envigo, Hsd:Athymic Nude-Foxn1^{nu}). When tumors were 100–200 mm^3 in size, 12 days after implantation, the mice were randomized and put into treatment groups. Mice were treated with PO doses of **33** three times daily (TID) at 100 and 25 mg/kg and BID at 100 and 50 mg/kg or with vehicle (30% PEG400, 20% Solutol HS15, 50% Phosal 53 MCT) TID for 14 days or with intravenous (IV) injections of 20 mg/mkg paclitaxel every other day (QOD) for 5 doses. Tumors and body weight were measured three times per week for the duration of the study. Plasma samples were collected from 3 animals per **33** treatment group for PK analysis by LCMS/MS at multiple time points shown on day 14. The remaining animals were monitored for an additional 27 days with tumor and body weight measurements.

In Vitro Safety and Metabolism Testing

Eurofins Discovery Services carried out the in vitro safety testing of **33**. The tests selected were from Eurofins product list and included i) The KINOMEscan™ kinase panel assay set containing 468 kinases; ii) The SAFETY scan47 E/IC50predominantly cell-based Functional Panel that includes 24 pharmacology targets tested against for both agonist and antagonist activities, 10 enzymes and transporters tested for antagonist activities, and an Ion-Profiler panel containing 6 voltage and ligand-gated ion channels; In each case **33** was tested at either a single concentration or at two test concentrations, **33** was also evaluated ADME-Tox In Vitro Metabolism Inhibition panel of 7 major human cytochrome P450 enzymes to determine the IC_{50} of inhibition against P450 enzymes.

ASSOCIATED CONTENT

Supporting Information. Supplementary figures; Solid-phase peptide synthesis including methods, building blocks used, and peptide sequences; Final compound purification; Analysis of final compounds; Solution phase synthesis methods including custom building blocks, key intermediates, and final compounds; Biochemical probe synthesis; DMPK analysis methods including MDCK-MDR1, Plasma Protein Binding, and Kinetic Solubility; MetID of Compound **2**; *In vitro* safety panel data

AUTHOR INFORMATION

Corresponding Author

*James B. Aggen – Circle Pharma, Inc. South San Francisco, CA, 94080, United States; Email: jim.aggen@circlepharma.com

Present Addresses

Miles W. Membreno – *University of California, Santa Cruz, CA 95064*
Ramesh Bambal – *Prelude Therapeutics, Wilmington, DE 19805*
Evelyn W. Wang – *Evelyn Wang Consulting, San Francisco, CA 94114*
Rajinder Singh – *Stealth Biotech, San Carlos, CA*
Jie Zheng – *Olema Oncology, San Francisco, CA 94103*
Yuliana Gritsenko – *New Culture, Inc., San Leandro, CA 94577*
Cayla M. McEwen – *Sangamo Therapeutics, Richmond, CA 94804*

Author Contributions

The manuscript was written through contributions of all authors. All authors have given approval to the final version of the manuscript. ‡These authors contributed equally.

Notes

All work described herein performed by authors while employed by Circle Pharma, Inc.

ACKNOWLEDGMENT

The authors thank Matthew P. Jacobson, William G. Kaelin Jr., Alan Ashworth, Bruce Stillman, John Josey, and George Tonn for their support and insightful discussions.

ABBREVIATIONS

CDK, cyclin dependent kinase; RB/RB1, retinoblastoma protein; E2F, early region 2 binding factor; HP, hydrophobic patch; CDX, cell line-derived xenograft; MRAIL, domain composed of methionine, arginine, alanine, isoleucine, leucine in cyclins; RxL, motif composed of arginine, a variable moiety, and leucine; PPI, protein-protein interaction; SCLC, small cell lung cancer; TAT, trans-activator of transcription; MDCK, Madin-Darby canine kidney cells; Papp, apparent permeability; FP, fluoresence polarization assay; LOQ, limit of quantitation; SAR, structure activity relationship; bRo5, beyond rule-of-five; HBD, hydrogen bond donor; HBA, hydrogen bond acceptor; IMHB, intramolecular hydrogen bond; TPSA, total polar surface area; PPB, plasma protein binding; IP, intraperiotoneal; PO, 'per os' oral dosing; QD, once daily dosing; QOD, every other day dosing; TGI, tumor growth inhibition; CR, complete regression; RCM, Ring Closing Metathesis; HATU, hexafluorophosphate azabenzotriazole tetramethyl uronium; TFA, trifluoroacetic acid; HFIP, hexafluoro-2-propanol; DCM, dichloromethane; DMF, dimethylformamide; DIEA, diisopropylethylamine; T3P, propanephosphonic acid anhydride; FAM, 5-carboxyfluorescein.

REFERENCES

(1) Camps-Fajol, C.; Cavero, D.; Minguillón, J.; Surrallés, J. Targeting Protein-Protein Interactions in Drug Discovery: Modulators Approved or in Clinical Trials for Cancer Treatment. *Pharmacol Res* **2025**, *211*, 107544. https://doi.org/10.1016/j.phrs.2024.107544.

(2) Fry, D. C.; Vassilev, L. T. Targeting Protein–Protein Interactions for Cancer Therapy. *J Mol Med (Berl)* **2005**, No. 12, 955–963. https://doi.org/10.1007/s00109-005-0705-x.

(3) Dougherty, P. G.; Qian, Z.; Pei, D. Macrocycles as Protein–Protein Interaction Inhibitors. *Biochem J* **2017**, No. 7, 1109–1125. https://doi.org/10.1042/BCJ20160619.

(4) Villar, E. A.; Beglov, D.; Chennamadhavuni, S.; Porco, J. A.; Kozakov, D.; Vajda, S.; Whitty, A. How Proteins Bind Macrocycles. *Nat Chem Biol* **2014**, No. 9, 723–731. https://doi.org/10.1038/nchembio.1584.

(5) Price, D. A.; Mathiowetz, A. M.; Liras, S. Designing Orally Bioavailable Peptide and Peptoid Macrocycles. *Practical Medicinal Chemistry with Macrocycles* **2017**, 59–76. https://doi.org/10.1002/9781119092599.ch3.

(6) Bonnet, P.; Agrafiotis, D. K.; Zhu, F.; Martin, E. Conformational Analysis of Macrocycles: Finding What Common Search Methods Miss. *J Chem Inf Model* **2009**, No. 10, 2242–2259. https://doi.org/10.1021/ci900238a.

(7) Li, S.; Pissarnitski, D.; Nowak, T.; Wleklinski, M.; Krska, S. W. Merging Late-Stage Diversification with Solid-Phase Peptide Synthesis Enabled by High-Throughput On-Resin Reaction Screening. *ACS Catal* **2022**, *12* (5), 3201–3210. https://doi.org/10.1021/acscatal.1c05502.

(8) Buyanova, M.; Pei, D. Targeting Intracellular Protein–Protein Interactions with Macrocyclic Peptides. *Trends Pharmacol Sci* **2022**, No. 3, 234–248. https://doi.org/10.1016/j.tips.2021.11.008.

(9) Crees, Z. D.; Rettig, M. P.; Bashey, A.; Devine, S. M.; Jaglowski, S.; Wan, F.; Zhou, A.; Harding, M.; Vainstein-Haras, A.; Sorani, E.; Gliko-Kabir, I.; Grossman, B. J.; Westervelt, P.; DiPersio, J. F.; Uy, G. L. Hematopoietic Stem Cell Mobilization for Allogeneic Stem Cell Transplantation by Motixafortide, a Novel CXCR4 Inhibitor. *Blood Adv* **2023**, *7* (18). https://doi.org/10.1182/bloodadvances.2023010407.

(10) Guerlavais, V.; Sawyer, T. K.; Carvajal, L.; Chang, Y. S.; Graves, B.; Ren, J.-G.; Sutton, D.; Olson, K. A.; Packman, K.; Darlak, K.; Elkin, C.; Feyfant, E.; Kesavan, K.; Gangurde, P.; Vassilev, L. T.; Nash, H. M.; Vukovic, V.; Aivado, M.; Annis, D. A. Discovery of Sulanemadlin (ALRN-6924), the First Cell-Permeating, Stabilized α-Helical Peptide in Clinical Development. *J Med Chem* **2023**, *66* (14). https://doi.org/10.1021/acs.jmedchem.3c00623.

(11) Li, H.; Thaisrivongs, D. A.; Shang, G.; Chen, Y.; Chen, Q.; Tan, L.; Xiao, K.-J.; Larson, R. T.; Kuethe, J. T.; Lee, J.; Deprez, N. R.; Nolting, A. F.; Poirier, M.; Bulger, P. G.; Regalado, E. L.; Biba, M.; Tsay, F.-R.; DaSilva, J.; Prier, C. K.; Strulson, C. A.; Zawatzky, K.; Liu, Z.; Newman, J. A.; Sokolowsky, K.; Tang, W.; Hullen, K.; Thakur, N.; Welch, C.; Patel, S.; He, Y.; Xu, J.; Variankaval, N.; Klapars, A.; Kong, J.; Desmond, R.; Varsolona, R.; Maligres, P. E.; Siepermann, C. A. P.; Robison, L.; Piou, T.; Hartmanshenn, C.; Chandra, A.; Patel, A.; Becker, M. R.; Liu, G.; Duan, J.; Wan, B.; Xiao, C.; Yuan, Y.; Cao, X.; Chen, L.; Yi, R.; Wu, Z.; Feng, M.; Li, D.; Song, Z.; Dong, Y.; Sun, J.; Li, B.; Shao, G.; Campeau, L.-C.; Yin, J. Total Synthesis of Enlicitide Decanoate. *J Am Chem Soc* **2025**, *147* (13). https://doi.org/10.1021/jacs.4c15966.

(12) Tanada, M.; Tamiya, M.; Matsuo, A.; Chiyoda, A.; Takano, K.; Ito, T.; Irie, M.; Kotake, T.; Takeyama, R.; Kawada, H.; Hayashi, R.; Ishikawa, S.; Nomura, K.; Furuichi, N.; Morita, Y.; Kage, M.; Hashimoto, S.; Nii, K.; Sase, H.; Ohara, K.; Ohta, A.; Kuramoto, S.; Nishimura, Y.; Iikura, H.; Shiraishi, T. Development of Orally Bioavailable Peptides Targeting an Intracellular Protein:

From a Hit to a Clinical KRAS Inhibitor. *J Am Chem Soc* **2023**, *145* (30), 16610–16620. https://doi.org/10.1021/jacs.3c03886.

(13) Ohta, A.; Tanada, M.; Shinohara, S.; Morita, Y.; Nakano, K.; Yamagishi, Y.; Takano, R.; Kariyuki, S.; Iida, T.; Matsuo, A.; Ozeki, K.; Emura, T.; Sakurai, Y.; Takano, K.; Higashida, A.; Kojima, M.; Muraoka, T.; Takeyama, R.; Kato, T.; Kimura, K.; Ogawa, K.; Ohara, K.; Tanaka, S.; Kikuchi, Y.; Hisada, N.; Hayashi, R.; Nishimura, Y.; Nomura, K.; Tachibana, T.; Irie, M.; Kawada, H.; Torizawa, T.; Murao, N.; Kotake, T.; Tanaka, M.; Ishikawa, S.; Miyake, T.; Tamiya, M.; Arai, M.; Chiyoda, A.; Akai, S.; Sase, H.; Kuramoto, S.; Ito, T.; Shiraishi, T.; Kojima, T.; Iikura, H. Validation of a New Methodology to Create Oral Drugs beyond the Rule of 5 for Intracellular Tough Targets. *J Am Chem Soc* **2023**, *145* (44), 24035–24051. https://doi.org/10.1021/jacs.3c07145.

(14) Lee, D.; Lee, S.; Choi, J.; Song, Y.-K.; Kim, M. J.; Shin, D.-S.; Bae, M. A.; Kim, Y.-C.; Park, C.-J.; Lee, K.-R.; Choi, J.-H.; Seo, J. Interplay among Conformation, Intramolecular Hydrogen Bonds, and Chameleonicity in the Membrane Permeability and Cyclophilin A Binding of Macrocyclic Peptide Cyclosporin O Derivatives. *J Med Chem* **2021**. https://doi.org/10.1021/acs.jmedchem.1c00211.

(15) Poongavanam, V.; Vo, D. D.; Kihlberg, J. Beware of Extreme Calculated Lipophilicity When Designing Cyclic Peptides. *Nat Chem Biol* **2024**. https://doi.org/10.1038/s41589-024-01715-0.

(16) Matsson, P.; Doak, B. C.; Over, B.; Kihlberg, J. Cell Permeability beyond the Rule of 5. *Adv Drug Deliv Rev* **2016**, 42–61. https://doi.org/10.1016/j.addr.2016.03.013.

(17) Doak, B. C.; Over, B.; Giordanetto, F.; Kihlberg, J. Oral Druggable Space beyond the Rule of 5: Insights from Drugs and Clinical Candidates. *Cell Metab* **2014**, No. 9, 1115–1142. https://doi.org/10.1016/j.chembiol.2014.08.013.

(18) Poongavanam, V.; Wieske, L. H. E.; Peintner, S.; Erdélyi, M.; Kihlberg, J. Molecular Chameleons in Drug Discovery. *Nat Rev Chem* **2023**, No. 1, 45–60. https://doi.org/10.1038/s41570-023-00563-1.

(19) Over, B.; Matsson, P.; Tyrchan, C.; Artursson, P.; Doak, B. C.; Foley, M. A.; Hilgendorf, C.; Johnston, S. E.; Lee, M. D.; Lewis, R. J.; McCarren, P.; Muncipinto, G.; Norinder, U.; Perry, M. W. D.; Duvall, J. R.; Kihlberg, J. Structural and Conformational Determinants of Macrocycle Cell Permeability. *Nat Chem Biol* **2016**, No. 12, 1065–1074. https://doi.org/10.1038/nchembio.2203.

(20) Matthews, H. K.; Bertoli, C.; Bruin, R. A. M. d. Cell Cycle Control in Cancer. *Nat Rev Mol Cell Biol* **2022**, No. 1, 74–88. https://doi.org/10.1038/s41580-021-00404-3.

(21) Hochegger, H.; Takeda, S.; Hunt, T. Cyclin-Dependent Kinases and Cell-Cycle Transitions: Does One Fit All? *Nat Rev Mol Cell Biol* **2008**, No. 11, 910–916. https://doi.org/10.1038/nrm2510.

(22) Kamb, A. Cyclin-Dependent Kinase Inhibitors and Human Cancer. *Cyclin Dependent Kinase (CDK) Inhibitors* **1998**, 139–148. https://doi.org/10.1007/978-3-642-71941-7_7.

(23) Ettl, T.; Schulz, D.; Bauer, R. J. The Renaissance of Cyclin Dependent Kinase Inhibitors. *Cancers* **2022**, No. 2, 293. https://doi.org/10.3390/cancers14020293.

(24) Putta, S.; Villegas, C. A.; Rubin, S. M. Differences in Binding Affinity among Cell-Cycle CDK and Cyclin Pairs. *J Mol Biol* **2025**, No. 5, 168952. https://doi.org/10.1016/j.jmb.2025.168952.

(25) Tatum, N. J.; Endicott, J. A. Chatterboxes: The Structural and Functional Diversity of Cyclins. *Semin Cell Dev Biol* **2020**, 4–20. https://doi.org/10.1016/j.semcdb.2020.04.021.

(26) Andzelm, E. R.; Lew, J.; Taylor, S. Bound to Activate: Conformational Consequences of Cyclin Binding to CDK2. *Structure* **1995**, *3* (11), 1135–1141. https://doi.org/10.1016/S0969-2126(01)00249-0.

(27) Schulman, B. A.; Lindstrom, D. L.; Harlow, E. Substrate Recruitment to Cyclin-Dependent Kinase 2 by a Multipurpose Docking Site on Cyclin A. *Proc Natl Acad Sci U S A* **1998**, No. 18, 10453–10458. https://doi.org/10.1073/pnas.95.18.10453.

(28) Morrison, L.; Loibl, S.; Turner, N. C. The CDK4/6 Inhibitor Revolution — a Game-Changing Era for Breast Cancer Treatment. *Nat Rev Clin Oncol* **2024**, No. 2, 89–105. https://doi.org/10.1038/s41571-023-00840-4.

(29) House, I.; Valore-Caplan, M.; Maris, E.; Falchook, G. S. Cyclin Dependent Kinase 2 (CDK2) Inhibitors in Oncology Clinical Trials: A Review. *J Immunother Precis Oncol* **2025**, *8* (1), 47–54. https://doi.org/10.36401/JIPO-24-22.

(30) Gerosa, R.; Sanctis, R. D.; Jacobs, F.; Benvenuti, C.; Gaudio, M.; Saltalamacchia, G.; Torrisi, R.; Masci, G.; Miggiano, C.; Agustoni, F.; Pedrazzoli, P.; Santoro, A.; Zambelli, A. Cyclin-Dependent Kinase 2 (CDK2) Inhibitors and Others Novel CDK Inhibitors (CDKi) in Breast Cancer: Clinical Trials, Current Impact, and Future Directions. *Crit Rev Oncol Hematol* **2024**, *196*, 104324. https://doi.org/10.1016/j.critrevonc.2024.104324.

(31) Łukasik, P.; Baranowska-Bosiacka, I.; Kulczycka, K.; Gutowska, I. Inhibitors of Cyclin-Dependent Kinases: Types and Their Mechanism of Action. *Int J Mol Sci* **2021**, No. 6, 2806. https://doi.org/10.3390/ijms22062806.

(32) Álvarez-Fernández, M.; Malumbres, M. Mechanisms of Sensitivity and Resistance to CDK4/6 Inhibition. *Cancer Cell* **2020**, No. 4, 514–529. https://doi.org/10.1016/j.ccell.2020.03.010.

(33) Chen, Y.-N. P.; Sharma, S. K.; Ramsey, T. M.; Jiang, L.; Martin, M. S.; Baker, K.; Adams, P. D.; Bair, K. W.; Kaelin, W. G. Selective Killing of Transformed Cells by Cyclin/Cyclin-Dependent Kinase 2 Antagonists. *Proc Natl Acad Sci U S A* **1999**, No. 8, 4325–4329. https://doi.org/10.1073/pnas.96.8.4325.

(34) (a) Andrews, M. J. I.; McInnes, C.; Kontopidis, G.; Innes, L.; Cowan, A.; Plater, A.; Fischer, P. M. Design, synthesis, biological activity and structural analysis of cyclic peptide inhibitors targeting the substrate recruitment site of cyclin-dependent kinase complexes. *Org Biomol Chem* **2004**, 2 (19), 2735–2741. https://10.1039/B409157D (b) Premnath, P. N.; Craig, S. N.; Liu, S.; Anderson, E. L.; Grigoroudis, A. I.; Kontopidis, G.; Perkins, T. L.; Wyatt, M. D.; Pittman, D. L.; McInnes, C. Iterative Conversion of Cyclin Binding Groove Peptides into Druglike CDK Inhibitors with Antitumor Activity. *J Med Chem* **2015**, No. 1, 433–442. https://doi.org/10.1021/jm5015023.

(35) Lane, D.; Fischer, P. Peptidomimetic Design of CDK Inhibitors Targeting the Recruitment Site of the Cyclin Subunit. *Curr Med Chem Anticancer Agents* **2003**, No. 1, 57–69. https://doi.org/10.2174/1568011033353506.

(36) Verwaltungsgesel, N. A. N.-E. Preparation of Peptides as Inhibitors of Binding of E2F-1 to Cyclin A for Cancer Therapy. *WO2002050102 A2* **2002**, 38.

(37) Castanedo, G.; Clark, K.; Wang, S.; Tsui, V.; Wong, M.; Nicholas, J.; Wickramasinghe, D.; Marsters, J. C.; Sutherlin, D. CDK2/cyclinA Inhibitors: Targeting the cyclinA Recruitment Site with Small Molecules Derived from Peptide Leads. *Bioorg Med Chem Lett* **2006**, No. 6, 1716–1720. https://doi.org/10.1016/j.bmcl.2005.12.004.

(38) Singh, S.; Gleason, C. E.; Fang, M.; Laimon, Y. N.; Khivansara, V.; Xie, S.; Durmaz, Y. T.; Sarkar, A.; Ngo, K.; Savla, V.; Li, Y.; Abu-Remaileh, M.; Li, X.; Locquet, M.-A.; Tuladhar, B.; Odeh, R.; Hamkins-Indik, F.; He, D.; Membreno, M. W.; Nosrati, M.; Gushwa, N. N.; Leung, S. S. F.; Fraga-Walton, B.; Hernandez, L.; Baldomero, M. P.; Lent, B. M.; Spellmeyer, D.; Luna, J. F.; Hoang, D.; Gritsenko, Y.; Chand, M.; DeMart, M. K.; Metobo, S.; Bhatt, C.; Shapiro, J. A.; Yang, K.; Dupper, N. J.; Bockus, A. T.; Fang, J.; Bambal, R.; Cremin, P.; Doench, J. G.; Aggen, J. B.; Liu, L.-F.; Levin, B.; Wang, E. W.; Vendrell, I.; Fischer, R.; Kessler, B.; Gokhale, P. C.; Signoretti, S.; Spektor, A.; Kreatsoulas, C.; Evangelista, M.; Singh, R.; Earp, D. J.; Nijhawan, D.; Garcia, P. D.; Oser, M. G. Targeting G1–S Checkpoint–Compromised Cancers with Cyclin A/B RxL Inhibitors. In Press, *Nature* **2025**.

(39) Bockus, A. T.; Leung, S. S. F.; Fraga-Walton, B.; Baldomero, M. P.; Hernandez, L.; Dupper, N. J.; Shapiro, J. A.; Lent, B. M.; Spellmeyer, D. C.; DeMart, M. K.; Luna, J.; Hoang, D.; Chand, M.; Gritsenko, Y.; Ramaseshan, M.; Gleason, C. E.; Hamkins-Indik, F.; Membreno, M. W.; Zheng, J.; Odeh, R.; Nosrati, M.; He, D.; Situ, G.; Bambal, R.; Cremin, P.; Fang, J.; Levin, B.; Wang, E. W.; Evangelista, M.; Earp, D. J.; Kreatsoulas, C.; Singh, R.; Garcia, P. D.; Aggen, J. B. Discovery of Cell-Permeable Macrocyclic Cyclin A/B RxL Inhibitors that Demonstrate Anti-Tumor Activity in E2F-driven Cancers. In Press, *Journal of Medicinal Chemistry* **2025.**

Authors are required to submit a graphic entry for the Table of Contents (TOC) that, in conjunction with the manuscript title, should give the reader a representative idea of one of the following: A key structure, reaction, equation, concept, or theorem, etc., that is discussed in the manuscript. Consult the journal's Instructions for Authors for TOC graphic specifications (3.5 x 1.75 inches).

Insert Table of Contents artwork here

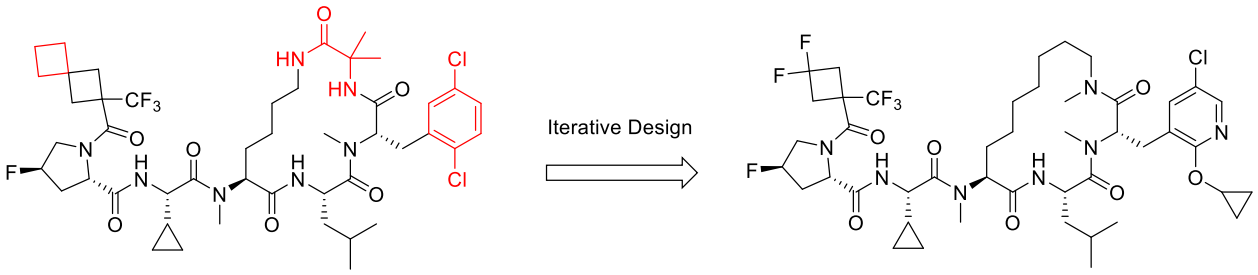

Early POC Compound

Cyclin A FP (IC_{50}): 0.079 μM, **B FP (IC_{50}):** <0.02 μM
MDCK: 3.6 x 10^{-6} cm/s, **H1048 (EC_{50}):** 0.042 μM
%F (mouse 30mpk): 2%, **Tumor Regression 100 mpk IP QD**

Optimized Lead

Cyclin A FP (IC_{50}): 0.050 μM, **B FP (IC_{50}):** <0.02 μM
MDCK: 13.2 x 10^{-6} cm/s, **H1048 (EC_{50}):** 0.016 μM
%F (mouse 30mpk): 27%, **Tumor Regression at 50 mpk PO BID**

Supporting Information

Orally Bioavailable Cyclin A/B RxL Inhibitors: optimization of a novel class of macrocyclic peptides to target E2F high and G1–S-checkpoint compromised cancers

Justin A. Shapiro,‡ Nathan J. Dupper,‡ Breena Fraga-Walton, Andrew T. Bockus, Siegfried S.F. Leung, Kai Yang, Chinmay Bhatt, Megan K. DeMart, Miguel P. Baldomero, Luis Hernandez, Gabriel Fung, Sammy Metobo, Steven Xie, Bryan M. Lent, David C. Spellmeyer, Joshua Luna, Dalena Hoang, Manesh Chand, Yuliana Gritsenko, Cayla M. McEwen, Catherine E. Gleason, Frances Hamkins-Indik, Miles W. Membreno, Jie Zheng, Ranya Odeh, Meisam Nosrati, Daphne He, Ramesh Bambal, Peadar Cremin, Jinshu Fang, Bernard Levin, Evelyn W. Wang, Marie Evangelista, David J. Earp, Constantine Kreatsoulas, Rajinder Singh, Pablo D. Garcia, James B. Aggen*

Circle Pharma, 169 Harbor Way, South San Francisco, CA 94080

Contents

Supplementary Figures

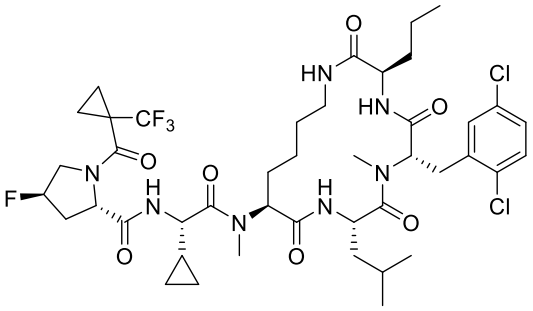

Compound 26 (from ref. 1)
ALogP = 4.5, CycA FP IC_{50} = 0.188 μM
H1048 GI_{50} = 0.096 μM, ***MDCK P_{app} A->B = 2.3 x 10^6 cm/s***

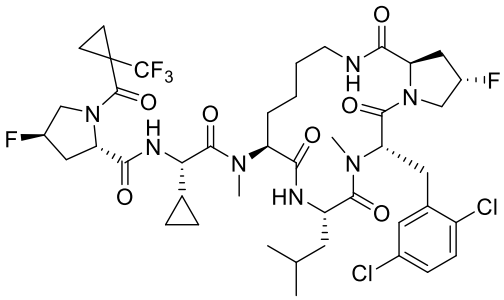

Compound 30 (from ref. 1)
ALogP = 4.1, CycA FP IC_{50} = 0.132 μM
H1048 GI_{50} = 0.176 μM, ***MDCK P_{app} A->B = 0.3 x 10^6 cm/s***

Supplementary Figure 1: Match-pair analysis of bridging residue between lariat *N*-*ε* and Phenylalanine residue. Despite reduction in H-bond donor count going from Compound 26 to Compound 30 (compound numbers taken from ref. 1), the MDCK value of 30 is dramatically reduced, suggesting the importance of macrocycle conformation in membrane permeability.

Solid Phase Peptide Synthesis

SPPS Methods

All peptides were synthesized using a Biotage Syro II automated peptide synthesizer. The reaction was were performed on a 50 μmol scale using 50-100 mg of 2-chlorotritylchloride polystyrene resin.

CTC Resin Loading: Fmoc-AA-OH (4 Equiv.) was dissolved in 1.0 mL of anhydrous NMP. Neat DIEA (8 Equiv.) was added to the Fmoc-AA-OH solution. The solution was dispensed in a peptide reactor vessel containing 100 mg of 2-chlorotrytl chloride (CTC) resin and was agitated for 2 hours at room temperature. The Fmoc-AA-OH solution was drained then the resin was washed with 1.0 mL DMF three times. Unreacted CTC resin was capped with 1.0 mL solution of methanol:DMF (50:50), and DIEA (8 Equiv.) for 10 minutes at room temperature. The methanol solution was drained then the resin was washed with 1.0 mL DMF three times.

Removal of Fmoc protecting group: A mixture of piperidine:DMF (20:80, 1 mL) was added to the resin and agitated for 10 to 15 minutes at room temperature. The piperidine solution was drained then the resin was washed with 1.0 mL DMF three times.

HATU Coupling: A solution of Fmoc-AA-OH (4 Equiv.), HATU (4 Equiv.), and DIEA (8 Equiv.) in 1.0 mL of anhydrous NMP was prepared. The mixture was allowed to react at room temperature for 5 minutes then was added to the resin and was agitated at 35 to 45°C for 10 to 90 minutes. The mixture was drained then the resin was washed with 1.0 mL of DMF three times.

HATU Coupling onto Secondary Amines: When coupling onto secondary amines, The HATU Coupling Method (above) was repeated.

On-Resin Mitsunobu Alkylation: This procedure is a modified version of the procedure outlined by Chatterjee et al.[1] After Fmoc Deprotection, 2,6-lutidine (6 Equiv.) dissolved in 0.5 mL of anhydrous DCE was added to the resin. 2-nitrobenzenesulfonyl chloride (5 Equiv.) dissolved in 0.5 mL anhydrous toluene was added to the resin then was agitated at 40 to 45°C for 10 to 15 minutes. The mixture was drained then the resin was washed with 1.0 mL of anhydrous toluene three times. The method was repeated twice.

Triphenylphosphine (10 Equiv.) dissolved in 0.7 mL anhydrous toluene was added to the resin. The appropriate primary alcohol (20 Equiv. Of methanol, ethanol, propanol, butanol, or other) was added to the resin suspension. Azodicarboxylate (10 Equiv.) was added to the resin and the

suspension was agitated at 35 to 45□C for 15 to 30 minutes. The mixture was drained then the resin was washed with 1.0 mL of anhydrous DMF three times. The method was repeated twice. 2-mercaptoethanol (5 Equiv.) and 1,8-Diazabicyclo[5.4.0]undec-7-ene (5 Equiv.) in 1.0 mL NMP was added to the resin and was agitated at 35 to 45□C for 15 to 30 minutes. The mixture was drained then the resin was washed with 1.0 mL of anhydrous DMF three times. The method was repeated twice.

Resin Cleavage: For peptide sequences with NMeKMe, KMe, and K, a solution of 30% TFA and 5% TIPS in DCM (2 mL) was added to 50-100 mg of resin in a solid phase reaction vessel. For peptide sequences containing **KMtt**, a solution of 90% HFIP, 2% TIPS in DCM (2 mL) was added to 50-100 mg of resin in a solid phase reaction vessel. The contents of the vessel were shaken for one hour. The liquid phase of the reaction was filtered into a 50 mL conical vial. The cleaved resin was washed with an additional DCM (2 mL) and the wash was collected in the conical vial. Toluene (2 mL) was added to the cleaved peptide solution and the solution was concentrated. Linear peptides could be purified at this stage or taken to the cyclization step without additional purification.

Cyclization of Linear Peptides: The deprotected linear product (50 μmol) was dissolved in NMP (500 uL), DIEA (250 uL), and DCM (0.75 mL). T3P (31uL, 3 Equiv.) is added, the solution was shaken for 1-10 minutes at room temperature. Reaction completion was confirmed via LCMS analysis.

Yamaguchi Cyclization of Compound 5: The deprotected linear product (25 μmol) was dissolved in TH F(500 uL). Then, 2,4,6-Trichlorobenzoyl chloride (6.0 mg, 3.8 μL, 1 Eq, 25 μmol), TEA (7.3 mg, 10 μL, 2.9 Eq, 72 μmol) and DMAP (0.3 mg, 0.1 Eq, 2 μmol) were added sequentially. The reaction was stirred overnight at ambient temperature. The reaction mixture was directly purified by RP-HPLC.

Table S1: SPPS Building Blocks Used

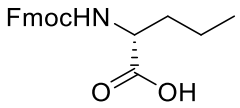	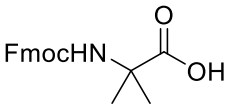	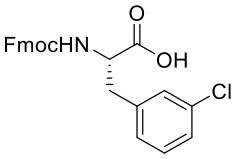	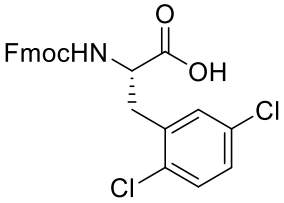
nva	**Aib**	**3ClF**	**25ClF**
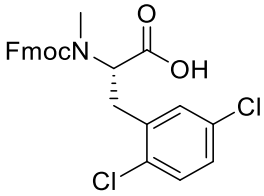	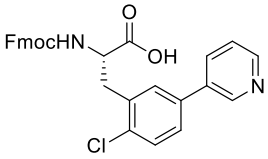	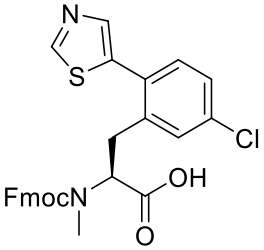	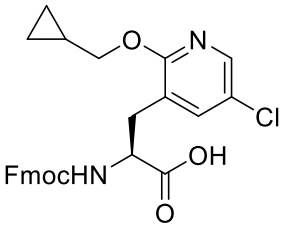
NMe25ClF	**23Pyr5ClF**	**NMe2H55ClF**	**Phe0042**
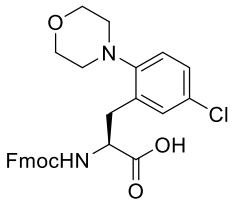	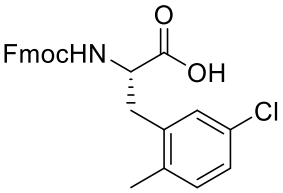	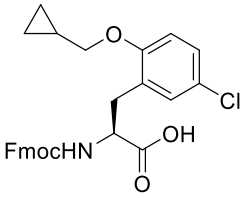	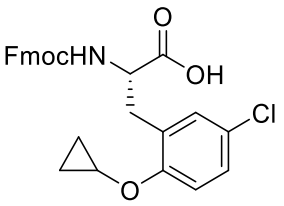
Phe0064	**2Me5ClF**	**5Cl2cPrF**	**Phe0034**
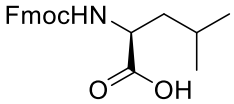	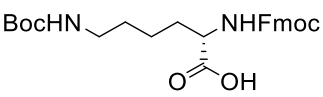	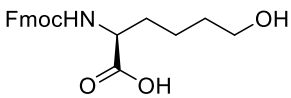	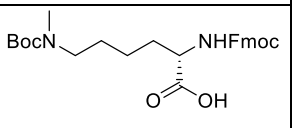
L	**K**	**LyxO**	**KMe**
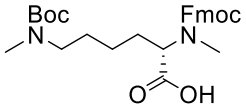	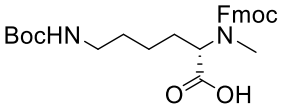	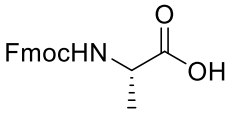	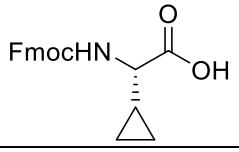
NMeKMe	**NMeK**	**A**	**cPrG**
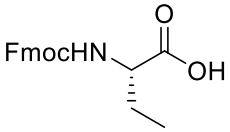	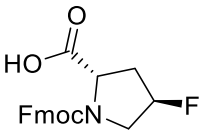	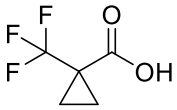	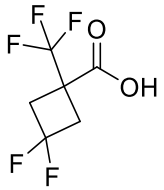
Abu	**AA0011**	**Acd0317**	**Acd0588**
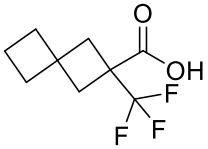			
Acd0540			

Table S2: SPPS Sequences

Comp #	R1	R2	R3	R4	R5	R6	R7
2	Aib	25ClF[A]	L	K[A]	cPrG	AA0011	Acd0540
3	Aib	25ClF[A]	L	K[A]	cPrG	AA0011	Acd0588
4	nva	3ClF[A]	L	K[A]	A	Abu	Acd0317
5	nva	3ClF[A]	L	LyxO[A]	A	Abu	Acd0317
6	nva	3ClF[A]	L	KMe[A]	A	Abu	Acd0317
7	Aib	2Me5ClF[A]	L	K[A]	cPrG	AA0011	Acd0540
8	Aib	Phe0034[A]	L	NMeK	cPrG	AA0011	Acd0540
9	Aib	NMe2H55ClF	L	NMeK	cPrG	AA0011	Acd0540
10	Aib	Phe0064[A]	L	NMeK	cPrG	AA0011	Acd0540
11	Aib	23Pyr5ClF[A]	L	NMeK	cPrG	AA0011	Acd0540
12	Aib	5Cl2cPrF[A]	L	NMeK	cPrG	AA0011	Acd0540
13	Aib	Phe0042[A]	L	NMeK	cPrG	AA0011	Acd0540
14	Aib	NMe25ClF	L	NMeKMe	cPrG	AA0011	Acd0540
15	nva	NMe25ClF	L	K[A]	cPrG	AA0011	Acd0540
16	nva	NMe25ClF	L	KMe[A]	cPrG	AA0011	Acd0540
17	nva	NMe25ClF	L	K[A]	cPrG	AA0011	Acd0588
18	nva	NMe25ClF	L	KMe[A]	cPrG	AA0011	Acd0588

[A] Mitsonobu

Final Compound Purification

Cyclic compounds were purified on a Xbridge (C18 column 10mm x 150mm) using a mass-triggered prep Waters HPLC system in a dual column set up. Components of the Waters HPLC system include: Waters 2767 Sample Manager, Waters 1525 Binary HPLC Pump, Waters 2545 Binary Gradient Module, Waters SFO System Fluidics Organizer, 515 HPLC Pump, Waters QDA and Waters 2998 Photodiode Array Detector. **Solvent A**: Water (+0.1% TFA). **Solvent B**: MeCN (+0.1% TFA). An exemplary method can be found below:

Time (min)	Flowrate (mL/min)	%A	%B
0	15.00	80	20
1.60	15.00	80	20

2.00	20.00	80	20
7.50	20.00	45	55
8.00	20.00	0	100
9.50	20.00	0	100
9.75	20.00	80	20
10.00	20.00	80	20

Analysis of Final Compounds

Method A: Purity of samples were analyzed using as Agilent Infinitylab LC/MSD with 6140 Quadrapole LCMS equipped with a BEH C18 Column (4.6x100mm; 3.5µm) using Solvent A (Water +0.1% TFA) and Solvent B (MeCN + 0.1% TFA). A ramp from 10-100% Solvent B was run over 8 min (flowrate: 1.2 mL/min). Ionization Mode: ESI+.

Method B: Purity of samples were analyzed using a Waters UPLC Aquity I-class with Acquity QDa equipped with a BEH C18 Column (4.6x100mm; 3.5µm) using Solvent A (Water +0.1% formic acid) and Solvent B (MeCN + 0.1% formic acid). A ramp from 10-100% Solvent B was run over 1 min (flowrate: 1.2 mL/min). Ionization Mode: ESI+.

Table S3: Analytical Data of SPPS Compounds

Compound ID	Analytical Method	Rt (min)	% Purity	Yield (mg)	*m/z* observed	Calcd *m/z*
5	A	7.11	91	0.6	843.9	843.4
6	A	6.87	99	13.0	856.6	856.43
7	B	0.812	99	46.95	952.43	952.46
8	B	0.830	99	45.43	994.40	994.48
9	B	0.789	96	42.47	1021.48	1021.43
10	B	0.793	99	9.4	1023.57	1023.5
11	B	0.748	88	2.2	1015.59	1015.48
12	B	0.843	99	1.60	1008.53	1008.49
13	B	0.857	99	4.13	1009.37	1009.49
14	B	0.822	99	29.76	986.97	986.43
15	B	0.861	99	22.64	986.53	986.43
16	B	0.910	99	17.01	1000.51	1000.44

17	B	0.800	99	5.27	982.44	982.38
18	B	0.838	99	46.23	996.39	996.39

SPPS compounds **2-4** were reported previously.[1]

Solution Phase Synthesis

All reactions were performed under open to air unless otherwise noted. Anhydrous solvents were used directly from commercial vendors. All chemicals were purchased from commercial vendors unless otherwise noted. Reactions were monitored using a Waters ACQUITY UPLC system coupled to a Waters SQ Detector 2 mass spectrometer with a Waters Acquity UPLC BEH C18 column (1.7 µm, 2.1 x 50 mm) using water (+0.5% Formic Acid) and MeCN (+0.5% Formic Acid) as mobile phases. NMR spectra were recorded with Bruker 400 Advance and Bruker 500 Advance instruments, Data for ^{1}H NMR spectra are reported as follows: chemical shift (δ ppm), multiplicity, coupling constant (Hz), and integration. The following abbreviations are used for the multiplicities: s = singlet; d = doublet; t = triplet; q = quartet; m = multiplet; br = broad; app = apparent.

Synthesis of Custom Building blocks

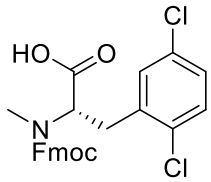

(S)-2-((((9H-fluoren-9-yl)methoxy)carbonyl)(methyl)amino)-3-(2,5-dichlorophenyl)propanoic acid (NMe25ClF) was synthesized as previously reported.[1]

LCMS: MS (ESI) mass calcd. for $C_{25}H_{22}Cl_2NO_4$: 470.08 m/z; found 470.00 $[M+H]^+$.

^{1}H NMR (400 MHz, DMSO) δ 13.12 (br. zzs, 1H), 7.87 (t, *J* = 7.4 Hz, 2H), 7.54 (dt, *J* = 14.3, 7.3 Hz, 2H), 7.49 – 7.24 (m, 7H), 5.76 (s, 1H), 4.89 (app. ddd, *J* = 23.3, 11.0, 4.6 Hz, 1H), 4.33 – 4.06 (m, 3H), 3.39 – 2.97 (m, 2H), 2.87 – 2.75 (m, , 3H). Reported as a mixture of rotamers.

^{13}C NMR (101 MHz, DMSO) δ 171.94, 171.77, 156.19, 155.91, 144.15, 144.07, 143.98, 141.17, 141.14, 141.11, 138.19, 138.09, 132.56, 132.52, 132.04, 132.00, 131.60, 131.51, 131.34, 131.30, 128.93, 128.81, 128.20, 128.15, 127.60, 125.45, 125.38, 125.26, 120.62, 67.48, 58.93, 58.77, 55.40, 47.07, 46.92, 40.60, 40.39, 40.19, 39.98, 39.77, 39.56, 39.35, 32.63, 32.48, 32.27, 26.82. Reported as a mixture of rotamers.

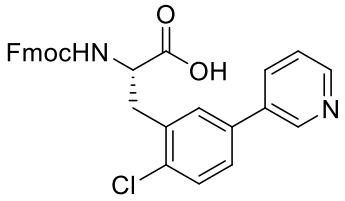

(S)-2-((((9H-fluoren-9-yl)methoxy)carbonyl)amino)-3-(2-chloro-5-(pyridin-3-yl)phenyl)propanoic acid (23Pyr5ClF) was synthesized as previously reported.[2]

LCMS: MS (ESI) mass calcd. for $C_{29}H_{24}ClN_2O_4$: 499.14 m/z; found 499.1 $[M+H]^+$.

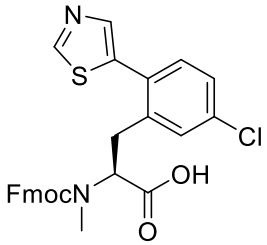

(S)-2-((((9H-fluoren-9-yl)methoxy)carbonyl)(methyl)amino)-3-(5-chloro-2-(thiazol-5-yl)phenyl)propanoic acid (NMe2H55ClF) The starting material, (S)-2-((((9H-fluoren-9-yl)methoxy)carbonyl)amino)-3-(5-chloro-2-(thiazol-5-yl)phenyl)propanoic acid, was synthesized as previously reported.[2]

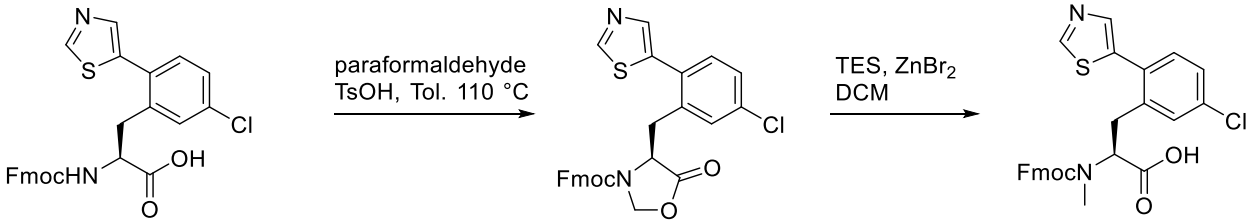

NMe2H55ClF: A mixture of (2S)-3-[5-chloro-2-(1,3-thiazol-5-yl)phenyl]-2-{[(9H-fluoren-9-ylmethoxy)carbonyl] amino}propanoic acid (10.0 g, 19.8 mmol, 1 Eq.), paraformaledyde (2.97g, 99 mmol, 5 Eq.) and 4-methylbenzene-1-sulfonic acid (341 mg, 1.98 mmol, 0.1 Eq.) in Toluene (100 mL) was stirred overnight at 90 ºC. The resulting mixture was filtered, concentrated. The resulting crude product was used in the next reaction without further purification.

LCMS: MS (ESI) mass calcd. for $C_{28}H_{22}ClN_2O_4S$: 517.10 m/z; found 517.00 $[M+H]^+$.

To a stirred mixture of 9H-fluoren-9-ylmethyl (4S)-4-{[5-chloro-2-(1,3-thiazol-5-yl)phenyl]methyl}-5-oxo-1,3-oxazolidine-3-carboxylate (10 g, 19.34 mmol, 1 Eq.) and $ZnBr_2$ (17.42 g, 77.37 mmol, 4 Eq.) in DCM (150 mL) was added TES (9.00 g, 77.37 mmol, 4 Eq.) dropwise at 0 ºC. The resulting mixture was stirred for 7 days at room temperature. The resulting mixture was diluted with EtOAc (100 mL), filtered, and concentrated to afford a crude residue.The residue was purified by RP chromatography (C18, 45 to 80% MeCN+0.1% formic acid in water+0.1% formic acid) This resulted in (2S)-3-[5-chloro-2-(1,3-thiazol-5-yl)phenyl]-2-{[(9H-fluoren-9-ylmethoxy)carbonyl] (methyl)amino}propanoic acid (6.32 g, 12.17 mmol, 62.9%) as a white solid.

LCMS: MS (ESI) mass calcd. for $C_{28}H_{24}ClN_2O_4S$: 519.12 m/z; found 519.01 $[M+H]^+$.

^{1}H NMR: (400 MHz, DMSO-d6): δ 2.61 (s, 3H), 2.99-3.24 (m, 1H), 3.37-3.50 (m, 1H), 4.00-4.30 (m, 3H), 4.61 (dd, J = 11.3, 4.7 Hz, 1H), 7.22-7.62 (m, 9H), 7.82-8.02 (m, 3H), 9.18 (d, J = 8.1 Hz, 1H), 12.97 (s, 1H).

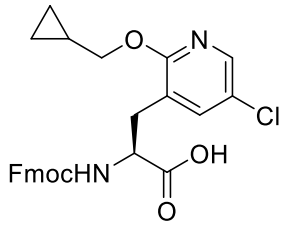

(S)-2-((((9H-fluoren-9-yl)methoxy)carbonyl)amino)-3-(5-chloro-2-(cyclopropylmethoxy)pyridin-3-yl)propanoic acid (Phe0042) was synthesized as previously reported.[2]

LCMS: MS (ESI) mass calcd. for $C_{27}H_{26}ClN_2O_5$: 493.16 m/z; found 493.0 $[M+H]^+$.

(S)-2-((((9H-fluoren-9-yl)methoxy)carbonyl)amino)-3-(5-chloro-2-morpholinophenyl)propanoic acid (Phe0064)

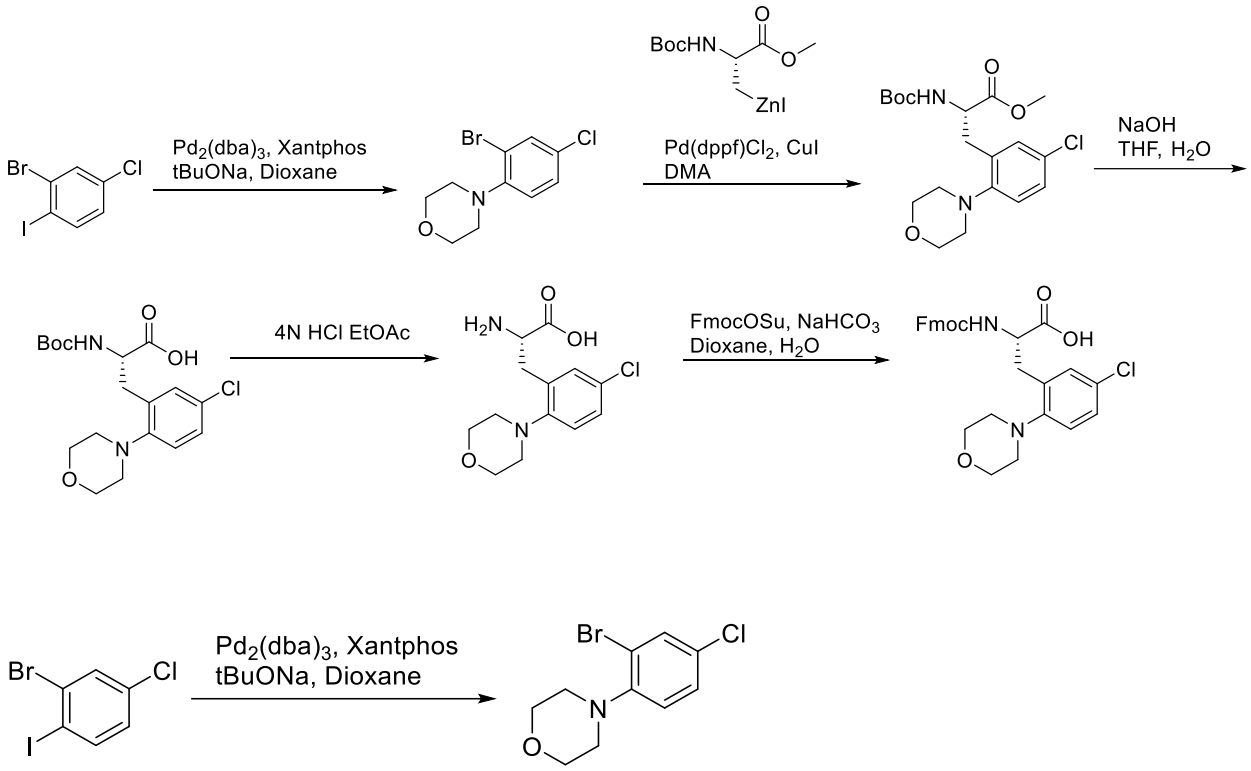

4-(2-bromo-4-chlorophenyl)morpholine: Into a 500ml round-bottom flask, 2-bromo-4-chloro-1-iodobenzene (25 g, 78.8 mmol, 1 Eq.), morpholine (6.86 g, 78.8 mmol, 1 Eq.), Xantphos (18.23 g, 31.5 mmol, 0.4 Eq.), $Pd_2(dba)_3$ (14.5 g, 15.8 mmol, 0.2 Eq.) and *t*-BuONa (22.71 g, 236.3 mmol, 3 Eq.) were dissolved / suspended in 1,4-dioxane (100 mL) at room temperature under a nitrogen atmosphere. The resulting mixture was stirred for 2 hr at 80 ºC. The reaction was quenched with ice water (500 ml) and extracted with EtOAc (3 x 200 mL). The combined organic layers were washed with brine (300 mL), dried with anhydrous Na_2SO_4, filtered and concentrated in vacuum to give the crude product. The residue was purified by silica gel column chromatography (Pet. 0-10% EtOAc in pet ether) to afford 4-(2-bromo-4-chlorophenyl)morpholine (14 g, 50.6 mmol, 64.26%) as a yellow solid.

LCMS: MS (ESI) mass calcd. for $C_{10}H_{12}BrClNO$: 275.98 m/z; found 275.90 $[M+H]^+$.

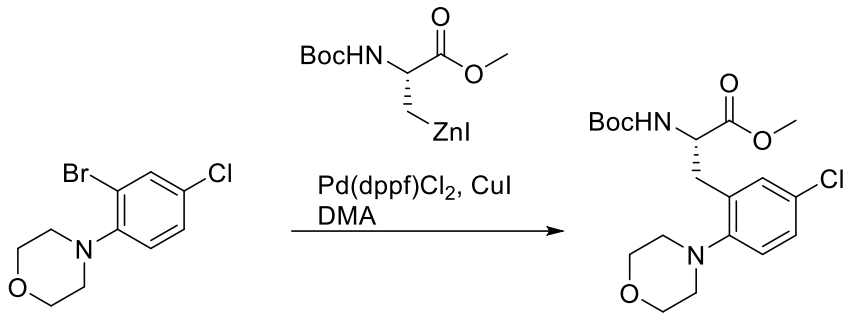

Methyl (S)-2-((tert-butoxycarbonyl)amino)-3-(5-chloro-2-morpholinophenyl)propanoate: To a suspension of Zn (5.63 g, 86.5 mmol, 1.7 Eq.) in DMA (40 mL) was added ethylene dibromide (1.3 g, 7.1 mmol, 0.14 Eq.) in one portion under a nitrogen atmosphere. Then TMSCl (0.6 g, 5.1 mmol, 0.1 Eq.) was added slowly. The zinc was allowed to activate for 30 min at room temperature. A solution of methyl (2R)-2-[(tert-butoxycarbonyl)amino]-3-iodopropanoate (25.1 g, 76.4 mmol, 1.5 Eq.) in DMA (40 mL) was added dropwise (over 30 min) to maintain temperature below 50 ºC. The resulting mixture was stirred at room temperature for 2 hr. the zincate solution was next added via a cannula to a solution of 4-(2-bromo-4-chlorophenyl)morpholine (14 g, 50.9 mmol, 1 Eq.), Pd(dppf)Cl_2.CH_2Cl_2 (8.3 g, 10.1 mmol, 0.2 Eq.) and CuI (1.9 g, 10.1 mmol, 0.2 Eq.) in DMA (80 mL),The mixture was stirred at room temperature for 5 min, then the mixture was heated and stirred at 80 ºC for 2 hr under nitrogen. The mixture was quenched with ice-water (500 mL) and extracted with EtOAc (3 x 200 mL). The organic layers were combined and washed with brine (300 mL), dried with anhydrous Na_2SO_4, filtered and concentrated in vacuum to give the crude product. The product was purified by silica gel chromatography (0-30% EtOAc in pet. ether) to give methyl (2S)-2-[(tert-butoxycarbonyl)amino]-3-[5-chloro-2-(morpholin-4-yl)phenyl]propanoate (3.2 g, 8.0 mmol, 15.85%) as a yellow oil.

LCMS: MS (ESI) mass calcd. for $C_{19}H_{28}ClN_2O_5$: 399.17 m/z; found 399.05 $[M+H]^+$.

^{1}H NMR: (400 MHz, DMSO-d6): δ 1.30 (s, 9H), 2.74 (ddd, J = 13.6, 9.7, 5.8 Hz, 3H), 2.87 (ddd, J = 11.8, 5.6, 3.2 Hz, 2H), 3.21 (dd, J = 13.7, 4.3 Hz, 1H), 3.64 (s, 3H), 3.73 (tt, J = 11.0, 5.6 Hz, 4H), 4.46 (ddd, J = 10.2, 8.3, 4.2 Hz, 1H), 7.20 (d, J = 8.4 Hz, 1H), 7.24 – 7.33 (m, 3H).

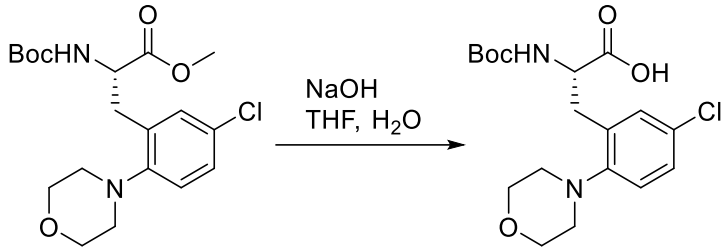

(S)-2-((tert-butoxycarbonyl)amino)-3-(5-chloro-2-morpholinophenyl)propanoic acid: Into a 100 mL round bottom was placed methyl (2S)-2-[(tert-butoxycarbonyl)amino]-3-[5-chloro-2-(morpholin-4-yl)phenyl]propanoate (3.2 g, 8.0 mmol, 1 equiv) in THF (40 mL). NaOH (1.6 g, 40.1 mmol, 5 equiv) in H_2O (8 mL) was added at 0 ºC. The resulting mixture was stirred for 2 hr at room temperature. The mixture was acidified to ~4 pH with 2N HCl (aq.). The acidified mixture was extracted with EtOAc (3 x 200 mL). The organic layers were combined, washed with brine and dried over with anhydrous Na_2SO_4, filtered, and the filtrate was concentrated under reduced pressure. The residue was purified by silica gel column chromatography (0-50% EtOAc in pet. ether) to afford (2S)-2-[(tert-butoxycarbonyl)amino]-3-[5-chloro-2-(morpholin-4-yl)phenyl]propanoic acid (3 g, 7.8 mmol, 97.17%) as a yellow oil.

LCMS: MS (ESI) mass calcd. for $C_{18}H_{26}ClN_2O_5$: 385.16 m/z; found 385.05 $[M+H]^+$.

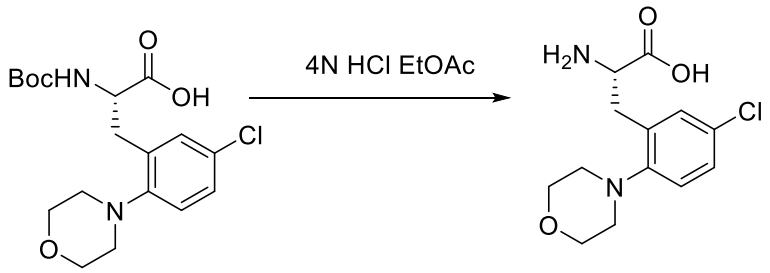

(S)-2-amino-3-(5-chloro-2-morpholinophenyl)propanoic acid: Into a 100 ml round bottom was placed (2S)-2-[(tert-butoxycarbonyl)amino]-3-[5-chloro-2-(morpholin-4-yl)phenyl]propanoic acid (3 g, 7.8 mmol, 1 equiv) in EtOAc (20 mL), 4N HCl in EtOAc (20 mL) was added at room temperature under an atmosphere of nitrogen. The resulting mixture was stirred for 2hr at room temperature. The solvent was removed under reduced pressure and crude product was used in the next step directly.

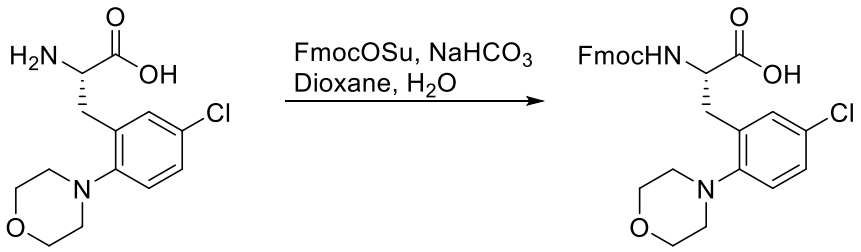

Phe0064: The above crude product was dissolved in 1,4-dioxane (30 mL) and H_2O (10 mL), $NaHCO_3$ (3.69 g, 43.90 mmol, 5.6 equiv) and FmocOSu (3.58 g, 7.02 mmol, 0.9 equiv) were added at room temperature. The resulting mixture was stirred at room temperature for 16hr. The mixture was acidified to pH ~2 with 2N HCl (aq) and extracted with EtOAc (3 x 100 mL). The organic layers were combined and dried over anhydrous Na_2SO_4. After filtration, the filtrate was concentrated under reduced pressure. The residue was purified by RP chromatography(C18, 10 to 50% MeCN+0.1% TFA in water+0.1% TFA). This resulted in (2S)-3-[5-chloro-2-(morpholin-4-yl)phenyl]-2-{[(9H-fluoren-9-ylmethoxy)carbonyl]amino}propanoic acid (1.63 g, 3.2 mmol, 41.0%) as a white solid after lyophilization.

LCMS: MS (ESI) mass calcd. for $C_{28}H_{28}ClN_2O_5$: 507.17 m/z; found 507.10. $[M+H]^+$.

^{1}H NMR: (400 MHz, DMSO-d6): δ 2.77 (dtd, J = 34.4, 11.6, 10.8, 4.1 Hz, 5H), 3.26 (dd, J = 13.7, 4.2 Hz, 1H), 3.69 (p, J = 6.1, 4.7 Hz, 4H), 4.04 – 4.32 (m, 3H), 4.46 (td, J = 9.8, 4.1 Hz, 1H), 7.18 (d, J = 8.5 Hz, 1H), 7.23 – 7.36 (m, 4H), 7.41 (t, J = 7.5 Hz, 2H), 7.64 (dd, J = 22.9, 8.0 Hz, 3H), 7.88 (d, J = 7.5 Hz, 2H), 12.72 (s, 1H).

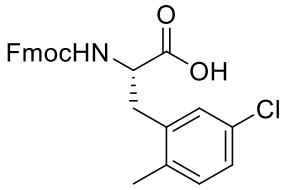

(S)-2-((((9H-fluoren-9-yl)methoxy)carbonyl)amino)-3-(5-chloro-2-methylphenyl)propanoic acid (2Me5ClF) was synthesized as previously reported.[2]

LCMS: MS (ESI) mass calcd. for $C_{25}H_{23}ClNO_4$: 436.13 m/z; found 436.13 $[M+H]^+$.

(S)-2-((((9H-fluoren-9-yl)methoxy)carbonyl)amino)-3-(5-chloro-2 (cyclopropylmethoxy)phenyl)propanoic acid (5Cl2cPrF):

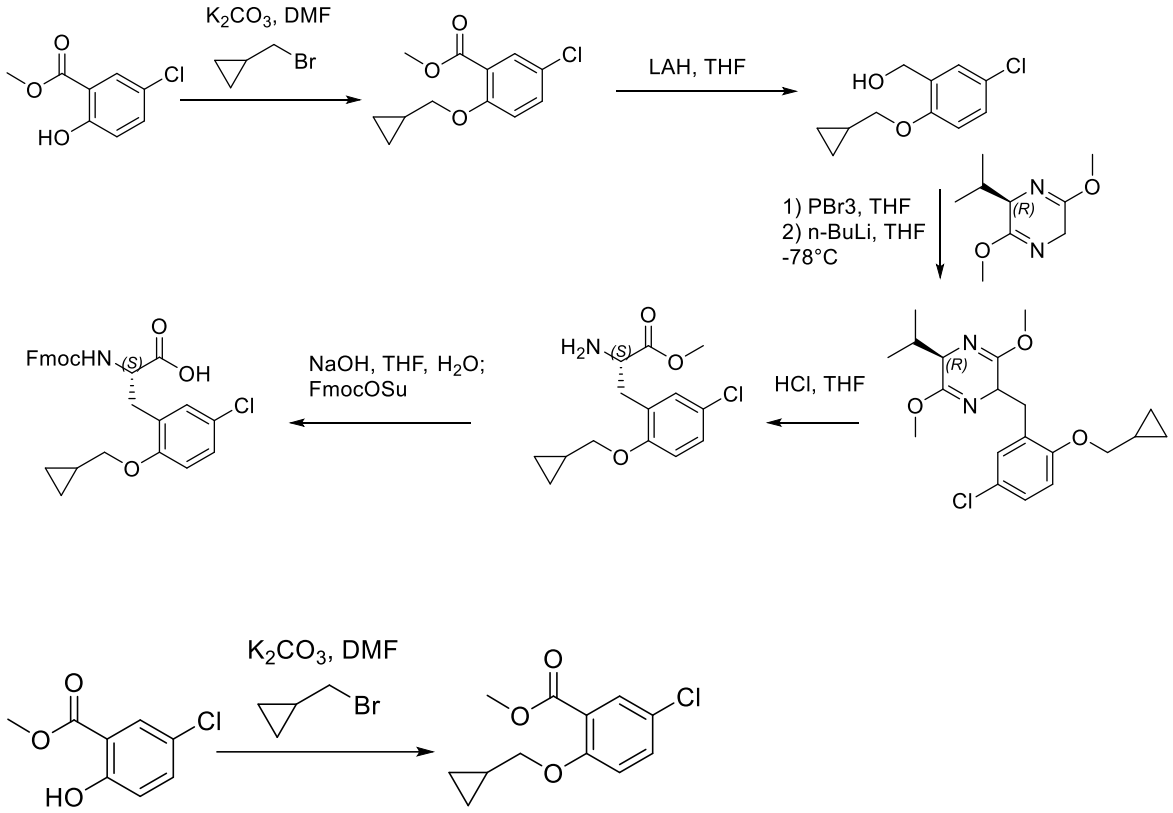

methyl 5-chloro-2-(cyclopropylmethoxy)benzoate: A solution of methyl 5-chloro-2-hydroxybenzoate (10 g, 53.59 mmol, 1 equiv), (bromomethyl)cyclopropane (7.24 g, 53.59 mmol, 1equiv) and K_2CO_3 (8.89 g, 64.31 mmol, 1.2 equiv) in DMF (150 mL) was stirred for 16hr at 40°C. The resulting mixture was diluted with water (300 mL) and extracted with EtOAc (3 x 100 mL). The organic layers were combined and dried over anhydrous Na_2SO_4. After filtration, the filtrate was concentrated under reduced pressure. The residue was purified by RP chromatography (C18, 0-100% MeCN+0.1% TFA in water+0.1%TFA). Methyl 5-chloro-2-(cyclopropylmethoxy) benzoate (9.8 g, 40.7 mmol, 75.9%) as a white solid after lyophilization.

LCMS: MS (ESI) mass calcd. for $C_{12}H_{14}ClO_3$: 241.07 m/z; found 241.06 $[M+H]^+$.

^{1}H NMR: (300 MHz, DMSO-d_6): δ 0.29 – 0.45 (m, 2H), 0.47 – 0.61 (m, 2H), 1.11 – 1.30 (m, 1H), 3.81 (s, 2H), 3.92 (d, J = 6.5 Hz, 2H), 7.16 (dd, J = 9.0, 1.3 Hz, 1H), 7.55 (dt, J = 8.9, 2.0 Hz, 1H), 7.63 (d, J = 2.7 Hz, 1H).

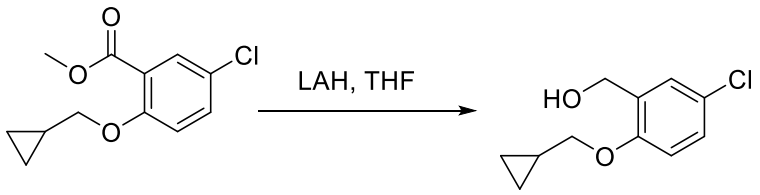

(5-chloro-2-(cyclopropylmethoxy)phenyl)methanol: A solution of methyl 5-chloro-2-(cyclopropylmethoxy) benzoate (9.8 g, 40.7 mmol, 1 equiv) and $LiAlH_4$ (3.09g, 81.4 mmol, 2 equiv) in THF (200 mL) was stirred for 3hr at 0°C under nitrogen atmosphere. The reaction was carefully quenched by the slow addition of water at 0°C. The resulting mixture was extracted with EtOAc (3 x 100 mL). The combined organic layers were washed with brine (50 mL), dried over anhydrous Na_2SO_4. After filtration, the filtration was concentrated under reduced pressure to afford [5-chloro-2-(cyclopropylmethoxy) phenyl] methanol (8.6g 40.7 mmol, quant.) as a light yellow oil. The resulting compound was used without further purification.

LCMS: MS (ESI) mass calcd. for $C_{11}H_{14}ClO_2$: 213.07 m/z; found 213.06 $[M+H]^+$.

^{1}H NMR: (400 MHz, DMSO-*d*$_6$): δ 0.24 – 0.37 (m, 2H), 0.47 – 0.62 (m, 2H), 1.13 – 1.26 (m, 1H), 3.83 (d, J = 6.8 Hz, 2H), 4.51 (s, 2H), 5.18 (s, 1H), 6.92 (d, J = 8.7 Hz, 1H), 7.20 (dd, J = 8.7, 2.8 Hz, 1H), 7.31 – 7.41 (m, 1H).

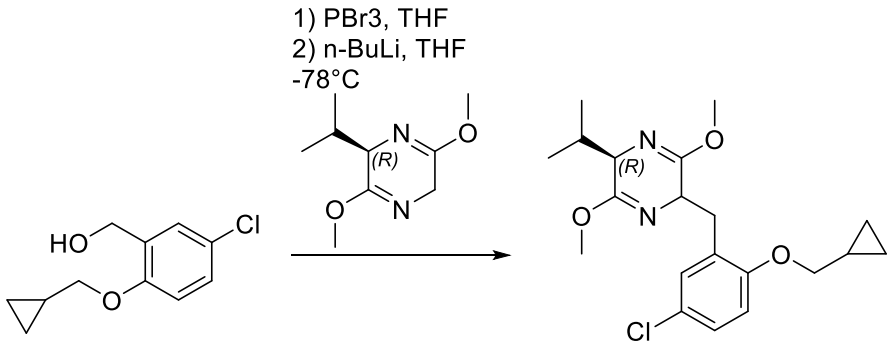

(5R)-2-(5-chloro-2-(cyclopropylmethoxy)benzyl)-5-isopropyl-3,6-dimethoxy-2,5-dihydropyrazine: A solution of [5-chloro-2-(cyclopropylmethoxy) phenyl] methanol (5 g, 23.51 mmol, 1 equiv) and PBr3 (8.27 g, 30.5 mmol, 1.3 equiv) in THF (100 mL) was stirred for 15 min at 0°C under an atmosphere of nitrogen. The reaction was quenched with water (25 mL) at 0°C. The resulting mixture was extracted with EtOAc (3 x 100mL). The combined organic layers were

dried over anhydrous Na_2SO_4. After filtration, the filtrate was concentrated under reduced pressure. 2-(bromomethyl)-4-chloro-1-(cyclopropylmethoxy) benzene (6.4g, 23.51 mmol, quant.)

A solution of (3R)-3-isopropyl-2,5-dimethoxy-3,6-dihydropyrazine (3.68 g, 19.96 mmol, 1.1equiv) and nBuLi (13.61 mL, 27.2 mmol, 1.5equiv) in THF (100 mL) was stirred for 1hr at -78°C under an atmosphere of nitrogen. 2-(bromomethyl)-4-chloro-1-(cyclopropylmethoxy) benzene (5 g, 18.14 mmol, 1equiv) in THF was added to the solution and stirred for 30 min. The reaction was quenched with water (50mL) at 0°C.The resulting mixture was extracted with EtOAc (3 x 50mL). The combined organic layers were dried over anhydrous Na_2SO_4. After filtration, the filtrate was concentrated under reduced pressure to afford (5R)-2-{[5-chloro-2-(cyclopropylmethoxy) phenyl]methyl }-5-isopropyl-3,6-dimethoxy-2,5-dihydropyrazine (6 g, 15.8 mmol, 87.27%) as a light-yellow oil. The product was used without further purification.

LCMS: MS (ESI) mass calcd. for $C_{20}H_{28}ClN_2O_3$: 379.18 m/z; found 379.15 $[M+H]^+$.

^{1}H NMR: (300 MHz, DMSO-d6): δ 0.25 – 0.39 (m, 2H), 0.56 (s, 2H), 0.49 – 0.71 (m, 9H), 0.98 (dd, J = 6.9, 2.4 Hz, 7H), 1.13 – 1.29 (m, 1H), 2.17 (dtq, J = 10.3, 6.9, 3.4 Hz, 2H), 2.71 (dd, J = 13.1, 8.1 Hz, 1H), 3.03 – 3.21 (m, 1H), 3.45 – 3.70 (m, 11H), 3.79 (dd, J = 9.4, 5.8 Hz, 1H), 3.79 – 3.94 (m, 1H), 3.89 – 4.00 (m, 4H), 4.27 (ddd, J = 8.2, 4.8, 3.5 Hz, 1H), 6.90 (d, J = 8.8 Hz, 1H), 7.05 – 7.22 (m, 2H).

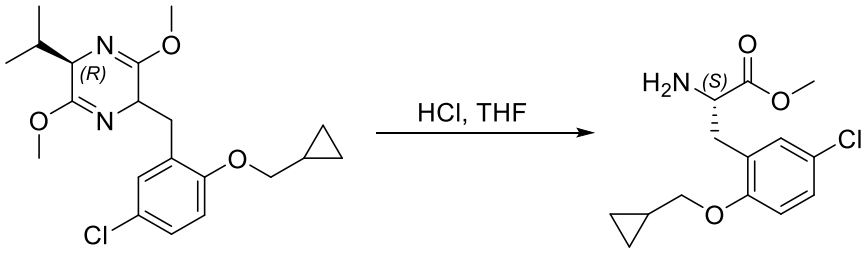

Methyl (S)-2-amino-3-(5-chloro-2-(cyclopropylmethoxy)phenyl)propanoate: A solution of (5R)-2-{[5-chloro-2-(cyclopropylmethoxy) phenyl] methyl}-5-isopropyl-3,6-dimethoxy-2,5-dihydropyrazine (6 g, 15.8 mmol, 1 equiv) was dissolved in 4N HCl in dioxane (50 mL). The reaction was stirred for 1 hr at room temperature.. The mixture was neutralized to pH 7 with 1 N NaOH. The resulting mixture was extracted with EtOAc (3 x 200mL). The combined organic layers were washed with brine (100 mL), dried over anhydrous Na_2SO_4. After filtration, the filtrate was concentrated under reduced pressure. The residue was purified by RP chromatography (C18,

0-100% MeCN+0.1% TFA in water+0.1%TFA). Pure fractions were evaporated to dryness to afford methyl (2S)-2-amino-3-[5-chloro-2-(cyclopropylmethoxy)phenyl] propanoate as the TFA salt (4.2 g, 11.9 mmol, 75.5%) as a white solid.

LCMS: MS (ESI) mass calcd. for $C_{14}H_{19}ClNO_3$: 284.11 m/z; found 284.20 $[M+H]^+$.

^{1}H NMR: (300 MHz, DMSO-d_6): δ 0.28 – 0.40 (m, 2H), 0.56 (ddt, J = 7.3, 3.9, 1.4 Hz, 2H), 1.15 – 1.29 (m, 1H), 2.51 (q, J = 1.9 Hz, 2H), 3.00 (dd, J = 13.8, 7.1 Hz, 1H), 3.17 (dd, J = 13.8, 7.5 Hz, 1H), 3.66 (s, 1H), 3.86 (dt, J = 6.9, 1.6 Hz, 2H), 4.23 (t, J = 7.2 Hz, 1H), 7.00 (dd, J = 8.8, 1.3 Hz, 1H), 7.23 (dd, J = 2.7, 1.3 Hz, 1H), 7.29 (ddd, J = 8.7, 2.8, 1.3 Hz, 1H), 8.50 (s, 3H).

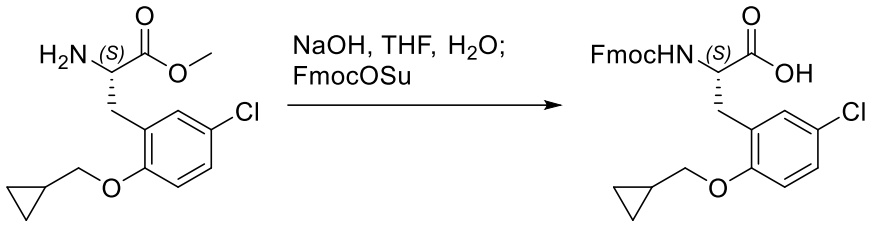

5Cl2cPrF: To a solution of methyl (2S)-2-amino-3-[5-chloro-2-(cyclopropylmethoxy) phenyl] propanoate (4.2 g, 11.9 mmol, 1.0 equiv) in THF (60 mL) a solution of NaOH (1.57g, 39.27 mmol, 3.3 equiv) in water (30mL) was added. The reaction was stirred for 2 hr. After the saponification was complete, 2N HCl was added to adjust the pH to ~8. FmocOSu (4.4 g, 13.09 mmol, 1.1 equiv). After the protection was compete the mixture was acidifed to pH ~3 and extracted with EtOAc (3 x 200mL). The combined organic layers were washed with brine (100 mL), dried over anhydrous Na_2SO_4. After filtration, the filtrate was concentrated under reduced pressure. The residue was purified by RP chromatography (C18, 0-100% MeCN+0.1% TFA in water+0.1%TFA). Pure fractions were evaporated to afford (2S)-3-[5-chloro-2-(cyclopropylmethoxy) phenyl]-2-{[(9H-fluoren-9-ylmethoxy) carbonyl] amino} propanoic acid (4.09 g, 8.3 mmol 69.8%) as a white solid.

LCMS: MS (ESI) mass calcd. for $C_{28}H_{27}ClNO_5$: 492.16 m/z; found 492.10 $[M+H]^+$.

^{1}H NMR: (300 MHz, DMSO-d_6): δ 0.35 (q, J = 5.3, 4.9 Hz, 2H), 0.54 (h, J = 3.9 Hz, 2H), 1.24 (s, 1H), 2.63 – 2.80 (m, 1H), 3.20 (dd, J = 13.6, 4.7 Hz, 1H), 3.77 – 3.95 (m, 2H), 4.18 (s, 3H), 4.33 (s, 1H), 6.95 (d, J = 8.7 Hz, 1H), 7.17 – 7.50 (m, 7H), 7.63 (t, J = 7.1 Hz, 3H), 7.88 (d, J = 7.6 Hz, 2H), 12.65 (s, 1H).

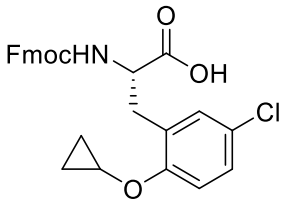

(S)-2-((((9H-fluoren-9-yl)methoxy)carbonyl)amino)-3-(5-chloro-2-cyclopropoxyphenyl)propanoic acid (Phe0034) was synthesized as previously reported.[2]

LCMS: MS (ESI) mass calcd. for $C_{27}H_{24}ClNO_5Na$: 500.12 m/z; found 500.10 $[M+Na]^+$.

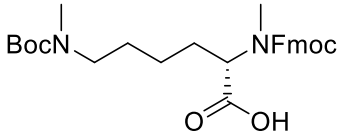

N2-(((9H-fluoren-9-yl)methoxy)carbonyl)-N6-(tert-butoxycarbonyl)-N2,N6-dimethyl-L-lysine (NMeKMe) was synthesized as previously reported.[1]

LCMS: MS (ESI) mass calcd. for $C_{28}H_{36}N_2NaO_6$: 519.25 *m/z*; found: 519.0 $[M+Na]^+$.

^{1}H NMR (400 MHz, DMSO) δ 7.89 (t, *J* = 7.3 Hz, 2H), 7.64 (ddd, *J* = 11.8, 7.4, 3.7 Hz, 2H), 7.44 – 7.27 (m, 4H), 4.40 – 4.22 (m, 3H), 3.14 (t, *J* = 7.2 Hz, 2H), 2.73 (si, 6H), 1.96 – 0.91 (m, 16H).

^{13}C NMR (101 MHz, DMSO) δ 173.09, 156.56, 156.12, 155.26, 144.27, 141.25, 128.13, 127.58, 125.45, 120.59, 78.69, 67.27, 58.36, 47.17, 33.93, 30.59, 28.49, 27.98, 27.13, 26.77, 23.25.

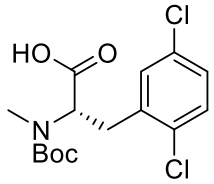

(S)-2-((tert-butoxycarbonyl)(methyl)amino)-3-(2,5-dichlorophenyl)propanoic acid (SI-1) was synthesized as previously reported.[3]

LCMS: MS (ESI) mass calcd. For $C_{15}H_{19}Cl_2NO_4Na$: 370.06 m/z; Found 370.0 $[M+H]^+$

^{1}H NMR: δ ppm 7.34 - 7.41 (m, 1 H) 7.20 - 7.32 (m, 2 H) 4.82 (dd, J=4.00, 4.00 Hz, 1 H) 3.39 - 3.48 (m, 1 H) 3.11 - 3.23 (m, 1 H) 2.69 - 2.81 (m, 3 H) 1.28 - 1.39 (m, 9 H)

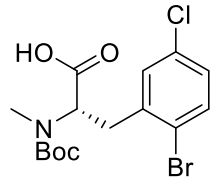

(S)-3-(2-bromo-5-chlorophenyl)-2-((tert-butoxycarbonyl)(methyl)amino)propanoic acid (SI-2) was synthesized as previously reported.[3]

LCMS: MS (ESI) mass calcd. For $C_{15}H_{20}BrClNO_4$: 392.03 m/z; Found 292.9 $[M\text{-}Boc]^+$

^{1}H NMR: (400 MHz, DMSO-*d_6*): 1.23 (d, 9H), 2.66 (s, 3H), 3.05 – 3.32 (m, 2H), 4.62 – 4.93 (m, 1H), 7.16 – 7.74 (m, 3H), 13.06 (s, 1H).

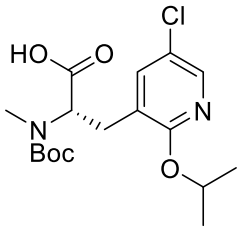

(S)-2-((tert-butoxycarbonyl)(methyl)amino)-3-(5-chloro-2-isopropoxypyridin-3-yl)propanoic acid (SI-3) was synthesized as previously reported.[3]

LCMS: MS (ESI) mass calcd. For $C_{17}H_{26}ClN_2O_5$: 373.15 m/z; Found 373.40 [M+H]+

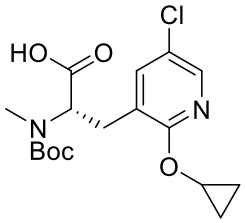

(S)-2-((tert-butoxycarbonyl)(methyl)amino)-3-(5-chloro-2-cyclopropoxypyridin-3-yl)propanoic acid (SI-4) was synthesized as previously reported.[3]

LCMS: MS (ESI) mass calcd. for $C_{17}H_{24}ClN_2O_5$: 371.13 m/z; Found 371.00. $[M+H]^+$

^{1}H NMR: (400 MHz, DMSO-*DF_6*) δ 0.79 – 0.61 (m, 4H), 1.21 (s, 9H), 2.95 – 2.84 (m, 2H), 3.00 (s, 3H), 3.09 – 3.01 (m, 1H), 4.86 (dd, J = 11.3, 4.6 Hz, 1H), 7.67 (d, J = 2.6 Hz, 1H), 8.11 (dd, J = 18.4, 2.6 Hz, 1H).

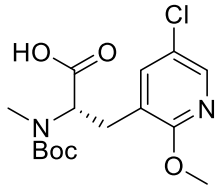

(S)-2-((tert-butoxycarbonyl)(methyl)amino)-3-(5-chloro-2-methoxypyridin-3-yl)propanoic acid (SI-5) was synthesized as previously reported.[3]

LCMS: MS (ESI) mass calcd. For $C_{15}H_{22}ClN_2O_5$: 345.12 m/z; Found 345.29 [M+H]+

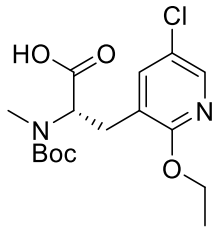

(S)-2-((tert-butoxycarbonyl)(methyl)amino)-3-(5-chloro-2-ethoxypyridin-3-yl)propanoic acid (SI-6) was synthesized as previously reported.[3]

LCMS: MS (ESI) mass calcd. For $C_{16}H_{23}ClN_2O_5$: 359.14 m/z; Found 359.31 [M+H]+

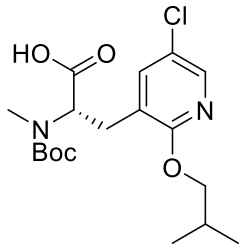

(S)-2-((tert-butoxycarbonyl)(methyl)amino)-3-(5-chloro-2-isobutoxypyridin-3-yl)propanoic acid (SI-7) was synthesized as previously reported.[3]

LCMS: MS (ESI) mass calcd. For $C_{18}H_{28}ClN_2O_5$: 387.17 m/z; Found 387.34 [M+H]+

(2S,4R)-1-(3,3-difluoro-1-(trifluoromethyl)cyclobutane-1-carbonyl)-4-fluoropyrrolidine-2-carboxylic acid (SI-8):

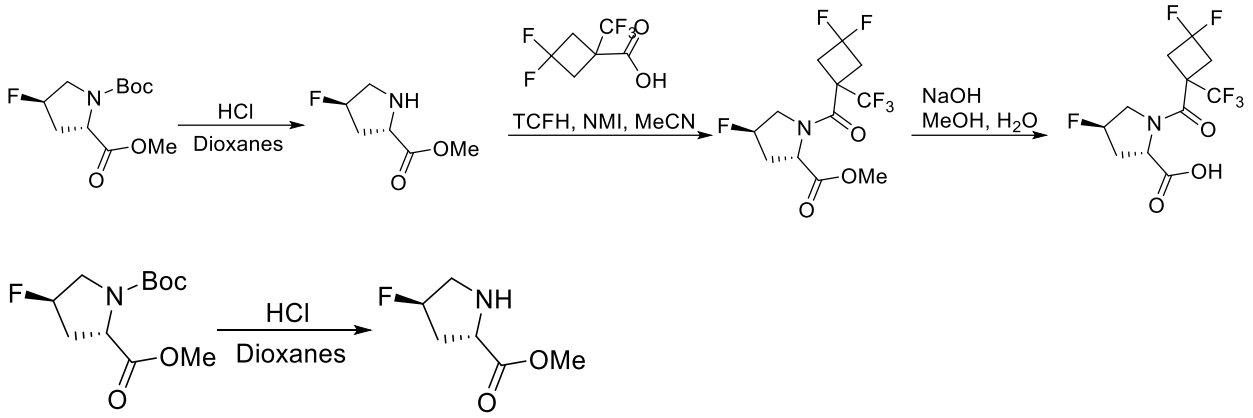

methyl (2S,4R)-4-fluoropyrrolidine-2-carboxylate: A solution of 1-tert-butyl 2-methyl (2S,4R)-4-fluoropyrrolidine-1,2-dicarboxylate (150 g, 606 mmol, 1 equiv) and 4N HCl 1,4-dioxane (758. mL) was stirred for 30 min at room temperature and then concentrated under vacuum to afford the desired product as the HCl salt (110 g, 599 mmol, 98%). The crude product was used in the next step directly without further purification.

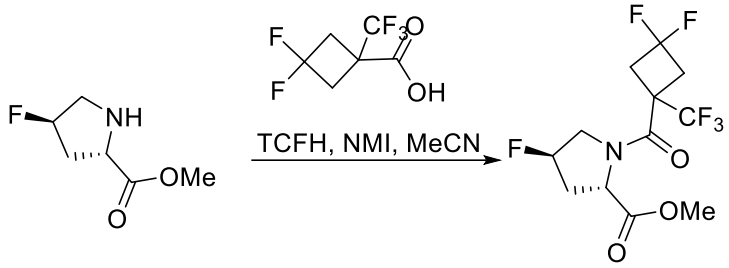

methyl (2S,4R)-1-(3,3-difluoro-1-(trifluoromethyl)cyclobutane-1-carbonyl)-4-fluoropyrrolidine-2-carboxylate: To a stirred solution of methyl (2S,4R)-4-fluoropyrrolidine-2-carboxylate (110 g, 599 mmol, 1 equiv), 3,3-difluoro-1-(trifluoromethyl)cyclobutane-1-carboxylic acid (122.06 g, 598 mmol, 1 equiv) and TCFH (251.69 g, 897 mmol, 1.5 equiv) in MeCN(1100 mL) was added NMI (245.51 g, 2.99 mol, 5 equiv) dropwise over 45 min at 0°C. The mixture was slowly warmed up to room temperature and stirred overnight at room temperature. The mixture was concentrated under vacuum at 28°C and diluted with EtOAc (1L) . The organic layer was and washed with 1N HCl (500 mL). The aqueous layer was extracted again with EtOAc (500mL) and the combined organic layers were washed with saturated $NaHCO_3$ (500mL) and brine (500mL), dried over anhydrous Na_2SO_4 and filtered. After filtration, the filtrate was concentrated under vacuum to afford the desired product (180 g, 540 mmol, 90%) as a light yellow solid. The crude product was used in the next step directly without further purification.

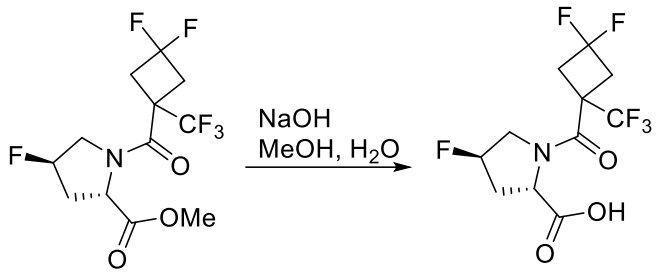

SI-8: To a stirred solution of methyl (2S,4R)-1-[3,3-difluoro-1-(trifluoromethyl)cyclobutanecarbonyl]-4-fluoropyrrolidine-2-carboxylate (180 g, 540 mmol, 1 equiv) in MeOH (1400 mL) was added dropwise NaOH (58.33 g, 1.45 mol, 2.7 equiv) in H_2O (400 mL) over 30 min at 0-20ºC. The mixture was stirred for 2 hr at room temperature. MeOH was evaporated under vacuum. The residue was diluted with water and acidified with 3N HCl at 0-20 ºC. Then the precipitated solids were collected by filtration and washed with water. The resulting filtrate was reacidified with 3N HCl and the resulting precipitate was filtered, washed with water and collected. The solids were combined and dried in an oven for 48hr at 40ºC. **SI-8** was isolated as a white solid and used with no further purification (150.65 g, 472 mmol, 87.4%) as a white solid.

LCMS: MS (ESI) mass calcd. For $C_{11}H_{12}F_6NO_3$: 320.07 m/z; Found 319.95 $[M+H]^+$

^{1}H NMR (400 MHz, DMSO-d_6): δ 2.11 (dddd, J = 40.2, 14.7, 8.8, 4.0 Hz, 1H), 2.53 – 2.65 (m, 1H), 3.10 (q, J = 14.1 Hz, 1H), 3.31 (tt, J = 10.5, 2.7 Hz, 3H), 3.58 – 3.88 (m, 2H), 4.49 (t, J = 8.7 Hz, 1H), 5.39 (dt, J = 52.5, 3.2 Hz, 1H), 12.88 (s, 1H).

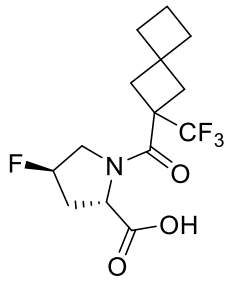

(2S,4R)-4-fluoro-1-(2-(trifluoromethyl)spiro[3.3]heptane-2-carbonyl)pyrrolidine-2-carboxylic acid (SI-9) was synthesized as previously reported.[1]

LCMS: MS (ESI): mass calcd. For $C_{14}H_{18}F_4NO_3$ 324.29 m/z found 324.41 [M+H]+.

^{1}H NMR (400 MHz, DMSO) δ 5.34 (dt, J = 52.5, 3.2 Hz, 1H), 4.41 (t, J = 8.7 Hz, 1H), 3.85 – 3.68 (m, 2H), 3.57 (ddd, J = 37.6, 12.8, 2.6 Hz, 1H), 2.71 – 2.54 (m, 1H), 2.47 – 2.43 (m, 1H), 2.29 – 2.08 (m, 1H), 2.04 (t, J = 7.6 Hz, 2H), 2.00 – 1.84 (m, 2H), 1.74 (q, J = 7.6 Hz, 2H).

^{13}C NMR (101 MHz, DMSO) δ 172.84, 167.06, 167.04, 131.47, 128.69, 125.90, 123.11, 94.04, 92.28, 58.69, 54.01, 53.80, 47.05, 46.78, 39.00, 36.78, 35.25, 34.96, 34.91, 34.69, 15.61.

Method A – Synthesis of Macrocyclic Core

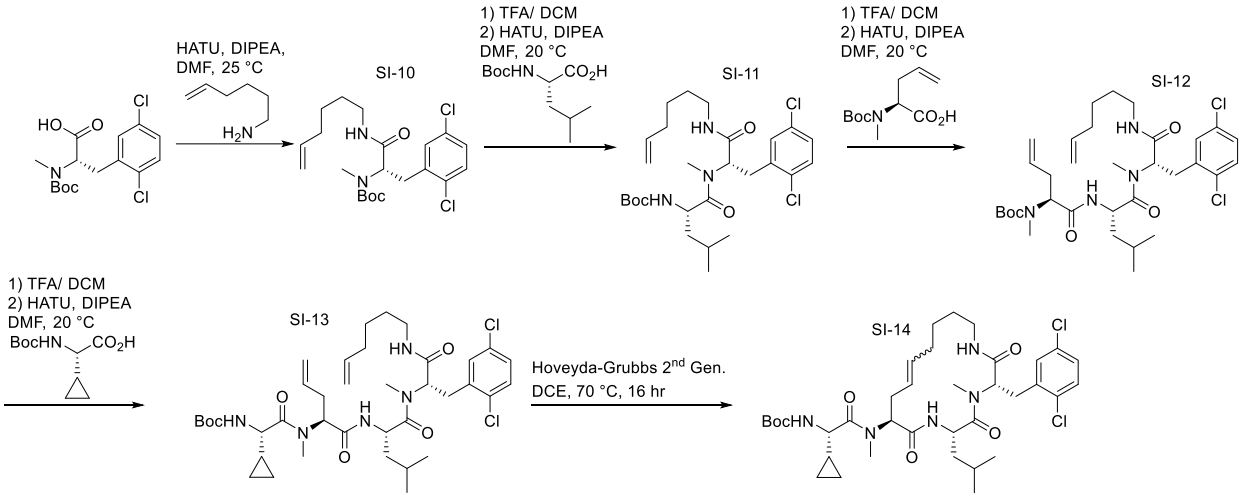

Representative procedure for Method A:

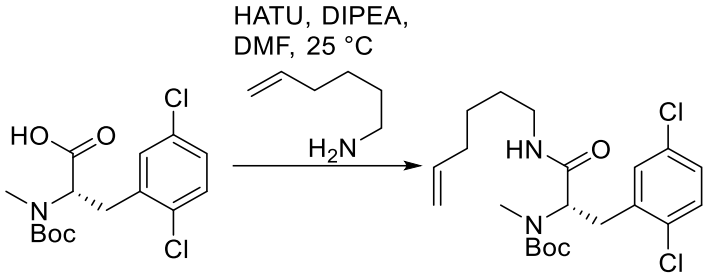

Tert-butyl (S)-(3-(2,5-dichlorophenyl)-1-(hex-5-en-1-ylamino)-1-oxopropan-2-yl)(methyl)carbamate (SI-10): To a 500mL round-bottom flask were added (S)-2-((tert-butoxycarbonyl)(methyl)amino)-3-(2,5-dichlorophenyl)propanoic acid (2.5 g, 7.2 mmol, 1 eq.) and HATU (3.3 g, 8.6 mmol, 1.2 eq.) The solids were dissolved in DMF (20 mL), and to the solution was added hex-5-en-1-amine (0.85 g, 1.0 mL, 8.6 mmol, 1.2 eq.) followed by DIPEA (3.2 g, 4.4 mL, 25 mmol, 3.5 eq.). The solution was confirmed basic by pH paper and stirred for 2 hours. The reaction mixture was diluted in water (100 mL) and extracted with ethyl acetate (100

mL x 3). The combined organics were washed with brine (150 mL), dried over anhydrous magnesium sulfate, and filtered over celite. The organic extract was concentrated under rotary evaporation to give a yellow-orange oil. The crude material was purified by silica gel chromatography (0-100% ethyl acetate in hexanes) and the eluent was concentrated to give tert-butyl (S)-(3-(2,5-dichlorophenyl)-1-(hex-5-en-1-ylamino)-1-oxopropan-2-yl)(methyl)carbamate (2.2 g, 5.1 mmol, 71% yield) as a colorless oil.

LCMS: MS (ESI) mass calcd. for : $C_{21}H_{30}Cl_2N_2O_3$: 438.16m/z; Found 373.1 [M-tBu].

^{1}H NMR: (400 MHz, D_3COD) δ = 7.49 - 7.16 (m, 3H), 5.85 - 5.72 (m, 1H), 5.04 - 4.93 (m, 4H), 3.50 - 3.35 (m, 1H), 3.27 - 3.14 (m, 2H), 3.11 - 2.98 (m, 1H), 2.77 (s, 3H), 2.08 (br d, J = 6.8 Hz, 2H), 1.52 (br s, 2H), 1.44 - 1.40 (m, 1H), 1.39 - 1.22 (m, 9H)

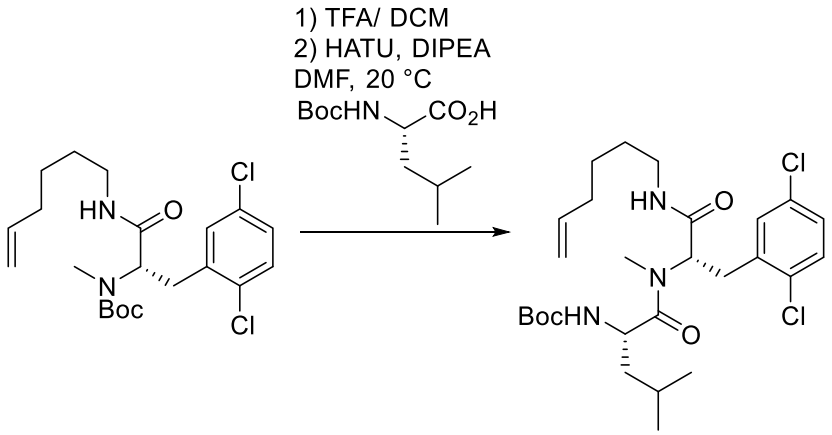

Tert-butyl ((S)-1-(((S)-3-(2,5-dichlorophenyl)-1-(hex-5-en-1-ylamino)-1-oxopropan-2-yl)(methyl)amino)-4-methyl-1-oxopentan-2-yl)carbamate (SI-11): tert-butyl (S)-(3-(2,5-dichlorophenyl)-1-(hex-5-en-1-ylamino)-1-oxopropan-2-yl)(methyl)carbamate (2.2 g, 5.1 mmol, 1 eq.) was dissolved in DCM (15 mL) and TFA (15 mL) and allowed to sit at room temperature for 30 minutes until the Boc group was removed as confirmed by LCMS. The reaction mixture was concentrated by rotary evaporation. The residue was resuspended in toluene and concentrated to remove residual TFA, and this procedure was repeated two times. The crude residue was used in the next reaction without further purification.

To a 500mL round-bottom flask containing the residue was added a solution of Boc-L-Leucine monohydrate (1.5 g, 6.1 mmol, 1.2 eq.), HATU (2.3 g, 6.1 mmol, 1.2 eq.), and DIPEA (2.3 g, 3.1 mL, 18 mmol, 3.5 eq.). in DMF (20 mL). The reaction mixture was checked by pH paper and

DIPEA was added in 1 eq. portions until the reaction was confirmed to be basic (pH ~9). The reaction was stirred for 2 hours at room temperature. The reaction mixture was diluted in water (100 mL) and extracted with ethyl acetate (100 mL x 3). The combined organics were washed with brine (150 mL), dried over anhydrous magnesium sulfate, and filtered over celite. The organic extract was concentrated under rotary evaporation to give a yellow-orange oil. The crude material was purified by silica gel chromatography (0-100% ethyl acetate in hexanes) and the eluent was concentrated to give tert-butyl ((S)-1-(((S)-3-(2,5-dichlorophenyl)-1-(hex-5-en-1-ylamino)-1-oxopropan-2-yl)(methyl)amino)-4-methyl-1-oxopentan-2-yl)carbamate (2.4 g, 4.4 mmol, 86% yield) as a colorless oil.

LCMS: MS (ESI) mass calcd. for $C_{27}H_{41}Cl_2N_3O_4$: 541.25 m/z; Found 442.2 [M-Boc].

^{1}H NMR: (400 MHz, D_3COD) δ= 7.48 - 7.35 (m, 1H), 7.31 (qd, J = 2.4, 4.5 Hz, 1H), 7.27 - 7.20 (m, 1H), 5.79 (tdd, J = 6.8, 10.3, 17.0 Hz, 1H), 5.03 - 4.91 (m, 4H), 4.58 (s, 2H), 4.50 - 4.18 (m, 1H), 3.55 - 3.36 (m, 1H), 3.28 - 3.20 (m, 1H), 3.20 - 3.06 (m, 2H), 3.01 (s, 1H), 2.90 (s, 1H), 2.13 - 1.98 (m, 2H), 1.73 - 1.62 (m, 1H), 1.61 - 1.52 (m, 2H), 1.51 - 1.45 (m, 2H), 1.42 (d, J = 1.2 Hz, 9H), 1.36 - 1.30 (m, 1H), 1.28 - 1.10 (m, 1H), 0.92 (dd, J = 6.8, 10.4 Hz, 3H), 0.71 (dd, J = 4.8, 6.4 Hz, 2H)

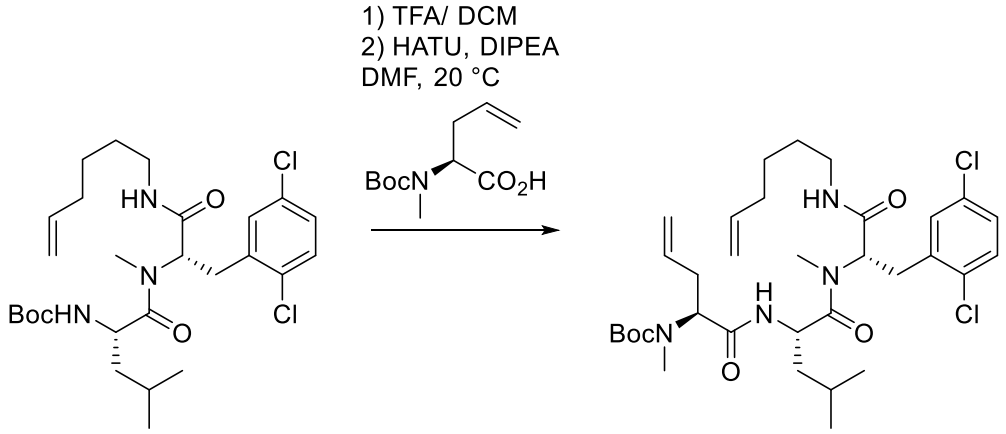

Tert-butyl ((S)-1-(((S)-1-(((S)-3-(2,5-dichlorophenyl)-1-(hex-5-en-1-ylamino)-1-oxopropan-2-yl)(methyl)amino)-4-methyl-1-oxopentan-2-yl)amino)-1-oxopent-4-en-2-yl)(methyl)carbamate (SI-12): tert-butyl ((S)-1-(((S)-3-(2,5-dichlorophenyl)-1-(hex-5-en-1-ylamino)-1-oxopropan-2-yl)(methyl)amino)-4-methyl-1-oxopentan-2-yl)carbamate (2.4 g, 4.4 mmol, 1 eq.) was dissolved in DCM (15 mL) and TFA (15 mL) and allowed to sit at room

temperature for 30 minutes until the Boc group was removed as confirmed by LCMS. The reaction mixture was concentrated by rotary evaporation. The residue was resuspended in toluene and concentrated to remove residual TFA, and this procedure was repeated two times. The crude residue was used in the next reaction without further purification.

To a 500mL round-bottom flask containing the residue was added a solution of (S)-2-((tert-butoxycarbonyl)(methyl)amino)pent-4-enoic acid (1.2 g, 5.3 mmol, 1.2 eq.), HATU (2.0 g, 5.3 mmol, 1.2 eq.), and DIPEA (2.0 g, 2.7 mL, 15 mmol, 3.5 eq.). in DMF (20 mL). The reaction mixture was checked by pH paper and DIPEA was added in 1 eq. portions until the reaction was confirmed to be basic (pH ~9). The reaction was stirred for 2 hours at room temperature. The reaction mixture was diluted in water (100 mL) and extracted with ethyl acetate (100 mL x 3). The combined organics were washed with brine (150 mL), dried over anhydrous magnesium sulfate, and filtered over celite. The organic extract was concentrated under rotary evaporation to give a yellow-orange oil. The crude material was purified by silica gel chromatography (0-100% ethyl acetate in hexanes) and the eluent was concentrated to give tert-butyl ((S)-1-(((S)-1-(((S)-3-(2,5-dichlorophenyl)-1-(hex-5-en-1-ylamino)-1-oxopropan-2-yl)(methyl)amino)-4-methyl-1-oxopentan-2-yl)amino)-1-oxopent-4-en-2-yl)(methyl)carbamate (2.72 g, 4.16 mmol, 94% yield) as a pale yellow oil.

LCMS: MS (ESI) mass calcd. for C $C_{33}H_{50}Cl_2N_4O_5$: 652.32 m/z; Found 553.2 [M-Boc].

^{1}H NMR: (400 MHz, D_3COD) δ=8.51 - 8.06 (m, 1H), 7.94 - 7.62 (m, 1H), 7.48 - 7.35 (m, 1H), 7.34 - 7.30 (m, 1H), 7.26 - 7.22 (m, 1H), 5.90 - 5.66 (m, 2H), 5.18 - 5.04 (m, 2H), 4.99 - 4.91 (m, 2H), 4.72 (ddd, J = 3.2, 7.5, 10.8 Hz, 1H), 4.67 - 4.42 (m, 2H), 3.51 - 3.36 (m, 1H), 3.28 - 3.22 (m, 1H), 3.21 - 3.09 (m, 2H), 3.03 (s, 1H), 2.90 (s, 1H), 2.82 (s, 2H), 2.58 (td, J = 5.2, 9.7 Hz, 1H), 2.49 - 2.39 (m, 1H), 2.17 - 2.00 (m, 2H), 1.69 - 1.52 (m, 3H), 1.45 (d, J = 8.4 Hz, 10H), 1.40 - 1.33 (m, 1H), 1.26 - 1.16 (m, 1H), 0.92 (br dd, J = 6.4, 13.3 Hz, 4H), 0.79 - 0.68 (m, 2H)

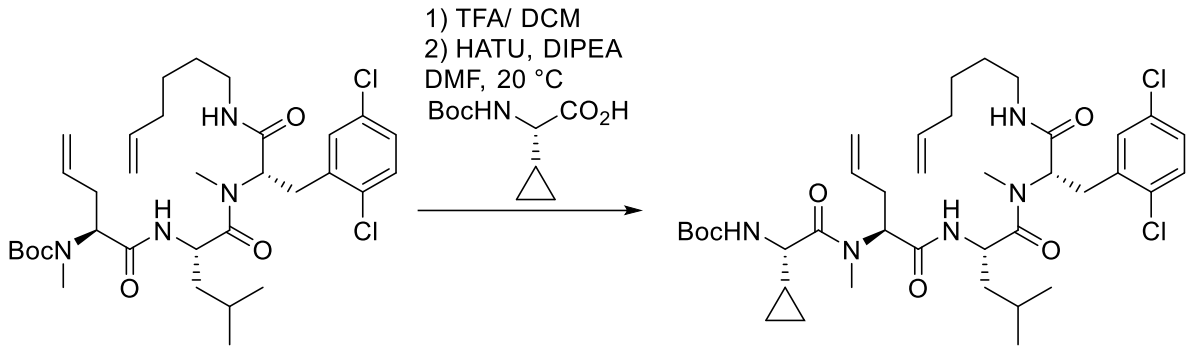

Tert-butyl ((1S,4S,7S,10S)-4-allyl-1-cyclopropyl-10-(2,5-dichlorobenzyl)-7-isobutyl-3,9-dimethyl-2,5,8,11-tetraoxo-3,6,9,12-tetraazaoctadec-17-en-1-yl)carbamate (SI-13) : tert-butyl ((S)-1-(((S)-1-(((S)-3-(2,5-dichlorophenyl)-1-(hex-5-en-1-ylamino)-1-oxopropan-2-yl)(methyl)amino)-4-methyl-1-oxopentan-2-yl)amino)-1-oxopent-4-en-2-yl)(methyl)carbamate (2.7 g, 4.1 mmol, 1 eq.) was dissolved in DCM (15 mL) and TFA (15 mL) and allowed to sit at room temperature for 30 minutes until the Boc group was removed as confirmed by LCMS. The reaction mixture was concentrated by rotary evaporation. The residue was resuspended in toluene and concentrated to remove residual TFA, and this procedure was repeated two times. The crude residue was used in the next reaction without further purification.

To a 500mL round-bottom flask containing the residue was added a solution of (S)-2-((tert-butoxycarbonyl)amino)-2-cyclopropylacetic acid (1.1 g, 5.0 mmol, 1.2 eq.), HATU (1.9 g, 5.0 mmol, 1.2 eq.), and DIPEA (1.9 g, 2.5 mL, 14 mmol, 3.5 eq.). in DMF (20 mL). The reaction mixture was checked by pH paper and DIPEA was added in 1 eq. portions until the reaction was confirmed to be basic (pH ~9). The reaction was stirred for 2 hours at room temperature. The reaction mixture was diluted in water (100 mL) and extracted with ethyl acetate (100 mL x 3). The combined organics were washed with brine (150 mL), dried over anhydrous magnesium sulfate, and filtered over celite. The organic extract was concentrated under rotary evaporation to give a yellow-orange oil. The crude material was purified by silica gel chromatography (0-100% ethyl acetate in hexanes) and the eluent was concentrated to give tert-butyl ((1S,4S,7S,10S)-4-allyl-1-cyclopropyl-10-(2,5-dichlorobenzyl)-7-isobutyl-3,9-dimethyl-2,5,8,11-tetraoxo-3,6,9,12-tetraazaoctadec-17-en-1-yl)carbamate (3.02 g, 4.02 mmol, 97 % yield) as a pale yellow oil.

LCMS: MS (ESI) mass calcd. for$C_{38}H_57Cl_2N_5O_6$: 749.37 m/z; Found 650.3 [M-Boc].

^{1}H NMR: (400 MHz, D_3COD) δ = 8.74 - 8.25 (m, 1H), 8.01 - 7.49 (m, 1H), 7.47 - 7.36 (m, 1H), 7.35 - 7.28 (m, 1H), 7.28 - 7.17 (m, 1H), 5.89 - 5.64 (m, 2H), 5.24 - 5.04 (m, 2H), 5.03 - 4.90 (m, 5H), 4.75 - 4.62 (m, 2H), 4.61 - 4.34 (m, 1H), 4.29 - 3.96 (m, 1H), 3.53 - 3.35 (m, 1H), 3.29 - 3.21 (m, 1H), 3.18 - 3.11 (m, 1H), 3.11 - 3.01 (m, 3H), 2.90 (s, 1H), 2.76 (d, J = 13.6 Hz, 1H), 2.65 - 2.36 (m, 2H), 2.12 - 1.75 (m, 2H), 1.65 - 1.47 (m, 3H), 1.46 - 1.42 (m, 9H), 1.42 - 1.39 (m, 2H), 1.38 - 1.04 (m, 3H), 0.95 - 0.85 (m, 3H), 0.74 - 0.67 (m, 2H), 0.66 - 0.56 (m, 1H), 0.56 - 0.30 (m, 4H)

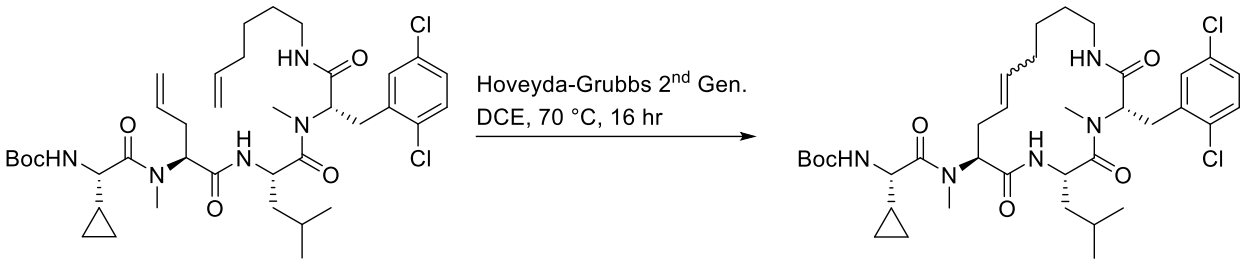

Tert-butyl ((S)-1-cyclopropyl-2-(((3S,6S,9S)-3-(2,5-dichlorobenzyl)-6-isobutyl-4-methyl-2,5,8-trioxo-1,4,7-triazacyclohexadec-11-en-9-yl)(methyl)amino)-2-oxoethyl)carbamate (SI-14): tert-butyl ((1S,4S,7S,10S)-4-allyl-1-cyclopropyl-10-(2,5-dichlorobenzyl)-7-isobutyl-3,9-dimethyl-2,5,8,11-tetraoxo-3,6,9,12-tetraazaoctadec-17-en-1-yl)carbamate (3.02 g, 4.02 mmol, 1 eq.) was dissolved in DCE (300 mL) to give a 13.4 mM solution. The solution was degassed with nitrogen for 20 minutes. To the solution was added Hoyveda-Grubbs II catalyst (M720 Umicore, 378 mgs, 0.15 eq.) and the solution was degassed for an additional 5 minutes. The reaction was heated to 70 ˚C and stirred under nitrogen overnight. Consumption of the starting material was confirmed by LCMS. The reaction was concentrated by rotary evaporation and purified by reverse-phase flash chromatography (50-100% acetonitrile in water, 0.1% TFA buffer) to give tert-butyl ((S)-1-cyclopropyl-2-(((3S,6S,9S)-3-(2,5-dichlorobenzyl)-6-isobutyl-4-methyl-2,5,8-trioxo-1,4,7-triazacyclohexadec-11-en-9-yl)(methyl)amino)-2-oxoethyl)carbamate (1.65 g, 2.3 mmol, 57.3 % yield) as a dark brown solid which was carried on without further purification. An aliquot was further purified by reverse-phase HPLC (50-100% acetonitrile in water, 0.05% formic acid buffer) for analytical purposes. Isolated as a mixture of isomers (~3:1). Analytical data given for major peak.

LCMS: MS (ESI) mass calcd. for $C_{36}H_{54}Cl_2N_5O_6$: 722.34 m/z; Found 722.4 $[M+H]^+$.

^{1}H NMR: (400 MHz, D_3COD) δ =7.48 - 7.38 (m, 1H), 7.35 - 7.27 (m, 1H), 7.16 - 7.02 (m, 1H), 5.56 - 5.40 (m, 1H), 5.40 - 5.07 (m, 1H), 4.67 (br dd, J = 2.0, 12.4 Hz, 2H), 4.59 (br s, 9H), 4.22 - 4.12 (m, 1H), 3.67 - 3.49 (m, 1H), 3.49 - 3.46 (m, 1H), 3.09 (s, 1H), 2.79 (d, J = 7.2 Hz, 4H), 2.21 - 1.84 (m, 2H), 1.83 - 1.52 (m, 2H), 1.52 - 1.39 (m, 9H), 1.38 - 1.21 (m, 2H), 1.20 - 1.06 (m, 1H), 1.01 - 0.70 (m, 6H), 0.70 - 0.30 (m, 4H)

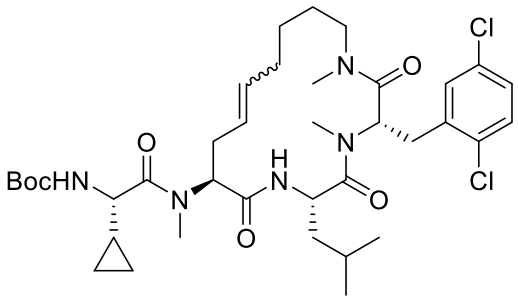

tert-butyl ((S)-1-cyclopropyl-2-(((3S,6S,9S)-3-(2,5-dichlorobenzyl)-6-isobutyl-1,4-dimethyl-2,5,8-trioxo-1,4,7-triazacyclohexadec-11-en-9-yl)(methyl)amino)-2-oxoethyl)carbamate (SI-15) SI-15 was synthesized via the procedure outlined in Method A using N-methylhex-5-en-1-amine as a starting material and was purified by reverse-phase flash chromatography (50-100% acetonitrile in water, 0.1% TFA buffer) to give tert-butyl ((S)-1-cyclopropyl-2-(((3S,6S,9S)-3-(2,5-dichlorobenzyl)-6-isobutyl-1,4-dimethyl-2,5,8-trioxo-1,4,7-triazacyclohexadec-11-en-9-yl)(methyl)amino)-2-oxoethyl)carbamate (2.31 g, 3.14 mmol) as a dark brown solid which was carried on without further purification. An aliquot was further purified by reverse-phase HPLC (50-100% acetonitrile in water, 0.05% formic acid buffer) for analytical purposes. Isolated as a mixture of isomers (~10:1). Analytical data given for major peak.

LCMS: MS (ESI) mass calcd. for $C_{37}H_{56}Cl_2N_5O_6$: 736.36 m/z; Found 736.4 $[M+H]^+$.

^{1}H NMR: (400 MHz, D_3COD) δ =7.40 (d, J = 8.4 Hz, 1H), 7.33 - 7.26 (m, 1H), 7.26 - 7.15 (m, 1H), 5.62 - 5.48 (m, 1H), 5.48 - 5.26 (m, 1H), 5.15 - 4.96 (m, 1H), 4.89 (br d, J = 1.6 Hz, 2H), 4.82 (br d, J = 3.6 Hz, 1H), 4.78 - 4.55 (m, 1H), 4.54 - 4.38 (m, 1H), 4.28 (dt, J = 5.6, 13.2 Hz, 1H), 4.22 - 4.09 (m, 1H), 3.53 - 3.32 (m, 2H), 3.29 - 3.14 (m, 1H), 3.13 - 3.01 (m, 2H), 2.98 - 2.86 (m, 3H), 2.82 - 2.73 (m, 3H), 2.64 - 2.47 (m, 1H), 2.16 - 1.76 (m, 3H), 1.73 - 1.54 (m, 2H), 1.53 - 1.41 (m, 9H), 1.41 - 1.21 (m, 3H), 1.18 - 0.97 (m, 2H), 0.97 - 0.87 (m, 3H), 0.79 (br d, J = 6.4 Hz, 2H), 0.69 - 0.24 (m, 4H)

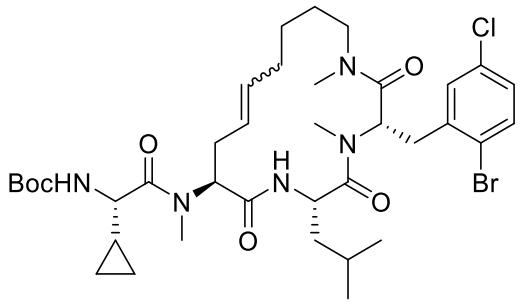

Tert-butyl ((S)-2-(((3S,6S,9S)-3-(2-bromo-5-chlorobenzyl)-6-isobutyl-1,4-dimethyl-2,5,8-trioxo-1,4,7-triazacyclohexadec-11-en-9-yl)(methyl)amino)-1-cyclopropyl-2-oxoethyl)carbamate (SI-16) was synthesized using the procedure outlined in Method A using N-methylhex-5-en-1-amine and **SI-2** as starting material. **SI-16** was purified column chromatography (SiO_2, 0 to 100% EtOAc in Hexane) and was isolated as a brown solid after concentration (10.35 g, 13.21 mmol). Isolated as a mixture of isomers (~10:1). Analytical data given for major peak.

LCMS: MS (ESI) mass calcd. For $C_{37}H_{56}BrClN_5O_6$ 780.30 m/z; Found 780.30 $[M+H]^+$.

^{1}H NMR (400 MHz, DMSO-d_6) δ 8.04-7.74 (m, 1H), 7.57 (br d, J = 8.2 Hz, 1H), 7.29 (br s, 1H), 7.22 (br d, J = 7.7 Hz, 1H), 6.62 - 6.20 (m, 1H), 5.56-5.43 (m, 1H), 5.40-5.20 (m, 1H), 4.93-4.93 (m, 1H), 4.91-4.88 (m, 1H), 5.01-4.55 (m, 2H), 4.35-4.09 (m, 2H), 3.36-3.11 (m, 2H), 3.06 (s, 3H), 3.00-2.79 (m, 8H), 2.78-2.58 (m, 2H), 2.09 (br s, 1H), 1.92 (br d, J = 10.0 Hz, 2H), 1.66-1.45 (m, 3H), 1.40 (br s, 9H), 1.29 (br s, 3H), 1.15-1.04 (m, 1H), 0.91-0.66 (m, 6H), 0.55-0.22 (m, 4H)

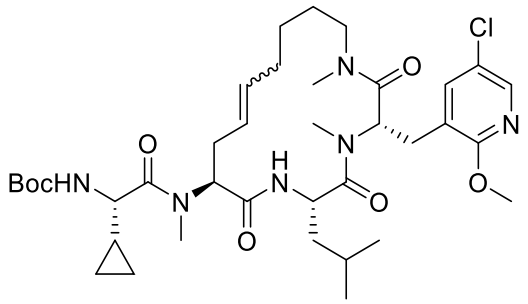

Tert-butyl ((S)-2-(((3S,6S,9S)-3-((5-chloro-2-methoxypyridin-3-yl)methyl)-6-isobutyl-1,4-dimethyl-2,5,8-trioxo-1,4,7-triazacyclohexadec-11-en-9-yl)(methyl)amino)-1-cyclopropyl-2-oxoethyl)carbamate (SI-17) was synthesized using the procedure outlined in Method A using N-methylhex-5-en-1-amine and **SI-5** as starting material. **SI-17** was purified by RP-HPLC (C18, 20% to 80% MeCN+0.1% TFA in water+0.1% TFA) and was isolated as a brown solid after lyophilization (2.5 g, 3.4 mmol, 68% yield). Isolated as a mixture of isomers.

LCMS: MS (ESI) mass calcd. for C37H57ClN6O7: 733.35 m/z; Found 733.77 $[M+H]^+$.

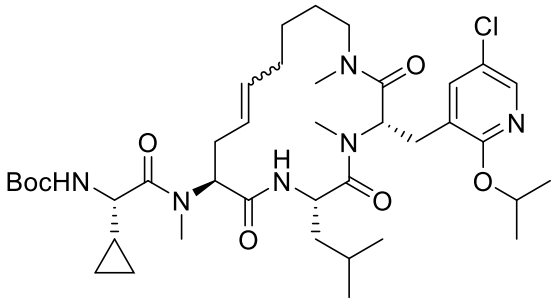

Tert-butyl ((S)-2-(((3S,6S,9S)-3-((5-chloro-2-isopropoxypyridin-3-yl)methyl)-6-isobutyl-1,4-dimethyl-2,5,8-trioxo-1,4,7-triazacyclohexadec-11-en-9-yl)(methyl)amino)-1-cyclopropyl-2-oxoethyl)carbamate (SI-18) was synthesized using the procedure outlined in Method A using N-methylhex-5-en-1-amine and **SI-3** as starting material. **SI-18** was purified by RP-HPLC (C18, 20% to 80% MeCN+0.1% TFA in water+0.1% TFA) and was isolated as a brown solid after lyophilization (0.74 g, 0.97 mmol, 40% yield). Isolated as a mixture of isomers.

LCMS: MS (ESI) mass calcd. for C39H61ClN6O7: 761.40 m/z; Found 761.98 $[M+H]^+$.

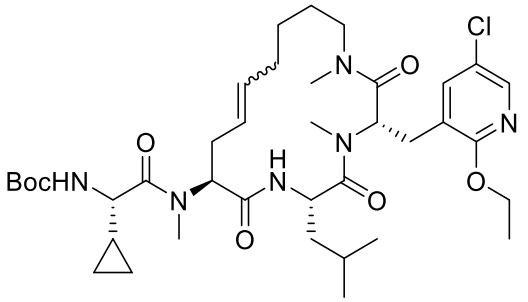

Tert-butyl ((S)-2-(((3S,6S,9S)-3-((5-chloro-2-ethoxypyridin-3-yl)methyl)-6-isobutyl-1,4-dimethyl-2,5,8-trioxo-1,4,7-triazacyclohexadec-11-en-9-yl)(methyl)amino)-1-cyclopropyl-2-oxoethyl)carbamate (SI-19) was synthesized using the procedure outlined in Method A using N-methylhex-5-en-1-amine and **SI-6** as starting material. **SI-19** was purified by RP-HPLC (C18, 20% to 80% MeCN+0.1% TFA in water+0.1% TFA) and was isolated as a brown solid after lyophilization (0.8 g, 1.00 mmol, 50% yield). Isolated as a mixture of isomers.

LCMS: MS (ESI) mass calcd. for C38H59ClN6O7: 747.38 m/z; Found 747.88 $[M+H]^+$.

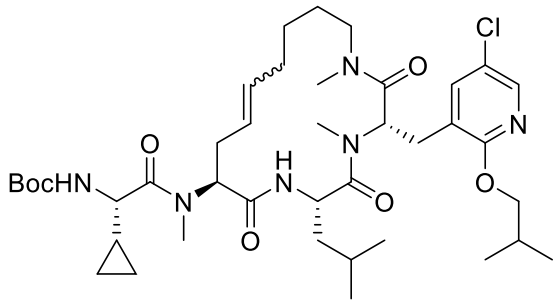

Tert-butyl ((S)-2-(((3S,6S,9S)-3-((5-chloro-2-isobutoxypyridin-3-yl)methyl)-6-isobutyl-1,4-dimethyl-2,5,8-trioxo-1,4,7-triazacyclohexadec-11-en-9-yl)(methyl)amino)-1-cyclopropyl-2-oxoethyl)carbamate (SI-20) was synthesized using the procedure outlined in Method A using N-methylhex-5-en-1-amine and **SI-7** as starting material. **SI-20** was purified by RP-HPLC (C18, 20% to 80% MeCN+0.1% TFA in water+0.1% TFA) and was isolated as a brown solid after lyophilization (1.65 g, 2.13 mmol, 57% yield). Isolated as a mixture of isomers.

LCMS: MS (ESI) mass calcd. for C40H63ClN6O7: 775.43 m/z; Found 775.94 $[M+H]^+$.

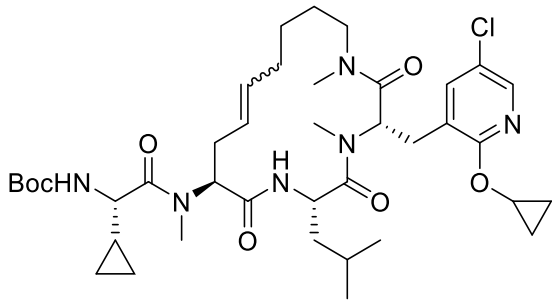

Tert-butyl ((S)-2-(((3S,6S,9S)-3-((5-chloro-2-cyclopropoxypyridin-3-yl)methyl)-6-isobutyl-1,4-dimethyl-2,5,8-trioxo-1,4,7-triazacyclohexadec-11-en-9-yl)(methyl)amino)-1-cyclopropyl-2-oxoethyl)carbamate (SI-21) was synthesized using the procedure outlined in Method A using N-methylhex-5-en-1-amine and **SI-4** as starting material. **SI-21** was purified by column chromatography (SiO_2, 0 to 100% EtOAc) and was isolated as a brown solid (52 g, 68.5 mmol)

LCMS: MS (ESI) mass calcd. for $C_{39}H_{60}ClN_6O_7$: 758.41 m/z; Found 759.4 $[M+H]^+$.

^{1}H NMR: (400 MHz, CD_3OD_3) δ= 8.17 - 8.05 (m, 1H), 8.00 - 7.80 (m, 1H), 7.53 - 7.30 (m, 1H), 5.55 - 5.07 (m, 2H), 5.00 - 4.83 (m, 1H), 4.45 - 4.02 (m, 4H), 3.17 - 2.89 (m, 5H), 2.86 - 2.65 (m,

7H), 2.61 - 2.43 (m, 1H), 1.91 (s, 3H), 1.88 - 1.75 (m, 1H), 1.63 - 1.46 (m, 2H), 1.43 - 1.21 (m, 13H), 1.10-0.96 (m, 2H), 0.86 - 0.63 (m, 11H), 0.50 - 0.15 (m, 4H)

Method B – Hydrogenation

Representative procedure for Method B:

Tert-butyl ((S)-1-cyclopropyl-2-(((3S,6S,9S)-3-(2,5-dichlorobenzyl)-6-isobutyl-4-methyl-2,5,8-trioxo-1,4,7-triazacyclohexadecan-9-yl)(methyl)amino)-2-oxoethyl)carbamate (SI-22):

tert-butyl ((S)-1-cyclopropyl-2-(((3S,6S,9S)-3-(2,5-dichlorobenzyl)-6-isobutyl-4-methyl-2,5,8-trioxo-1,4,7-triazacyclohexadec-11-en-9-yl)(methyl)amino)-2-oxoethyl)carbamate (1.6 g, 2.2 mmol, 1 eq.) was dissolved in EtOAc (200 mL). To the solution was added 10% Palladium on Carbon (1.6 g, 1.5 mmol, 0.68 eq.) as a solid. The reaction vessel was evacuated and backfilled with hydrogen gas 10 times. The reaction was stirred under 1 atm of hydrogen for 2 hours. Consumption of the starting material was confirmed by LCMS. The reaction was filtered through a pad of Celite and the filtrate was concentrated by rotary evaporation to give tert-butyl ((S)-1-cyclopropyl-2-(((3S,6S,9S)-3-(2,5-dichlorobenzyl)-6-isobutyl-4-methyl-2,5,8-trioxo-1,4,7-triazacyclohexadecan-9-yl)(methyl)amino)-2-oxoethyl)carbamate (1.5 g, 2.1 mmol, 93 % yield) as a pale brown solid which was carried on without further purification. An aliquot was further purified by reverse-phase HPLC (50-100% acetonitrile in water, 0.05% formic acid buffer) for analytical purposes.

LCMS: MS (ESI) mass calcd. for $C_{36}H_{56}Cl_2N_5O_6$: 724.36 m/z; Found 724.4 $[M+H]^+$.

^{1}H NMR: (400 MHz, CD_3OD_3) δ=7.66 - 7.57 (m, 1H), 7.53 - 7.45 (m, 1H), 7.37 - 7.20 (m, 1H), 5.38 - 5.23 (m, 1H), 4.93 - 4.84 (m, 2H), 4.73 - 4.64 (m, 1H), 4.62 - 4.31 (m, 2H), 3.94 - 3.76 (m, 1H), 3.72 - 3.64 (m, 1H), 3.48 - 3.26 (m, 1H), 3.26 - 3.19 (m, 1H), 3.18 - 2.91 (m, 5H), 1.90 - 1.74

(m, 1H), 1.73 - 1.54 (m, 17H), 1.51 - 1.35 (m, 2H), 1.31 - 1.21 (m, 1H), 1.12 - 1.04 (m, 2H), 1.00 - 0.95 (m, 2H), 0.93 - 0.78 (m, 3H), 0.75 (br s, 1H)

^{13}C NMR (400 MHz, CD_3OD_3) δ = 223.748, 209.755, 174.41, 174.118, 172.277, 172.145, 171.86, 171.784, 171.481, 170.779, 170.487, 170.115, 168.84, 156.235, 156.227, 137.786, 137.354, 132.933, 132.444, 132.341, 132.273, 132.144, 131.795, 131.184, 130.588, 128.854, 128.763, 128.289, 79.341, 79.277, 59.963, 58.878, 56.484, 55.896, 53.145, 52.432, 48.759, 48.736, 48.709, 48.531, 48.227, 47.802, 47.587, 47.374, 46.949, 46.668, 39.432, 39.235, 38.95, 37.926, 36.81, 31.889, 31.775, 31.688, 30.136, 30.003, 29.1, 28.891, 28.622, 28.478, 28.383, 28.079, 27.95, 27.635, 27.464, 27.411, 27.271, 26.967, 26.315, 26.265, 26.14, 25.84, 24.418, 23.924, 23.757, 23.617, 23.386, 23.044, 22.911, 22.494, 22.35, 22.126, 22.069, 21.09, 19.614, 19.269, 18.923, 12.598, 12.461, 12.203, 2.524, 2.437, 2.247, 1.788, 1.727, 1.53, 0.767

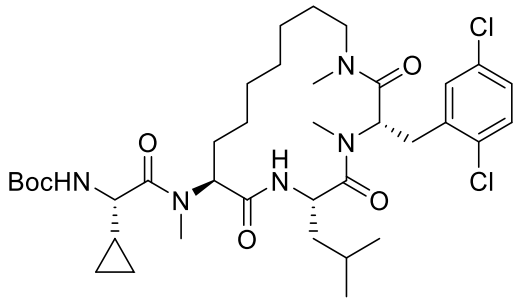

Tert-butyl ((S)-1-cyclopropyl-2-(((3S,6S,9S)-3-(2,5-dichlorobenzyl)-6-isobutyl-1,4-dimethyl-2,5,8-trioxo-1,4,7-triazacyclohexadecan-9-yl)(methyl)amino)-2-oxoethyl)carbamate (SI-23) was synthesized using the procedure outlined in Method B using **SI-15** as a starting material to give tert-butyl ((S)-1-cyclopropyl-2-(((3S,6S,9S)-3-(2,5-dichlorobenzyl)-6-isobutyl-1,4-dimethyl-2,5,8-trioxo-1,4,7-triazacyclohexadecan-9-yl)(methyl)amino)-2-oxoethyl)carbamate (2.1 g, 2.8 mmol) as a pale brown solid which was carried on without further purification. An aliquot was further purified by reverse-phase HPLC (50-100% acetonitrile in water, 0.05% formic acid buffer) for analytical purposes.

LCMS: MS (ESI) mass calcd. for $C_{37}H_{58}Cl_2N_5O_6$: 738.37 m/z; Found 738.4 $[M+H]^+$.

^{1}H NMR: (400 MHz, CD_3OD_3) δ = 8.30 - 8.04 (m, 1H), 7.24 - 7.13 (m, 1H), 7.09 - 6.96 (m, 2H), 6.91 - 6.36 (m, 1H), 4.75 - 4.66 (m, 1H), 4.31 (br s, 1H), 4.25 - 3.91 (m, 3H), 3.19 (br s, 1H), 3.01 (br s, 3H), 2.82 - 2.71 (m, 3H), 2.69 - 2.58 (m, 3H), 2.53 (s, 1H), 2.06 - 1.72 (m, 1H), 1.54 - 1.40

(m, 2H), 1.39 - 1.31 (m, 1H), 1.31 - 1.18 (m, 13H), 1.18 - 1.07 (m, 5H), 1.07 (br s, 2H), 0.92 - 0.85 (m, 1H), 0.65 (br s, 4H), 0.61 - 0.51 (m, 3H), 0.40 - -0.04 (m, 4H)

^{13}C NMR (400 MHz, CD_3OD_3) δ = 224.022, 223.908, 223.46, 223.156, 223.13, 223.084, 222.758, 221.415, 221.195, 221.153, 220.975, 220.967, 220.865, 220.857, 220.755, 220.732, 220.182, 218.994, 215.556, 212.005, 211.007, 210.885, 206.579, 197.499, 192.87, 192.854, 188.605, 184.7, 183.251, 182.325, 172.941, 172.338, 172.076, 171.985, 171.871, 171.264, 169.314, 156.223, 137.582, 132.831, 132.125, 132.038, 130.516, 128.828, 128.221, 126.362, 119.979, 112.694, 79.201, 58.821, 56.294, 52.534, 48.77, 48.645, 48.588, 48.25, 48.167, 47.954, 47.825, 47.61, 47.396, 46.971, 39.011, 38.908, 34.848, 34.662, 32.659, 30.007, 29.362, 28.565, 27.859, 27.457, 27.294, 27.085, 26.869, 26.228, 25.78, 24.399, 24.308, 24.008, 23.867, 23.56, 23.446, 23.15, 22.494, 21.113, 20.058, 20.043, 19.739, 13.554, 13.069, 12.26, 2.179, 2.031, 1.788, 0.9.

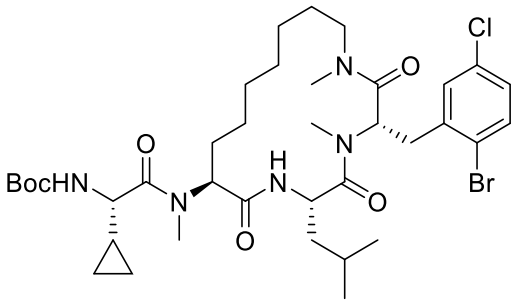

Tert-butyl ((S)-2-(((3S,6S,9S)-3-(2-bromo-5-chlorobenzyl)-6-isobutyl-1,4-dimethyl-2,5,8-trioxo-1,4,7-triazacyclohexadecan-9-yl)(methyl)amino)-1-cyclopropyl-2-oxoethyl)carbamate (SI-24) was synthesized using the procedure outlined in Method B with the following modification: 0.1 equiv of Pt_2O was used instead of Pd/C. **SI-24** was isolated as an off white solid (11.8 g, 15.3 mmol, 98% yield). The reaction was used without further purification.

LCMS: MS (ESI) mass calcd. for $C_{37}H_{58}BrClN_5O_6$: 782.32 m/z; Found 782.20 $[M+H]^+$.

^{1}H NMR: (400 MHz, DMSO-d6) δ 8.21-8.50 (m, 1H), 7.49-7.64 (m, 1H), 7.13-7.38 (m, 2H), 6.81 (d, J = 3.6 Hz, 1H), 4.81 (d, J = 12.4 Hz, 1H), 4.32-4.50 (m, 1H), 4.13-4.27 (m, 2H), 3.03-3.36 (m, 2H), 2.69-2.98 (m, 10H), 2.53-2.64 (m, 1H), 1.79-2.04 (m, 1H), 1.49-1.65 (m, 2H), 1.31-1.43 (m, 14H), 0.99-1.27 (m, 8H), 0.80-0.87 (m, 3H), 0.66 (d, J = 5.6 Hz, 3H), 0.31-0.47 (m, 2H), 0.11-0.28 (m, 2H)

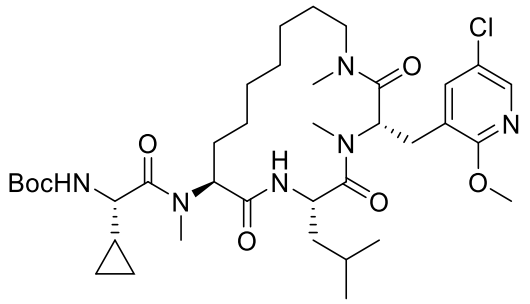

Tert-butyl ((S)-2-(((3S,6S,9S)-3-((5-chloro-2-methoxypyridin-3-yl)methyl)-6-isobutyl-1,4-dimethyl-2,5,8-trioxo-1,4,7-triazacyclohexadecan-9-yl)(methyl)amino)-1-cyclopropyl-2-oxoethyl)carbamate (SI-25) was synthesized using the procedure outlined in Method B. **SI-25** was isolated as an off white solid (0.45 g, 0.614 mmol, 100% yield). The reaction was used without further purification.

LCMS: MS (ESI) mass calcd. for C37H59ClN6O7: 735.36 m/z; Found 735.78 $[M+H]^+$.

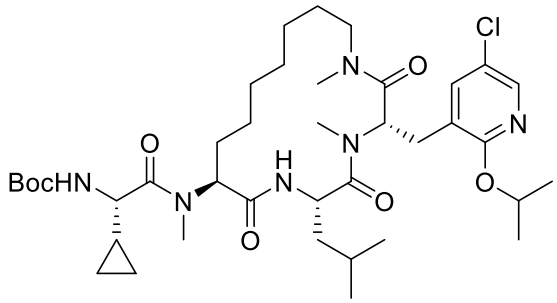

Tert-butyl ((S)-2-(((3S,6S,9S)-3-((5-chloro-2-isopropoxypyridin-3-yl)methyl)-6-isobutyl-1,4-dimethyl-2,5,8-trioxo-1,4,7-triazacyclohexadecan-9-yl)(methyl)amino)-1-cyclopropyl-2-oxoethyl)carbamate (SI-26) was synthesized using the procedure outlined in Method B. **SI-26** was isolated as an off white solid (0.3 g, 0.4 mmol, 99% yield). The reaction was used without further purification.

LCMS: MS (ESI) mass calcd. for C39H63ClN6O7: 763.42 m/z; Found 763.95 $[M+H]^+$.

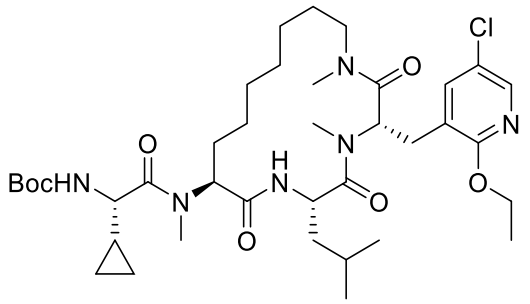

Tert-butyl ((S)-2-(((3S,6S,9S)-3-((5-chloro-2-ethoxypyridin-3-yl)methyl)-6-isobutyl-1,4-dimethyl-2,5,8-trioxo-1,4,7-triazacyclohexadecan-9-yl)(methyl)amino)-1-cyclopropyl-2-oxoethyl)carbamate (SI-27) was synthesized using the procedure outlined in Method B. **SI-27** was isolated as an off white solid (0.46 g, 0.602 mmol, 100% yield). The reaction was used without further purification.

LCMS: MS (ESI) mass calcd. for C38H61ClN6O7: 749.39 m/z; Found 749.85 $[M+H]^+$.

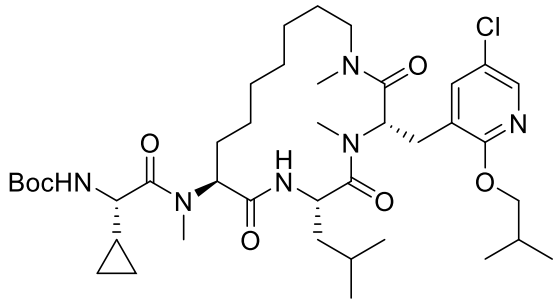

Tert-butyl ((S)-2-(((3S,6S,9S)-3-((5-chloro-2-isobutoxypyridin-3-yl)methyl)-6-isobutyl-1,4-dimethyl-2,5,8-trioxo-1,4,7-triazacyclohexadecan-9-yl)(methyl)amino)-1-cyclopropyl-2-oxoethyl)carbamate (SI-28) was synthesized using the procedure outlined in Method B . **SI-28** was isolated as an off white solid (0.44 g, 0.580 mmol, 99% yield). The reaction was used without further purification.

LCMS: MS (ESI) mass calcd. for C40H65ClN6O7: 777.45 m/z; Found 777.96 $[M+H]^+$.

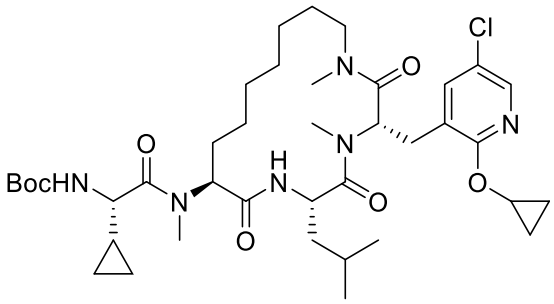

Tert-butyl ((S)-2-(((3S,6S,9S)-3-((5-chloro-2-cyclopropoxypyridin-3-yl)methyl)-6-isobutyl-1,4-dimethyl-2,5,8-trioxo-1,4,7-triazacyclohexadecan-9-yl)(methyl)amino)-1-cyclopropyl-2-oxoethyl)carbamate (SI-29) was synthesized using the procedure outlined in Method B. **SI-29** was isolated as a off-white solid (52g, 68.5 mmol, quant.) which was used without further purification.

LCMS: MS (ESI) mass calcd. for $C_{39}H_{62}ClN_6O_7$: 761.43 m/z; Found 761.4 $[M+H]^+$.

^{1}H NMR: (400 MHz, CD_3OD) δ 7.85 - 7.78 (d, J = 2.4 Hz, 1H), 7.37 - 7.29 (d, J = 2.4 Hz, 1H), 4.19 - 4.01 (m, 4H), 2.98 - 2.79 (m, 5H), 2.78 - 2.67 (m, 7H), 2.54 - 2.43 (m, 1H), 1.48 - 1.29 (m, 4H), 1.26 - 1.20 (m, 13H), 1.18 - 1.08 (m, 5H), 0.96 - 0.82 (m, 2H), 0.79 - 0.67 (m, 5H), 0.53- 0.64 (m, 7H), 0.33 - 0.12 (m, 3H), 0.02 (m, 1H).

Method C – Suzuki Coupling

Representative procedure for Method C:

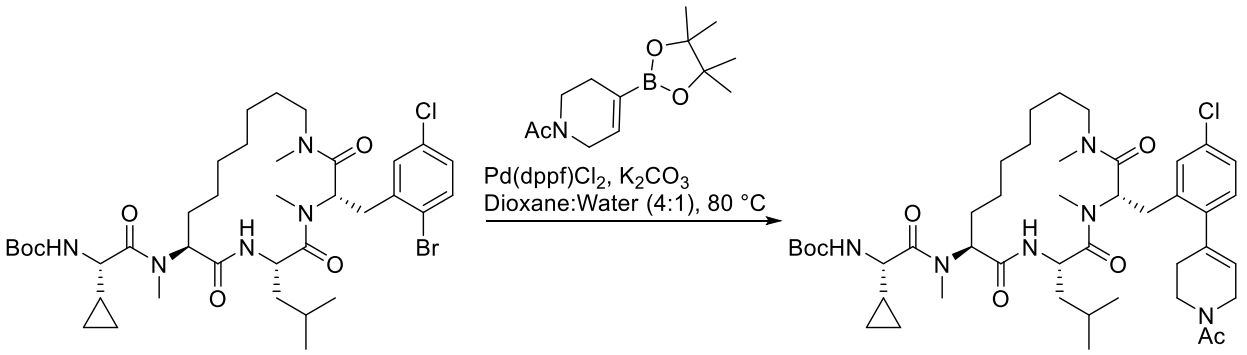

tert-butyl ((S)-2-(((3S,6S,9S)-3-(2-(1-acetyl-1,2,3,6-tetrahydropyridin-4-yl)-5-chlorobenzyl)-6-isobutyl-1,4-dimethyl-2,5,8-trioxo-1,4,7-triazacyclohexadecan-9-yl)(methyl)amino)-1-cyclopropyl-2-oxoethyl)carbamate (SI-30): SI-24 (100 mg, 1 Eq, 128 µmol), 1-(4-(4,4,5,5-tetramethyl-1,3,2-dioxaborolan-2-yl)-3,6-dihydropyridin-1(2H)-yl)ethan-1-one (48.1 mg, 1.5 Eq,

192 µmol), and $PdCl_2$(dppf) (14.0 mg, 0.15 Eq, 19.2 µmol) were dissolved in 1,4-dioxane (1 mL). 2 M K_2CO_3 (, 200 µL) was added and the reaction was degassed with a stream of N_2 (5 min). The reaction was then heated to 80 °C and stirred until the complete consumption of starting material (~2 hr). The reaction was diluted with MeCN (2 mL), filtered and directly purified by RP chromatography (15.5g C18, 30-80% MeCN+0.1% TFA in Water+0.1% TFA). **SI-30** (79.3 mg, 95.8 µmol, 75.1 %) was isolated as an off-white solid after lyophilization.

LCMS: MS (ESI) mass calcd. for $C_{44}H_{68}ClN_6O_7$: 827.48; m/z Found 827.80 $[M+H]^+$.

^{1}H NMR: (400 MHz, CD_3OD_3) δ= 7.30 - 7.20 (m, 1H), 7.17 (br s, 1H), 7.10 (br d, J = 8.2 Hz, 1H), 5.81 (br d, J = 8.2 Hz, 1H), 4.38 - 4.27 (m, 2H), 4.18 (br d, J = 8.8 Hz, 2H), 3.96 - 3.65 (m, 2H), 3.31 (t, J = 1.6 Hz, 3H), 3.18 (br d, J = 7.4 Hz, 1H), 3.09 (s, 3H), 3.00 - 2.82 (m, 6H), 2.66 (br d, J = 12.8 Hz, 1H), 2.59 - 2.36 (m, 2H), 2.35 - 2.18 (m, 1H), 2.16 (d, J = 10.8 Hz, 2H), 2.05 (br d, J = 10.6 Hz, 1H), 1.81 - 1.62 (m, 2H), 1.61 - 1.49 (m, 2H), 1.46 (br s, 3H), 1.43 (s, 9H), 1.38 - 1.15 (m, 7H), 1.15 - 0.99 (m, 2H), 0.98 - 0.86 (m, 3H), 0.85 - 0.69 (m, 3H), 0.65 - 0.15 (m, 4H)

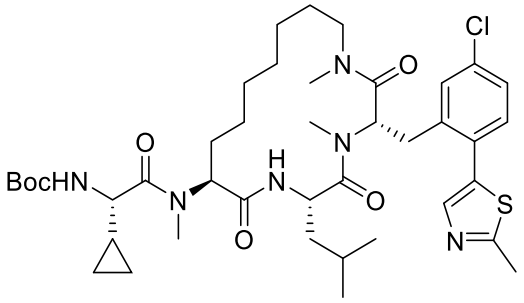

Tert-butyl ((S)-2-(((3S,6S,9S)-3-(5-chloro-2-(2-methylthiazol-5-yl)benzyl)-6-isobutyl-1,4-dimethyl-2,5,8-trioxo-1,4,7-triazacyclohexadecan-9-yl)(methyl)amino)-1-cyclopropyl-2-oxoethyl)carbamate (SI-31) was synthesized using the procedure outlined in Method C using **SI-24** and 2-methyl-5-(4,4,5,5-tetramethyl-1,3,2-dioxaborolan-2-yl)thiazole as starting material. **SI-31** was purified by RP-HPLC (C18, 20% to 80% MeCN+0.1% TFA in water+0.1% TFA) and was isolated as a fluffy off-white solid after lyophilization (101 mg, 131 µmol, 85% yield).

LCMS: MS (ESI) mass calcd. for **(SI-31)** : 772.37 m/z; Found 772.90 $[M+H]^+$.

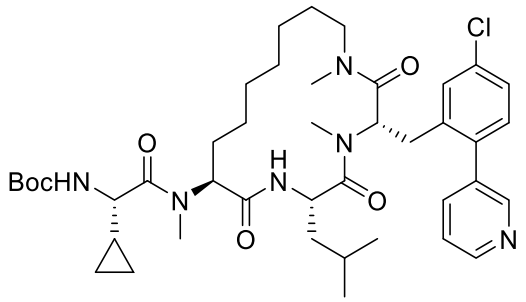

Tert-butyl ((S)-2-(((3S,6S,9S)-3-(5-chloro-2-(pyridin-3-yl)benzyl)-6-isobutyl-1,4-dimethyl-2,5,8-trioxo-1,4,7-triazacyclohexadecan-9-yl)(methyl)amino)-1-cyclopropyl-2-oxoethyl)carbamate (SI-32) was synthesized using the procedure outlined in Method C using **SI-24** and pyridin-3-ylboronic acid as starting material. **SI-32** was purified by RP-HPLC (C18, 20% to 80% ACN+0.1% TFA in water+0.1% TFA) and was isolated as a fluffy off-white solid after lyophilization (0.055 g, 0.070 mmol, 92% yield).

LCMS: MS (ESI) mass calcd. for $C_{42}H_{62}ClN_6O_6$: 781.44 m/z; Found 781.20 $[M+H]^+$.

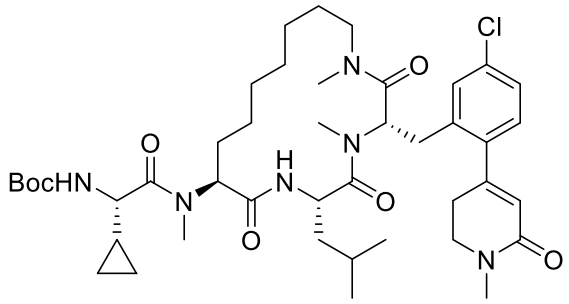

tert-butyl ((S)-2-(((3S,6S,9S)-3-(5-chloro-2-(1-methyl-6-oxo-1,2,3,6-tetrahydropyridin-4-yl)benzyl)-6-isobutyl-1,4-dimethyl-2,5,8-trioxo-1,4,7-triazacyclohexadecan-9-yl)(methyl)amino)-1-cyclopropyl-2-oxoethyl)carbamate (SI-33) was synthesized using the procedure outlined in Method C using **SI-24** and 1-methyl-4-(trifluoro-l4-boraneyl)-5,6-dihydropyridin-2(1H)-one, potassium salt as starting material. **SI-33** was purified by RP-HPLC (C18, 20% to 80% MeCN+0.1% TFA in water+0.1% TFA) and was isolated as a fluffy off-white solid after lyophilization (0.045 g, 0.055 mmol, 43% yield).

LCMS: MS (ESI) mass calcd. for C43H65ClN6O7: 813.48 m/z; Found 813.93 $[M+H]^+$.

Method D – Dipeptide Addition

Representative procedure for Method D:

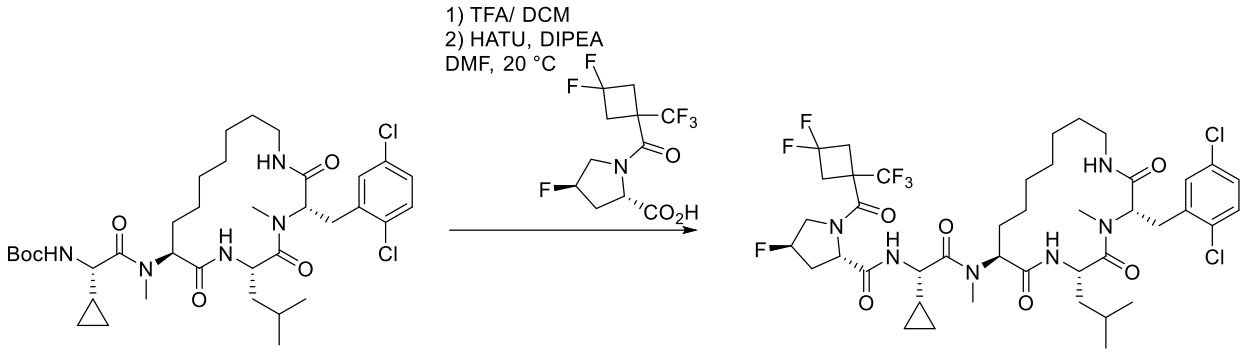

(2S,4R)-N-((S)-1-cyclopropyl-2-(((3S,6S,9S)-3-(2,5-dichlorobenzyl)-6-isobutyl-4-methyl-2,5,8-trioxo-1,4,7-triazacyclohexadecan-9-yl)(methyl)amino)-2-oxoethyl)-1-(3,3-difluoro-1-(trifluoromethyl)cyclobutane-1-carbonyl)-4-fluoropyrrolidine-2-carboxamide (Compound 23): tert-butyl ((S)-1-cyclopropyl-2-(((3S,6S,9S)-3-(2,5-dichlorobenzyl)-6-isobutyl-4-methyl-2,5,8-trioxo-1,4,7-triazacyclohexadecan-9-yl)(methyl)amino)-2-oxoethyl)carbamate (0.05 g, 0.069 mmol, 1 eq.) was dissolved in DCM (1 mL) and TFA (1 mL) and allowed to sit at room temperature for 30 minutes until the Boc group was removed as confirmed by LCMS. The reaction mixture was concentrated by rotary evaporation. The residue was resuspended in toluene and concentrated to remove residual TFA, and this procedure was repeated two times. The crude residue was used in the next reaction without further purification.

To a vial containing the residue was added a solution of (2S,4R)-1-(3,3-difluoro-1-(trifluoromethyl)cyclobutane-1-carbonyl)-4-fluoropyrrolidine-2-carboxylic acid (0.026 g, 0.083 mmol, 1.2 eq.), HATU (0.031 g, 0.083 mmol, 1 eq.), and DIPEA (0.031 g, 0.042 mL, 0.24 mmol, 3.5 eq.). in DMF (1 mL). The reaction mixture was checked by pH paper and DIPEA was added in 1 eq. portions until the reaction was confirmed to be basic (pH ~9). The reaction was allowed to sit for 2 hours at room temperature. The reaction mixture was diluted in water (100 mL) and extracted with ethyl acetate (100 mL x 3). The combined organics were washed with brine (150 mL), dried over anhydrous magnesium sulfate, and filtered over celite. The organic extract was concentrated under rotary evaporation to give a yellow-orange oil. The crude material was purified by reverse-phase HPLC (50-100% acetonitrile in water, 0.05% formic acid buffer) and the eluent was lyophilized to give (2S,4R)-N-((S)-1-cyclopropyl-2-(((3S,6S,9S)-3-(2,5-dichlorobenzyl)-6-isobutyl-4-methyl-2,5,8-trioxo-1,4,7-triazacyclohexadecan-9-yl)(methyl)amino)-2-oxoethyl)-1-(3,3-difluoro-1-(trifluoromethyl)cyclobutane-1-carbonyl)-4-fluoropyrrolidine-2-carboxamide (0.044 g, 0.048 mmol, 69 % yield) as a fluffy white solid.

LCMS: MS (ESI) mass calcd. For $C_{42}H_{57}Cl_2F_6N_6O_6$: 925.36 m/z; Found 925.36 $[M+H]^+$.

^{1}H NMR: (400 MHz, CD_3OD_3) δ = 7.66 - 7.56 (m, 1H), 7.53 - 7.42 (m, 2H), 7.35 - 7.21 (m, 1H), 5.61 - 5.37 (m, 1H), 5.11 - 5.05 (m, 1H), 4.95 - 4.65 (m, 4H), 4.55 - 4.29 (m, 1H), 4.15 - 4.00 (m, 1H), 3.96 - 3.78 (m, 2H), 3.72 - 3.61 (m, 2H), 3.45 - 3.27 (m, 6H), 3.27 - 3.21 (m, 1H), 3.13 - 3.04 (m, 2H), 3.03 - 2.92 (m, 2H), 2.84 - 2.68 (m, 1H), 2.44 - 2.09 (m, 2H), 1.96 - 1.73 (m, 2H), 1.68 (br s, 13H), 1.11 - 1.02 (m, 2H), 0.99 - 0.95 (m, 2H), 0.92 - 0.87 (m, 1H), 0.86 - 0.77 (m, 2H), 0.76 - 0.47 (m, 4H)

^{13}C NMR (400 MHz, CD_3OD_3) δ = 174.156, 172.13, 171.644, 171.625, 171.105, 170.585, 170.13, 168.836, 165.626, 137.889, 137.441, 132.971, 132.501, 132.395, 132.319, 132.205, 131.863, 131.207, 131.135, 130.615, 128.786, 128.3, 126.362, 118.913, 116.185, 93.096, 91.324, 63.697, 63.663, 60.256, 60.017, 59.557, 59.231, 56.404, 55.831, 54.344, 54.219, 52.762, 52.045, 48.778, 48.531, 48.25, 47.611, 46.971, 46.725, 41.291, 41.029, 40.764, 39.553, 39.436, 39.261, 39.034, 38.491, 37.956, 36.818, 34.966, 31.942, 31.726, 30.189, 30.03, 28.884, 28.368, 28.132, 27.013, 26.436, 26.319, 25.829, 24.6, 24.524, 23.867, 23.773, 23.681, 23.116, 22.923, 22.513, 22.399, 22.228, 22.092, 21.113, 19.64, 19.307, 19.132, 11.999, 11.714, 2.486, 1.989, 1.921, 1.856, 1.207

Final Compounds Made Using Method D

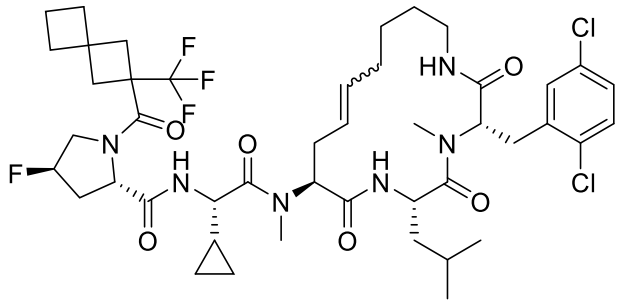

(2S,4R)-N-((S)-1-cyclopropyl-2-(((3S,6S,9S)-3-(2,5-dichlorobenzyl)-6-isobutyl-4-methyl-2,5,8-trioxo-1,4,7-triazacyclohexadec-11-en-9-yl)(methyl)amino)-2-oxoethyl)-4-fluoro-1-(2-(trifluoromethyl)spiro[3.3]heptane-2-carbonyl)pyrrolidine-2-carboxamide (Compound 19) was synthesized using method D using **SI-14** and **SI-9** as starting materials. **Compound 19** was purified using RP-HPLC. **Compound 19** (11.46 mg, 0.012 mmol, 28.0% Yield) was isolated as a

fluffy white solid after lyophilization. Isolated as a~9:1 mixture of E:Z isomers. Major isomer was not elucidated. Data given for major isomer

LCMS: MS (ESI) mass calcd. for $C_{45}H_{61}Cl_2F_4N_6O_6$: 927.3966 m/z; Found 927.3941 $[M+H]^+$.

^{1}H NMR: (400 MHz, 7621) δ 7.68 - 7.55 (m, 1H), 7.55 - 7.45 (m, 1H), 7.39 - 7.21 (m, 1H), 5.74 - 5.58 (m, 1H), 5.57 - 5.36 (m, 2H), 5.36 - 5.23 (m, 1H), 4.90 - 4.69 (m, 3H), 4.64 - 4.54 (m, 1H), 4.34 - 4.00 (m, 2H), 3.95 - 3.75 (m, 2H), 3.73 - 3.63 (m, 2H), 3.43 - 3.24 (m, 3H), 3.01 - 2.90 (m, 5H), 2.81 - 2.61 (m, 4H), 2.45 - 2.04 (m, 8H), 2.03 - 1.89 (m, 3H), 1.88 - 1.54 (m, 6H), 1.53 - 1.28 (m, 3H), 1.19 - 0.95 (m, 6H), 0.93 - 0.64 (m, 5H)

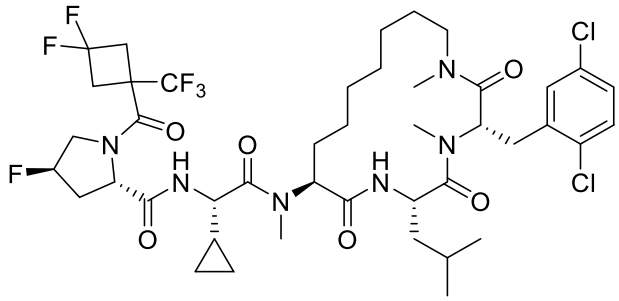

(2S,4R)-N-((S)-1-cyclopropyl-2-(((3S,6S,9S)-3-(2,5-dichlorobenzyl)-6-isobutyl-4-methyl-2,5,8-trioxo-1,4,7-triazacyclohexadec-11-en-9-yl)(methyl)amino)-2-oxoethyl)-1-(3,3-difluoro-1-(trifluoromethyl)cyclobutane-1-carbonyl)-4-fluoropyrrolidine-2-carboxamide (Compound 20): was synthesized using method D using **SI-8** and **SI-14** as starting materials. **Compound 20** was purified using RP-HPLC. **Compound 20** (29.78 mg, 0.032 mmol, 23.3% Yield) was isolated as a fluffy white solid after lyophilization. Isolated as a~9:1 mixture of E:Z isomers. Major isomer was not elucidated. Data given for major isomer

LCMS: MS (ESI) mass calcd. for $C_{42}H_{55}Cl_2F_6N_6O_6$: 923.3464 m/z; Found 923.3491 $[M+H]^+$.

^{1}H NMR: (400 MHz, D_3COD) δ 7.60 - 7.45 (m, 1H), 7.36 - 7.27 (m, 1H), 7.18-7.24 (m, 1H), 7.08 - 6.95 (m, 1H), 5.02 (dd, J = 3.0, 11.8 Hz, 3H), 4.95 (br dd, J = 3.6, 10.8 Hz, 1H), 4.72 - 4.54 (m, 2H), 4.52 - 4.42 (m, 1H), 4.37 (s, 1H), 4.09 - 3.72 (m, 2H), 3.43-3.66 (m, 2H), 3.41 - 3.23 (m, 3H), 3.18 - 2.96 (m, 5H), 2.77 (s, 1H), 2.74 - 2.60 (m, 5H), 2.56 - 2.38 (m, 1H), 2.20 - 1.72 (m, 4H), 1.72 - 1.41 (m, 2H), 1.40 - 1.24 (m, 2H), 1.24 - 1.00 (m, 3H), 0.98 - 0.70 (m, 6H), 0.70 - 0.27 (m, 5H)

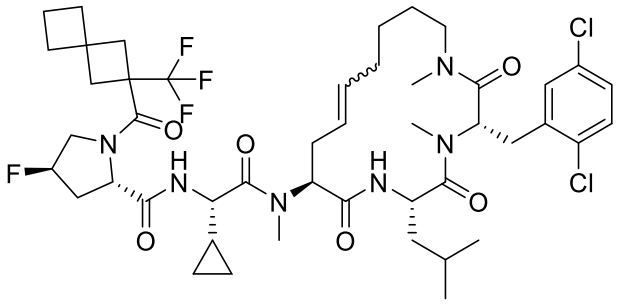

(2S,4R)-N-((S)-1-cyclopropyl-2-(((3S,6S,9S)-3-(2,5-dichlorobenzyl)-6-isobutyl-1,4-dimethyl-2,5,8-trioxo-1,4,7-triazacyclohexadec-11-en-9-yl)(methyl)amino)-2-oxoethyl)-4-fluoro-1-(2-(trifluoromethyl)spiro[3.3]heptane-2-carbonyl)pyrrolidine-2-carboxamide (Compound 21) was synthesized using method D using **SI-15** and **SI-9** as starting materials. **Compound 21** was purified using RP-HPLC. **Compound 21** (23.2 mg, 0.025 mmol, 53.50% Yield) was isolated as a fluffy white solid after lyophilization.

LCMS: MS (ESI) mass calcd. for $C_{46}H_{63}Cl_2F_4N_6O_6$: 941.4122 m/z; Found 941.4153 $[M+H]^+$.

^{1}H NMR: (400 MHz, D_3COD) δ 7.37 - 7.26 (m, 1H), 7.22 - 7.03 (m, 2H), 5.53 - 5.35 (m, 1H), 5.34 - 5.09 (m, 2H), 4.91 (br s, 1H), 4.47 (br s, 2H), 4.42 - 4.32 (m, 1H), 4.31 - 4.25 (m, 1H), 4.24 - 4.09 (m, 1H), 3.94 - 3.72 (m, 1H), 3.65 - 3.45 (m, 1H), 3.32 - 3.24 (m, 1H), 3.18 - 2.92 (m, 4H), 2.91 - 2.81 (m, 3H), 2.80 - 2.59 (m, 6H), 2.55 - 2.35 (m, 5H), 2.10 - 1.81 (m, 8H), 1.43 (br s, 6H), 1.32 - 1.14 (m, 3H), 1.13 - 1.02 (m, 1H), 1.01 - 0.90 (m, 1H), 0.88 - 0.82 (m, 2H), 0.78 (br d, J = 6.4 Hz, 1H), 0.73 - 0.64 (m, 3H), 0.62 - 0.27 (m, 4H)

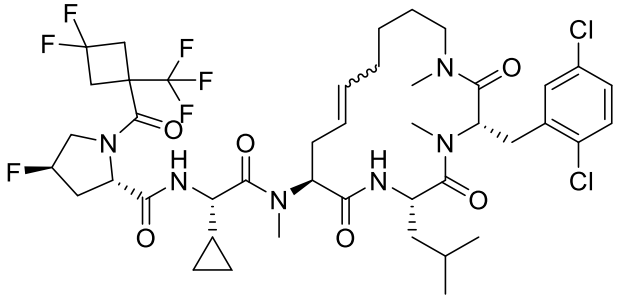

(2S,4R)-N-((S)-1-cyclopropyl-2-(((3S,6S,9S)-3-(2,5-dichlorobenzyl)-6-isobutyl-1,4-dimethyl-2,5,8-trioxo-1,4,7-triazacyclohexadec-11-en-9-yl)(methyl)amino)-2-oxoethyl)-1-(3,3-difluoro-1-(trifluoromethyl)cyclobutane-1-carbonyl)-4-fluoropyrrolidine-2-carboxamide

(Compound 22) was synthesized using method D using **SI-15** and **SI-8** as starting materials. **Compound 22** was purified using RP-HPLC. **Compound 22** (11.66 mg, 0.012 mmol, 28.20% Yield) was isolated as a fluffy white solid after lyophilization.

LCMS: MS (ESI) mass calcd. for $C_{43}H_{57}Cl_2F_6N_6O_6$: 937.3621 m/z; Found 937.3528 $[M+H]^+$.

^{1}H NMR: (400 MHz, D_3COD) δ 8.20 - 7.99 (m, 1H), 7.37 - 7.26 (m, 1H), 7.25 - 7.04 (m, 2H), 5.55 - 5.36 (m, 1H), 5.33 - 5.17 (m, 3H), 4.44 - 4.04 (m, 4H), 3.93 - 3.38 (m, 5H), 3.13 - 3.01 (m, 4H), 2.78 (s, 5H), 2.75 - 2.61 (m, 4H), 2.39 (br s, 2H), 2.15 - 1.95 (m, 2H), 1.92 - 1.78 (m, 1H), 1.71 (br d, J = 14.2Hz, 2H), 1.49 - 1.37 (m, 1H), 1.31 (br s, 8H), 0.94 - 0.60 (m, 7H), 0.58 - 0.25 (m, 3H)

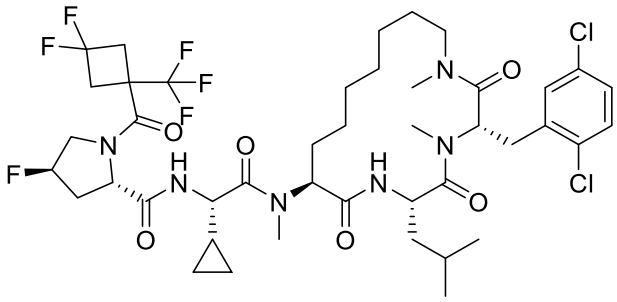

(2S,4R)-N-((S)-1-cyclopropyl-2-(((3S,6S,9S)-3-(2,5-dichlorobenzyl)-6-isobutyl-1,4-dimethyl-2,5,8-trioxo-1,4,7-triazacyclohexadecan-9-yl)(methyl)amino)-2-oxoethyl)-1-(3,3-difluoro-1-(trifluoromethyl)cyclobutane-1-carbonyl)-4-fluoropyrrolidine-2-carboxamide (Compound 24) was synthesized using method D using **SI-23** and **SI-8** as starting materials. **Compound 24** was purified using RP-HPLC. **Compound 24** (22.34 mg, 0.024 mmol, 25.30% Yield) was isolated as a fluffy white solid after lyophilization.

LCMS: MS (ESI) mass calcd. for $C_{43}H_{59}Cl_2F_6N_6O_6$: 939.3777 m/z; Found 939.3799 $[M+H]^+$.

^{1}H NMR: (400 MHz, D_3COD) δ= 7.31 - 7.25 (m, 1H), 7.23 - 7.13 (m, 2H), 5.29 - 5.11 (m, 1H), 4.80 (br s, 2H), 4.71 (br s, 2H), 4.52 (br s, 2H), 4.35 - 4.15 (m, 2H), 3.89 - 3.74 (m, 1H), 3.68 - 3.50 (m, 1H), 3.44 - 3.30 (m, 2H), 3.18 - 2.95 (m, 7H), 2.94 - 2.70 (m, 6H), 2.66 - 2.36 (m, 2H), 2.29 - 1.85 (m, 2H), 1.71 - 1.44 (m, 3H), 1.40 - 0.99 (m, 11H), 0.95 - 0.76 (m, 4H), 0.74 - 0.64 (m, 3H), 0.56 - 0.16 (m, 4H)

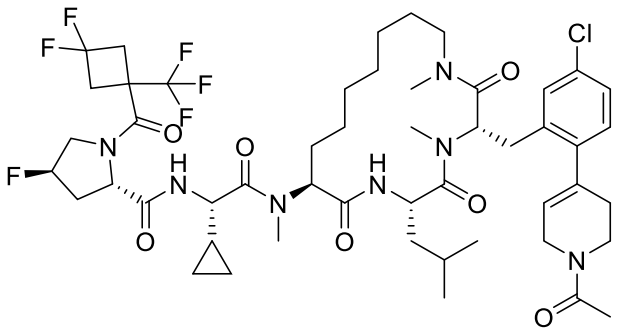

(2S,4R)-N-((S)-2-(((3S,6S,9S)-3-(2-(1-acetyl-1,2,3,6-tetrahydropyridin-4-yl)-5-chlorobenzyl)-6-isobutyl-1,4-dimethyl-2,5,8-trioxo-1,4,7-triazacyclohexadecan-9-yl)(methyl)amino)-1-cyclopropyl-2-oxoethyl)-1-(3,3-difluoro-1-(trifluoromethyl)cyclobutane-1-carbonyl)-4-fluoropyrrolidine-2-carboxamide (Compound 25) was synthesized using method D using **SI-30** and **SI-8** as starting materials. **Compound 25** was purified using RP-HPLC. **Compound 25** (26.32 mg, 0.025 mmol, 20.10% Yield) was isolated as a fluffy white solid after lyophilization.

LCMS: MS (ESI) mass calcd. for $C_{51}H_{68}ClF_6N_7O_7$: 1028.48 m/z; Found 1028.4835 $[M+H]^+$.

^{1}H NMR: (400 MHz, D_3COD) δ = 7.31 - 7.20 (m, 1H), 7.17 (br s, 1H), 7.10 (d, J = 8.2 Hz, 1H), 5.81 (br d, J = 8.4 Hz, 1H), 5.40 - 5.21 (m, 1H), 4.90 (br s, 1H), 4.79 - 4.63 (m, 2H), 4.60 - 4.51 (m, 1H), 4.37 - 4.23 (m, 2H), 4.23 - 4.09 (m, 2H), 4.08 - 3.77 (m, 2H), 3.77 - 3.66 (m, 2H), 3.54 - 3.41 (m, 1H), 3.25 - 3.15 (m, 3H), 3.15 - 3.10 (m, 3H), 3.09 - 3.00 (m, 1H), 2.99 - 2.91 (m, 3H), 2.90 - 2.79 (m, 3H), 2.70 - 2.62 (m, 1H), 2.60 - 2.33 (m, 3H), 2.16 (d, J = 10.8 Hz, 3H), 2.13 - 1.91 (m, 2H), 1.77 - 1.60 (m, 2H), 1.60 - 1.52 (m, 1H), 1.52 - 1.33 (m, 6H), 1.33 - 1.21 (m, 4H), 1.21 - 1.11 (m, 2H), 1.11 - 1.00 (m, 1H), 0.97 (br d, J = 6.2 Hz, 2H), 0.94 - 0.84 (m, 1H), 0.84 - 0.70 (m, 3H), 0.70 - 0.27 (m, 4H)

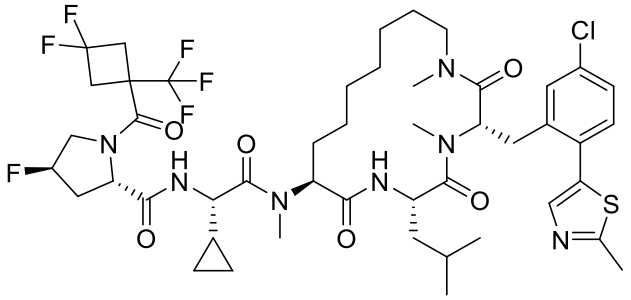

(2S,4R)-N-((S)-2-(((3S,6S,9S)-3-(5-chloro-2-(2-methylthiazol-5-yl)benzyl)-6-isobutyl-1,4-dimethyl-2,5,8-trioxo-1,4,7-triazacyclohexadecan-9-yl)(methyl)amino)-1-cyclopropyl-2-oxoethyl)-1-(3,3-difluoro-1-(trifluoromethyl)cyclobutane-1-carbonyl)-4-fluoropyrrolidine-2-carboxamide (Compound 26) was synthesized using method D using **SI-31** and **SI-8** as starting materials. **Compound 26** was purified using RP-HPLC. **Compound 26** (22 mg, 39 μmol 58% Yield) was isolated as a fluffy white solid after lyophilization.

LCMS: MS (ESI) mass calcd. for $C_{47}H_{63}ClF_6N_7O_6S$: 1002.4153 m/z; Found 1002.4130 $[M+H]^+$.

^{1}H NMR: (400 MHz, D_3COD) δ 7.74 - 7.65 (m, 1H), 7.39 - 7.28 (m, 3H), 5.42 - 5.23 (m, 1H), 4.95 - 4.89 (m, 2H), 4.82 - 4.69 (m, 2H), 4.67 - 4.52 (m, 2H), 4.40 - 4.20 (m, 2H), 4.02 - 3.85 (m, 1H), 3.81 - 3.61 (m, 1H), 3.57 - 3.36 (m, 2H), 3.29 - 3.10 (m, 7H), 2.90 - 2.82 (m, 6H), 2.65 - 2.49 (m, 2H), 2.23 - 1.98 (m, 2H), 1.78 - 1.61 (m, 2H), 1.58 - 1.12 (m, 14H), 1.05 - 0.88 (m, 4H), 0.86 - 0.75 (m, 3H), 0.63 - 0.27 (m, 4H)

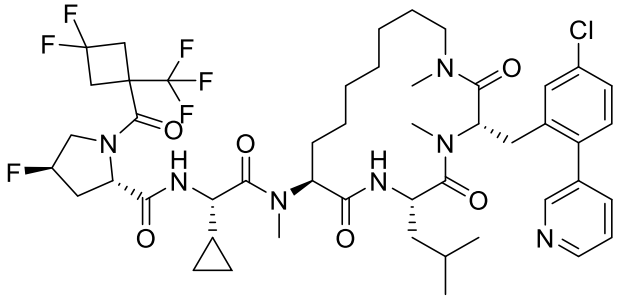

(2S,4R)-N-((S)-2-(((3S,6S,9S)-3-(5-chloro-2-(pyridin-3-yl)benzyl)-6-isobutyl-1,4-dimethyl-2,5,8-trioxo-1,4,7-triazacyclohexadecan-9-yl)(methyl)amino)-1-cyclopropyl-2-oxoethyl)-1-(3,3-difluoro-1-(trifluoromethyl)cyclobutane-1-carbonyl)-4-fluoropyrrolidine-2-carboxamide (Compound 27) was synthesized using method D using **SI-32** and **SI-8** as starting

materials. **Compound 27** was purified using RP-HPLC. **Compound 27** (36.17 mg, 0.037 mmol, 45.80% Yield) was isolated as a fluffy white solid after lyophilization.

LCMS: MS (ESI) mass calcd. for $C_{48}H_{63}ClF_6N_7O_6$: 982.4433 m/z; Found 982.4423 $[M+H]^+$.

^{1}H NMR: (400 MHz, D_3COD) δ 8.72 - 8.55 (m, 2H), 8.41 - 8.25 (m, 1H), 8.00 - 7.91 (m, 1H), 7.61 - 7.50 (m, 1H), 7.44 - 7.29 (m, 2H), 7.27 - 7.18 (m, 1H), 5.43 - 5.21 (m, 1H), 4.77 - 4.65 (m, 1H), 4.70 - 4.45 (m, 1H), 4.37 (br s, 1H), 4.03 - 3.84 (m, 1H), 3.81 - 3.60 (m, 1H), 3.54 - 3.42 (m, 1H), 3.26 - 3.07 (m, 7H), 2.92 - 2.73 (m, 6H), 2.64 - 2.48 (m, 2H), 2.27 - 1.90 (m, 2H), 1.77 - 1.60 (m, 2H), 1.56 (br s, 1H), 1.04 - 0.87 (m, 4H), 0.84 - 0.73 (m, 3H), 0.71 - 0.28 (m, 4H)

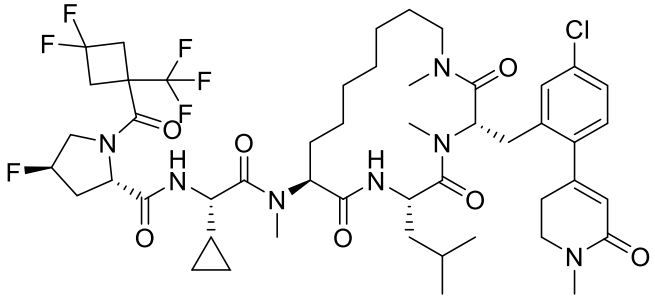

(2S,4R)-N-((S)-2-(((3S,6S,9S)-3-(5-chloro-2-(1-methyl-6-oxo-1,2,3,6-tetrahydropyridin-4-yl)benzyl)-6-isobutyl-1,4-dimethyl-2,5,8-trioxo-1,4,7-triazacyclohexadecan-9-yl)(methyl)amino)-1-cyclopropyl-2-oxoethyl)-1-(3,3-difluoro-1-(trifluoromethyl)cyclobutane-1-carbonyl)-4-fluoropyrrolidine-2-carboxamide (Compound 28) was synthesized using method D using **SI-34** and **SI-8** as starting materials. **Compound 28** was purified using RP-HPLC. **Compound 28** (57.61 mg, 0.057 mmol, 57.60% Yield) was isolated as a fluffy white solid after lyophilization.

LCMS: MS (ESI) mass calcd. for $C_{49}H_{67}ClF_6N_7O_7$: 1014.4695 m/z; Found 1014.4672 $[M+H]^+$.

^{1}H NMR: (400 MHz, D_3COD) δ 8.45 - 8.31 (m, 1H), 7.40 - 7.27 (m, 2H), 7.23 - 7.13 (m, 1H), 5.98 - 5.88 (m, 1H), 5.44 - 5.19 (m, 1H), 4.95 - 4.90 (m, 1H), 4.78 - 4.69 (m, 1H), 4.63 - 4.53 (m, 2H), 4.43 - 4.24 (m, 2H), 4.02 - 3.83 (m, 1H), 3.79 - 3.59 (m, 3H), 3.53 - 3.43 (m, 1H), 3.29 - 3.14 (m, 5H), 3.03 (s, 6H), 3.01 - 2.89 (m, 6H), 2.86 - 2.77 (m, 3H), 2.64 - 2.49 (m, 1H), 2.20 - 2.01 (m, 2H), 1.72 - 1.15 (m, 15H), 1.05 - 0.88 (m, 4H), 0.85 - 0.74 (m, 3H), 0.68 - 0.31 (m, 4H)

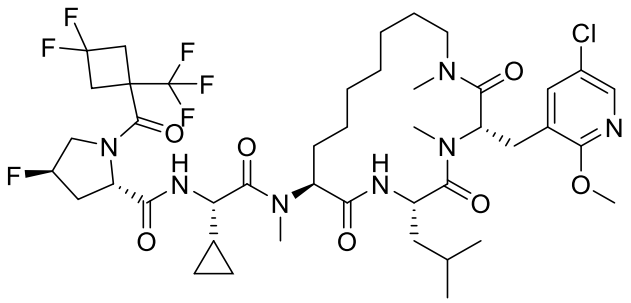

(2S,4R)-N-((S)-2-(((3S,6S,9S)-3-((5-chloro-2-methoxypyridin-3-yl)methyl)-6-isobutyl-1,4-dimethyl-2,5,8-trioxo-1,4,7-triazacyclohexadecan-9-yl)(methyl)amino)-1-cyclopropyl-2-oxoethyl)-1-(3,3-difluoro-1-(trifluoromethyl)cyclobutane-1-carbonyl)-4-fluoropyrrolidine-2-carboxamide (Compound 29) was synthesized using method D using **SI-25** and **SI-8** as starting materials. **Compound 29** was purified using RP-HPLC. **Compound 29** (59.95 mg, 0.064 mmol, 31.40% Yield) was isolated as a fluffy white solid after lyophilization.

LCMS: MS (ESI) mass calcd. for $C_{43}H_{61}ClF_6N_7O_7$: 936.4225 m/z; Found 936.4215 $[M+H]^+$.

^{1}H NMR: (400 MHz, D_3COD) δ 8.03 (d, J = 2.5 Hz, 1H), 7.56 - 7.45 (m, 1H), 5.41 - 5.24 (m, 1H), 4.99 - 4.94 (m, 1H), 4.73 (br t, J = 8.7 Hz, 1H), 4.65 - 4.53 (m, 3H), 4.45 - 4.28 (m, 2H), 4.07 - 3.86 (m, 4H), 3.43 (br d, J = 4.9 Hz, 3H), 3.23 - 3.09 (m, 7H), 3.05 - 2.80 (m, 7H), 2.65 - 2.46 (m, 1H), 2.22 - 1.95 (m, 2H), 1.79 - 1.54 (m, 3H), 1.47 - 1.29 (m, 9H), 1.26 - 1.12 (m, 3H), 0.98 - 0.75 (m, 7H), 0.65 - 0.43 (m, 3H), 0.37 - 0.28 (m, 1H)

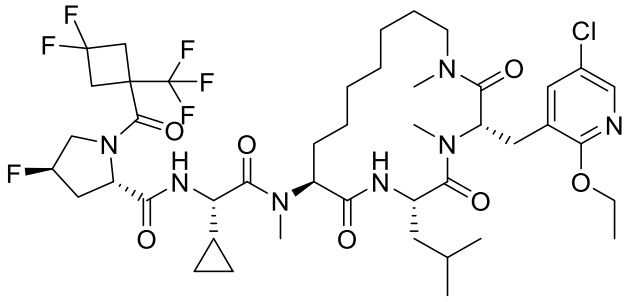

(2S,4R)-N-((S)-2-(((3S,6S,9S)-3-((5-chloro-2-ethoxypyridin-3-yl)methyl)-6-isobutyl-1,4-dimethyl-2,5,8-trioxo-1,4,7-triazacyclohexadecan-9-yl)(methyl)amino)-1-cyclopropyl-2-oxoethyl)-1-(3,3-difluoro-1-(trifluoromethyl)cyclobutane-1-carbonyl)-4-fluoropyrrolidine-

2-carboxamide (Compound 30) was synthesized using method D using **SI-27** and **SI-8** as starting materials. **Compound 30** was purified using RP-HPLC. **Compound 30** (61.87 mg, 0.065 mmol, 33.10% Yield) was isolated as a fluffy white solid after lyophilization.

LCMS: MS (ESI) mass calcd. for $C_{44}H_{63}ClF_6N_7O_7$: 950.4382 m/z; Found 950.4404 $[M+H]^+$.

^{1}H NMR: (400 MHz, D_3COD) δ 8.20 - 7.95 (m, 1H), 7.65 - 7.42 (m, 1H), 5.43 - 5.21 (m, 1H), 4.96 - 4.93 (m, 1H), 4.73 (br t, J = 8.6 Hz, 1H), 4.64 - 4.54 (m, 3H), 4.47 - 4.27 (m, 4H), 4.00 - 3.83 (m, 1H), 3.78 - 3.59 (m, 1H), 3.57 - 3.41 (m, 2H), 3.21 (br d, J = 3.9 Hz, 7H), 3.02 - 2.81 (m, 7H), 2.65 - 2.50 (m, 1H), 2.24 - 1.98 (m, 2H), 1.74 - 1.54 (m, 3H), 1.52 - 1.42 (m, 7H), 1.40 - 1.28 (m, 5H), 1.25 - 1.16 (m, 2H), 1.01 - 0.78 (m, 7H), 0.61 - 0.28 (m, 4H)

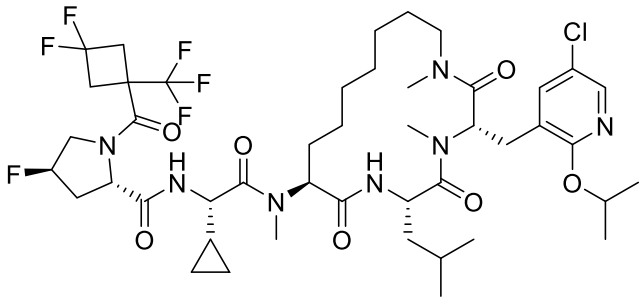

(2S,4R)-N-((S)-2-(((3S,6S,9S)-3-((5-chloro-2-isopropoxypyridin-3-yl)methyl)-6-isobutyl-1,4-dimethyl-2,5,8-trioxo-1,4,7-triazacyclohexadecan-9-yl)(methyl)amino)-1-cyclopropyl-2-oxoethyl)-1-(3,3-difluoro-1-(trifluoromethyl)cyclobutane-1-carbonyl)-4-fluoropyrrolidine-2-carboxamide (Compound 31) was synthesized using method D using **SI-26** and **SI-8** as starting materials. **Compound 31** was purified using RP-HPLC. **Compound 31** (34.54 mg, 0.035 mmol, 27.3% Yield) was isolated as a fluffy white solid after lyophilization.

LCMS: MS (ESI) mass calcd. for $C_{45}H_{65}ClF_6N_7O_7$: 964.4538 m/z; Found 964.4506 $[M+H]^+$.

^{1}H NMR: (400 MHz, D_3COD) δ 8.45 - 8.29 (m, 1H), 8.11 - 7.91 (m, 1H), 7.64 - 7.32 (m, 1H), 5.45 - 5.21 (m, 2H), 4.95 - 4.90 (m, 1H), 4.76 - 4.70 (m, 1H), 4.66 - 4.53 (m, 2H), 4.45 - 4.29 (m, 2H), 4.01 - 3.84 (m, 1H), 3.80 - 3.39 (m, 2H), 3.02 (br d, J = 6.8 Hz, 8H), 2.99 - 2.80 (m, 6H), 2.78 (s, 1H), 2.63 - 2.51 (m, 1H), 2.21 - 1.98 (m, 2H), 1.74 - 1.53 (m, 3H), 1.49 - 1.14 (m, 17H), 1.03 - 0.87 (m, 4H), 0.84 - 0.77 (m, 3H), 0.67 - 0.29 (m, 4H)

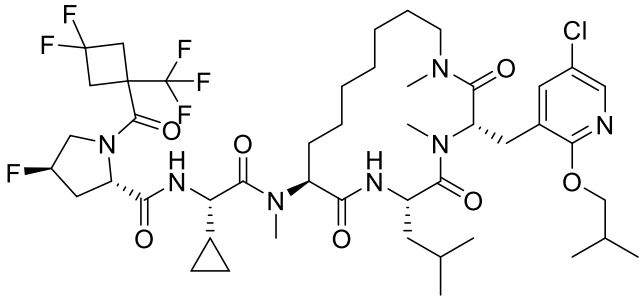

(2S,4R)-N-((S)-2-(((3S,6S,9S)-3-((5-chloro-2-isobutoxypyridin-3-yl)methyl)-6-isobutyl-1,4-dimethyl-2,5,8-trioxo-1,4,7-triazacyclohexadecan-9-yl)(methyl)amino)-1-cyclopropyl-2-oxoethyl)-1-(3,3-difluoro-1-(trifluoromethyl)cyclobutane-1-carbonyl)-4-fluoropyrrolidine-2-carboxamide (Compound 32) was synthesized using method D using **SI-28** and **SI-8** as starting materials. **Compound 32** was purified using RP-HPLC. **Compound 32** (55.65 mg, 0.057 mmol, 29.10% Yield) was isolated

LCMS: MS (ESI) mass calcd. for $C_{46}H_{67}ClF_6N_7O_7$: 978.4695 m/z; Found 978.4709 $[M+H]^+$.

^{1}H NMR: (400 MHz, D_3COD) δ 8.13 - 7.93 (m, 1H), 7.59 - 7.44 (m, 1H), 5.44 - 5.23 (m, 1H), 4.94 - 4.90 (m, 1H), 4.77 - 4.69 (m, 1H), 4.66 - 4.54 (m, 2H), 4.40 - 4.26 (m, 2H), 4.23 - 4.07 (m, 2H), 3.98 - 3.84 (m, 1H), 3.79 - 3.59 (m, 1H), 3.56 - 3.40 (m, 1H), 3.24 - 3.07 (m, 7H), 3.03 (s, 7H), 2.64 (br s, 1H), 2.25 - 2.01 (m, 3H), 1.72 - 1.53 (m, 3H), 1.50 - 1.16 (m, 12H), 1.12 - 1.03 (m, 6H), 1.00 - 0.87 (m, 4H), 0.85 - 0.72 (m, 3H), 0.63 - 0.28 (m, 4H)

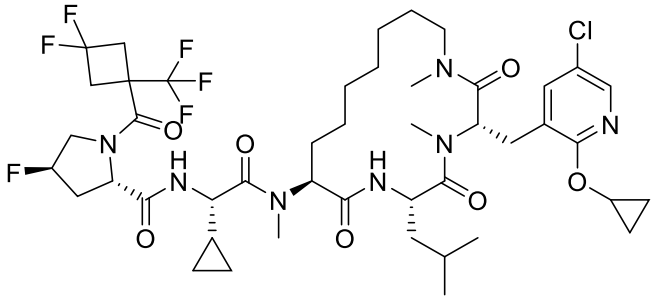

(2S,4R)-N-((S)-2-(((3S,6S,9S)-3-((5-chloro-2-cyclopropoxypyridin-3-yl)methyl)-6-isobutyl-1,4-dimethyl-2,5,8-trioxo-1,4,7-triazacyclohexadecan-9-yl)(methyl)amino)-1-cyclopropyl-2-oxoethyl)-1-(3,3-difluoro-1-(trifluoromethyl)cyclobutane-1-carbonyl)-4-fluoropyrrolidine-2-carboxamide (Compound 33) was synthesized using method D using **SI-29** and **SI-8** as starting

materials. **Compound 33** was purified using RP-HPLC. **Compound 33** (24.3 g, 25.3 mmol, 37% yield) was isolated as a fluffy white solid after lyophilization.

LCMS: MS (ESI) mass calcd. for $C_{45}H_{63}ClF_6N_7O_7$: 962.4382 m/z; Found 962.4399 $[M+H]^+$.

^{1}H NMR: (400 MHz, D_3COD) δ 8.09 (d, J=2.4 Hz, 0.3H, active hydrogen that has not been completely exchanged), 7.79 (d, J=3.2 Hz, 1H), 7.30 (d, J=3.6 Hz, 1H), 5.08 (d, J=23.6 Hz, 1H), 4.67 (s, 1H), 4.37-4.60 (m, 2H), 4.35 - 4.28 (m, 1H), 4.26 - 4.01 (m, 3H), 3.78 - 3.59 (m, 1H), 3.57 - 3.35 (m, 1H), 3.32 - 3.12 (m, 1H), 3.06 - 2.85 (m, 6H), 2.85 - 2.78 (m, 1H), 2.77 - 2.53 (m, 7H), 2.50 - 2.23 (m, 2H), 2.09 - 1.70 (m, 2H), 1.49 - 1.27 (m, 3H), 1.27 - 0.86 (m, 11H), 0.48 (br s, 11H), 0.43 - 0.04 (m, 4H).

^{13}C NMR: (101 MHz, D_3COD) δ 172.088, 172.046, 171.913, 171.769, 171.583, 171.447, 171.143, 171.01, 169.671, 169.413, 169.352, 165.622, 165.413, 161.365, 143.061, 139.729, 139.274, 127.28, 127.242, 124.491, 124.457, 123.884, 122.317, 121.71, 118.947, 116.223, 113.499, 93.138, 93.02, 91.362, 91.241, 59.573, 59.079, 56.473, 56.203, 55.911, 54.67, 54.454, 54.253, 52.891, 52.174, 50.99, 50.371, 48.322, 47.894, 47.681, 47.469, 47.044, 42.031, 41.933, 41.891, 41.796, 41.743, 41.644, 41.602, 41.504, 41.314, 41.064, 40.809, 39.607, 39.345, 39.083, 38.863, 35.072, 34.981, 34.852, 34.765, 34.533, 34.446, 30.121, 29.373, 28.576, 27.863, 26.22, 25.734, 25.275, 24.471, 23.64, 23.439, 23.131, 22.577, 22.467, 22.278, 22.266, 22.133, 20.631, 20.547, 19.88, 12.83, 12.082, 11.813, 5.074, 4.918, 2.812, 2.228, 2.152, 1.962, 1.386

Biochemical Probe Synthesis

Synthesis of fluorescence polarization probe ("FP-2") performed as previously described.[1]

Synthesis of FP2 Probe:

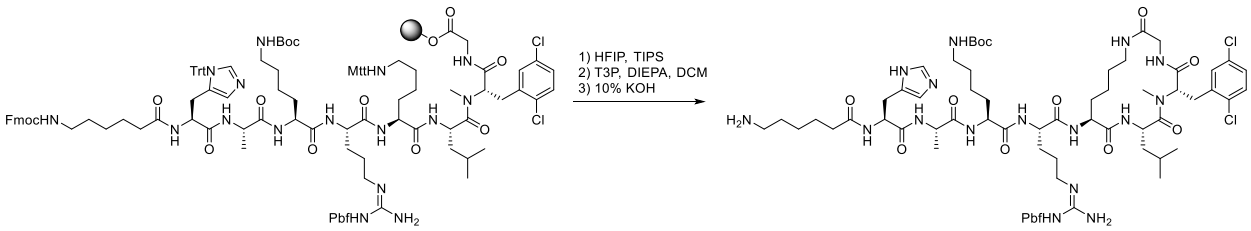

tert-butyl ((S)-6-(((S)-5-(((Z)-amino((2,2,4,6,7-pentamethyl-2,3-dihydrobenzofuran)-5-sulfonamido)methylene)amino)-1-(((6S,9S,12S)-6-(2,5-dichlorobenzyl)-9-isobutyl-7-methyl-2,5,8,11-tetraoxo-1,4,7,10-tetraazacyclohexadecan-12-yl)amino)-1-oxopentan-2-yl)amino)-

5-((S)-2-((S)-2-(6-aminohexanamido)-3-(1H-imidazol-5-yl)propanamido)propanamido)-6-oxohexyl)carbamate: The FP2 Probe Linear Intermediate in **Table 2b** with Fmoc-Ahx still intact was cleaved from the solid phase with a 2 mL solution of 24% HFIP, 2% TIPS, in DCM. The material was concentrated under reduced pressure and purified via reverse-phase chromatography to yield a white powder. **LCMS:** MS (ESI) mass calcd. For cleaved linear intermediate $C_{103}H_{132}Cl_2N_{16}O_{17}S$ 1966.91 m/z found 1968.65 $[M+H]^+$.

The deprotected and purified linear product was transferred to a 50 mL conical vial and dissolved in 1 mL NMP followed by the addition of DIEA (0.5 mL) and DCM (35 mL). T3P (3 eqv) was added to the solution and the reaction pH was adjusted to pH 9 via dropwise addition of DIPEA. The closed conical vial was agitated at room temperature for 2 hours at 150 rotations per minute. The solution was concentrated at 45°C under reduced pressure in a Genevac system. The Fmoc group was then removed with the addition of a 10% of KOH/Water solution (5 mL) heated at 70°C for 30 minutes. The resulting LCMS trace revealed that the trityl group had been unexpectedly removed during the cyclization and Fmoc-deprotection steps. The cyclic peptide was then purified via reverse phase HPLC using an Acetonitrile/Water gradient with 0.05% formic acid. The purified fractions were pooled and lyophilized. **LCMS:** MS (ESI) mass calcd. For $C_{69}H_{106}Cl_2N_{16}O_{14}S$ 1484.72 m/z found 1485.94 $[M+H]^+$.

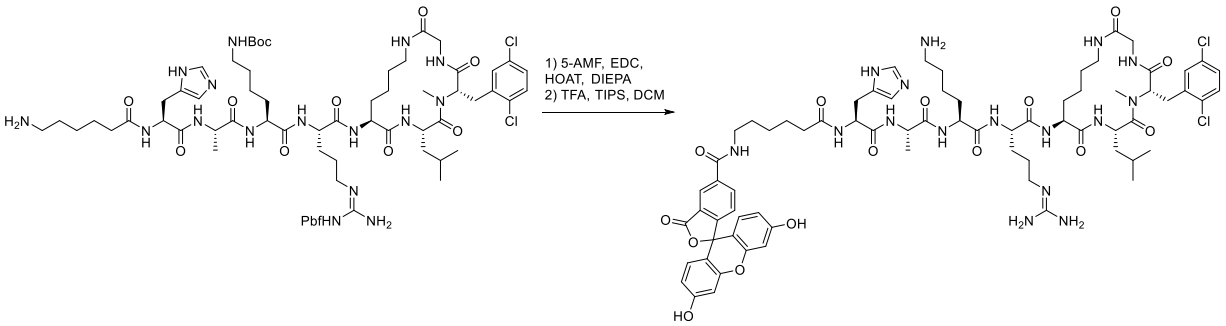

N-((6S,9S,12S,15S)-15-((1H-imidazol-5-yl)methyl)-1,1-diamino-9-(4-aminobutyl)-6-(((6S,9S,12S)-6-(2,5-dichlorobenzyl)-9-isobutyl-7-methyl-2,5,8,11-tetraoxo-1,4,7,10-tetraazacyclohexadecan-12-yl)carbamoyl)-12-methyl-8,11,14,17-tetraoxo-2,7,10,13,16-pentaazadocos-1-en-22-yl)-3',6'-dihydroxy-3-oxo-3H-spiro[isobenzofuran-1,9'-xanthene]-5-carboxamide (FP2 Probe): The probe was fluorescently labeled via a peptide coupling in solution. A solution of 5-carboxyfluorescein (4 Equiv.), EDC (4 Equiv.), HOAt (3.9 Equiv.) and DIPEA (8 Equiv.) in 1.0 mL of anhydrous DCM was prepared. The mixture was allowed to pre-

activate at room temperature for 5 minutes. The macrocycle with free N-terminal amine was added to the coupling solution, and the reaction was agitated at room temperature until starting material was not observed by LCMS.

LCMS: MS (ESI) mass calcd. For $C_{90}H_{116}Cl_2N_{16}O_{20}S$ 1842.76 m/z found 1844.29 $[M+H]^+$.
The Boc and Pbf protecting groups were removed by dissolving the cyclic peptide in a 1 mL solution of 90% TFA, 5% TIPS, 5% DCM and agitating for 1 hour. The reaction was monitored by LCMS for the disappearance of starting material. Upon completion, the reaction was concentrated. The crude material was co-evaporated with DCE (5 mL x 2), and then purified via reverse phase-HPLC to yield **FP2 Probe** (0.7 mg, >99% purity by UV). **LCMS:** MS (ESI) mass calcd. For $C_{72}H_{92}Cl_2N_{16}O_{15}$ 1490.63 m/z found 1493.4 $[M+H]^+$.

DMPK Assays

MDCK-MDR1 Permeability: Cell-based compound permeability was measured in Madin Darby Canine Kidney (MDCK) cells transfected with the human MDR1 gene, which encoded the P-glycoprotein (P-gp) efflux transporter. In this experiment, MDCK-MDR1 cells were plated into 96-well plates at 7,500 cells per well (75 µL) and incubated for three days at 37ºC with 5% CO2. Cells were washed with Hank's Balanced Salt Solution (HBSS) with 5 mM HEPES for 30 minutes before starting the experiment. Test compound solutions were prepared by diluting DMSO stock into HBSS buffer with 10 µM of P-gp inhibitor Elacridar, resulting in a final test compound concentration at 6 µM with final DMSO concentration of 0.2% (v/v). Prior to the experiment, cell monolayer integrity is verified by transendothelial electrical resistance (TEER). Transport experiment was initiated by adding test compounds to the apical (75 µL) side and blank HBSS buffer with Elacridar in the basolateral (250 µL) side. Assay is carried out in duplicate. Transport plates were incubated at 37ºC for one hour in a humidified incubator with 5% CO2. Samples were taken from the apical and basolateral compartments after one hour and analyzed by liquid chromatography with tandem mass spectrometry (LC/MS/MS). Cyclosporin was used as a reference control. Apparent permeability (Papp) values are calculated using the following equation

$$Papp = (dQ/dt)/A/C0$$

Where dQ/dt is the initial rate of amount of test compound transported across cell monolayer, A is the surface area of the filter membrane, and C0 is the initial concentration of the test compound, calculated for each direction using a 4-point calibration curve by LC/MS/MS. All samples were analyzed on LC/MS/MS using an AB Sciex API 4000 instrument, coupled to a Shimadzu LC-20AD LC Pump system. Analytical samples were separated using a Waters Atlantis T3 dC18 reverse phase HPLC column (20 mm x 2.1 mm) at a flow rate of 0.5 mL/min. The mobile phase consists of 0.1% formic acid in water (solvent A) and 0.1% formic acid in 100% acetonitrile (solvent B).

Plasma Protein Binding: Plasma protein binding was evaluated using ultracentrifugation method. Mouse plasma (K2-EDTA) was obtained from BioIVT, pH was adjusted to 7.4 before the assay. Test compounds in DMSO stock solution at 1 mM were spiked into the plasma to make a final concentration of 2 μM and incubate for 30 minutes at 37°C prior to the centrifugation. An equal volume of blank phosphate buffer saline (PBS) was added to the plate to make the matrix at 50:50 plasma: buffer. Spiked plasma was transferred (200 μL/tube) to four centrifuge tubes (Polycarbonate, 7x20 mm, Beckman Coulter, Inc., Brea, CA). Two tubes were used for actual ultracentrifugation samples and two other tubes are used for reference samples. Actual samples were centrifuged at 85,000 rpm (346,000 xg) for 4 hours at 37ºC, while the reference samples were incubated at 37°C for 4 hours. After 4 hours, gently mix the reference samples. The supernatants (30 μL) were removed from the two replicate samples and the mixed reference samples (30 uL) were removed from the two mixed reference samples. The supernatant and mixed plasma samples were diluted with an equal volume of blank plasma and pH 7.4 PBS, respectively. At last, 150 μL of quench solution (50% acetonitrile, 50% methanol and 0.05% formic acid) containing internal standards (bucetin) was added to each well. Plates were sealed and vortex for 20 minutes, then centrifuged at 4°C for 15 minutes at 4,000 rpm (163,000 xg). The supernatant was transferred to fresh plates for LC/MS/MS analysis. Reference compound propranolol was included in every experiment. All samples were analyzed on LC/MS/MS using an AB Sciex API 4000 instrument, coupled to a Shimadzu LC-20AD LC Pump system. Analytical samples were separated using a Waters Atlantis T3 dC18 reverse phase HPLC column (20 mm x 2.1 mm) at a flow rate of 0.5 mL/min. The mobile phase consisted of 0.1% formic acid in water (solvent A) and 0.1% formic acid in acetonitrile (solvent B).

The percentage of test compound bound to protein was calculated by the following equation:

% Free = (Concentration of supernatant/Concentration of reference plasma) × 100%

% Bound = 100% - % Free

Kinetic Solubility: Kinetic solubility was measured based on samples supplied in DMSO solution. Test compounds at 10 mM in DMSO were diluted with PBS buffer (pH 7.4) resulting in a final DMSO concentration of 5% and mixed by shaking for 1.5 hours at room temperature followed by vacuum filtration. The samples were then assayed via reverse phase HPLC with UV detection. Quantitation was achieved by reference to a three-point standard curve constructed via serial dilution of drug substance dissolved in 100% DMSO. Amiodarone and testosterone were used as reference controls.

Met ID of Compound 2

Metabolite Identification: Metabolite identification was performed using mouse plasma samples pooled from mouse samples collected between 5 min to 1 hour post an Intravenous (IV) dose at 5 mg/kg. 25 µL of blood was taken from each mouse. 60 µL of pooled mouse sample was precipitated with 120 µL of Acetonitrile (ACN) following by vigorous vortex mixing for 5 minutes. The samples were then centrifuged at 4°C, 20,000 g for 30 minutes. The clear supernatant was collected and transferred prior to liquid chromatography – high resolution mass spectrometry (LC-HRMS) analysis. 15 µL of sample was injected, with autosampler temperature at 5°C. The metabolite profiling was performed using LC-HRMS. 0.1% (v/v) Formic Acid in purified water was used as mobile phase A, and pure ACN was used as mobile phase B for the LC. Thermo Accucore C18, 2.1 × 150 mm, 2.6 µm column was used with column compartment temperature at 40°C. The LC gradient started with 10% B from 0 to 0.3 minutes and gradually increased to 50% B from 0.3 to 10.5 minutes, followed by increasing from 50% to 90% from 10.5 to 14 minutes. Then the gradient was held at 90% B for 4 minutes, and re-equilibration back to 10%B from 18 minutes to 22 minutes. A full MS scan from 100 to 1500 m/z in both positive and negative mode was performed. Data dependent-MS^2 (tandem mass spectrometry) was performed with stepped collision energy (CE) at 10, 25, and 40V.

Compound 2 was dosed in mouse at 5 mg/kg IV, and mouse blood samples were collected and pooled from 5 min to 1 hour post dose to perform metabolite identification analysis. The parent

compound 2, and its metabolites were detected in positive mode using liquid chromatography – high resolution mass spectrometry (LC-HRMS). Based on relative MS abundance (calculated based on MS peak area), 90.6% of parent compound 2 was observed. 2 was observed as $[M+H]^+$ at 15.1 min. Oxidation metabolite of compound 2 M988 with the relative abundance of 2.5%, was observed as $[M+H]^+$ at retention time 13.2 minutes. Its isomer, M988-Isomer with the relative abundance of 1.3%, was observed as $[M+H]^+$ at retention time 13.3 minutes. An unknown peak, with m/z same as the parent compound, was observed at retention time of 14 minutes.

In Vitro Safety Panels

KINOMEscan™ Profiling Assay conducted by Eurofins

Compound **33** was tested in this panel of 468 kinase assays using standard conditions to identify potential off-target activity.

Protocol Description for Kinase Assays.

For most assays, kinase-tagged T7 phage strains were grown in parallel in 24-well blocks in an E. coli host derived from the BL21 strain. E. coli were grown to log-phase and infected with T7 phage from a frozen stock (multiplicity of infection = 0.4) and incubated with shaking at 32°C until lysis (90-150 minutes). The lysates were centrifuged (6,000 x g) and filtered (0.2µm) to remove cell debris. The remaining kinases were produced in HEK-293 cells and subsequently tagged with DNA for qPCR detection. Streptavidin-coated magnetic beads were treated with biotinylated small molecule ligands for 30 minutes at room temperature to generate affinity resins for kinase assays. The liganded beads were blocked with excess biotin and washed with blocking buffer (SeaBlock (Pierce), 1 % BSA, 0.05 % Tween 20, 1 mM DTT) to remove unbound ligand and to reduce non-specific phage binding. Binding reactions were assembled by combining kinases, liganded affinity beads, and test compounds in 1x binding buffer (20 % SeaBlock, 0.17x PBS, 0.05 % Tween 20, 6 mM DTT). Test compounds were prepared as 40x stocks in 100% DMSO and directly diluted into the assay. All reactions were performed in polypropylene 384-well plates in a final volume of 0.02 ml. The assay plates were incubated at room temperature with shaking for 1 hour and the affinity beads were washed with wash buffer (1x PBS, 0.05 % Tween 20). The beads were then re-suspended in elution buffer (1x PBS, 0.05

% Tween 20, 0.5 µM non-biotinylated affinity ligand) and incubated at room temperature with shaking for 30 minutes. The kinase concentration in the eluates was measured by qPCR. Confidential CIR001-01-p-00001 9/20/2021 2 of 19 Percent Control (%Ctrl). The compound(s) were screened at the concentration(s) requested, and results for primary screen binding interactions are reported as '% Ctrl', where lower numbers indicate stronger hits in the matrix on the following page(s).

Percent Control (%Ctrl) Calculation:

$$\text{Percent Control (\%Ctrl)} = \left(\frac{\text{Test compound signal} - \text{positive control signal}}{\text{Negative control signal} - \text{positive control signal}} \right) \text{X } 100$$

Where:

test compound = compound submitted by Circle Pharma Inc

negative control = DMSO (100%Ctrl)

positive control = control compound (0%Ctrl)

Table S4. Results from KINOMEscan™ Profiling Assay with Compound 33 at 1 µM and 10 µM test concentrations Target Gene Symbol	**%Control at 1 µM**	**%Control at 10 µM**
AAK1	100	100
ABL1(E255K)-phosphorylated	92	100
ABL1(F317I)-nonphosphorylated	100	94
ABL1(F317I)-phosphorylated	81	93
ABL1(F317L)-nonphosphorylated	100	100
ABL1(H396P)-nonphosphorylated	87	92
ABL1(H396P)-phosphorylated	91	100
ABL1(M351T)-phosphorylated	75	82
ABL1(Q252H)-nonphosphorylated	82	83
ABL1(Q252H)-phosphorylated	100	100

Table S4. Results from KINOMEscan™ Profiling Assay with Compound 33 at 1 µM and 10 µM test concentrations **Target Gene Symbol**	**%Control at 1 µM**	**%Control at 10 µM**
ABL1(T315I)-nonphosphorylated	100	93
ABL1(T315I)-phosphorylated	83	85
ABL1(Y253F)-phosphorylated	100	100
ABL1-nonphosphorylated	83	84
ABL1-phosphorylated	100	100
ABL2	100	100
ACVR1	100	100
ACVR1B	83	100
ACVR2A	88	100
ACVR2B	72	98
ACVRL1	100	100
ADCK3	100	99
ADCK4	100	87
AKT1	87	95
AKT2	100	100
AKT3	100	98
ALK	89	99
ALK(C1156Y)	53	60
ALK(L1196M)	71	76
AMPK-alpha1	100	64
AMPK-alpha2	100	96
ANKK1	92	68
ARK5	99	93
ASK1	100	100
ASK2	90	100
AURKA	91	83
AURKB	95	90
AURKC	100	100

Table S4. Results from KINOMEscan™ Profiling Assay with Compound 33 at 1 µM and 10 µM test concentrations **Target Gene Symbol**	**%Control at 1 µM**	**%Control at 10 µM**
AXL	100	100
BIKE	100	100
BLK	100	100
BMPR1A	100	96
BMPR1B	72	72
BMPR2	79	61
BMX	100	88
BRAF	100	93
BRAF(V600E)	98	88
BRK	85	86
BRSK1	100	79
BRSK2	88	98
BTK	100	100
BUB1	92	88
CAMK1	100	100
CAMK1B	100	100
CAMK1D	100	100
CAMK1G	100	100
CAMK2A	100	100
CAMK2B	100	100
CAMK2D	100	100
CAMK2G	97	100
CAMK4	100	100
CAMKK1	93	100
CAMKK2	94	100
CASK	85	100
CDC2L1	92	83
CDC2L2	88	95

Table S4. Results from KINOMEscan™ Profiling Assay with Compound 33 at 1 µM and 10 µM test concentrations **Target Gene Symbol**	**%Control at 1 µM**	**%Control at 10 µM**
CDC2L5	76	80
CDK11	95	89
CDK2	100	100
CDK3	90	100
CDK4	100	91
CDK4-cyclinD1	99	100
CDK4-cyclinD3	73	82
CDK5	92	99
CDK7	70	100
CDK8	88	90
CDK9	100	81
CDKL1	100	96
CDKL2	100	97
CDKL3	97	77
CDKL5	100	100
CHEK1	100	100
CHEK2	92	95
CIT	100	100
CLK1	88	100
CLK2	100	100
CLK3	82	100
CLK4	100	96
CSF1R	100	80
CSF1R-autoinhibited	100	100
CSK	90	99
CSNK1A1	85	58
CSNK1A1L	100	100
CSNK1D	100	100

Table S4. Results from KINOMEscan™ Profiling Assay with Compound 33 at 1 µM and 10 µM test concentrations **Target Gene Symbol**	**%Control at 1 µM**	**%Control at 10 µM**
CSNK1E	100	100
CSNK1G1	100	86
CSNK1G2	85	100
CSNK1G3	100	100
CSNK2A1	73	80
CSNK2A2	82	83
CTK	100	88
DAPK1	97	100
DAPK2	100	100
DAPK3	100	100
DCAMKL1	86	74
DCAMKL2	82	93
DCAMKL3	100	100
DDR1	100	100
DDR2	100	100
DLK	62	79
DMPK	100	100
DMPK2	100	92
DRAK1	99	100
DRAK2	100	100
DYRK1A	100	100
DYRK1B	100	100
DYRK2	100	81
EGFR	100	100
EGFR(E746-A750del)	100	93
EGFR(G719C)	100	100
EGFR(G719S)	100	100
EGFR(L747-E749del, A750P)	100	92

Table S4. Results from KINOMEscan™ Profiling Assay with Compound 33 at 1 µM and 10 µM test concentrations **Target Gene Symbol**	**%Control at 1 µM**	**%Control at 10 µM**
EGFR(L747-S752del, P753S)	97	100
EGFR(L747-T751del,Sins)	100	100
EGFR(L858R)	100	90
EGFR(L858R,T790M)	72	82
EGFR(L861Q)	100	100
EGFR(S752-I759del)	100	100
EGFR(T790M)	71	91
EIF2AK1	74	81
EPHA1	100	99
EPHA2	97	73
EPHA3	78	94
EPHA4	100	100
EPHA5	93	96
EPHA6	100	87
EPHA7	100	100
EPHA8	100	100
EPHB1	100	100
EPHB2	91	86
EPHB3	100	92
EPHB4	100	89
EPHB6	100	100
ERBB2	96	91
ERBB3	42	100
ERBB4	98	100
ERK1	91	100
ERK2	93	100
ERK3	100	100
ERK4	100	82

Table S4. Results from KINOMEscan™ Profiling Assay with Compound 33 at 1 µM and 10 µM test concentrations **Target Gene Symbol**	**%Control at 1 µM**	**%Control at 10 µM**
ERK5	100	95
ERK8	86	100
ERN1	100	75
FAK	100	100
FER	100	100
FES	100	83
FGFR1	100	100
FGFR2	100	86
FGFR3	100	97
FGFR3(G697C)	100	80
FGFR4	100	91
FGR	92	74
FLT1	100	100
FLT3	92	96
FLT3(D835H)	100	100
FLT3(D835V)	79	80
FLT3(D835Y)	98	100
FLT3(ITD)	97	100
FLT3(ITD,D835V)	78	77
FLT3(ITD,F691L)	100	100
FLT3(K663Q)	73	92
FLT3(N841I)	86	100
FLT3(R834Q)	100	100
FLT3-autoinhibited	73	69
FLT4	100	100
FRK	100	90
FYN	85	88
GAK	92	81

Table S4. Results from KINOMEscan™ Profiling Assay with Compound 33 at 1 µM and 10 µM test concentrations **Target Gene Symbol**	**%Control at 1 µM**	**%Control at 10 µM**
GCN2(Kin.Dom.2,S808G)	100	100
GRK1	80	82
GRK2	91	100
GRK3	70	66
GRK4	100	100
GRK7	72	92
GSK3A	87	88
GSK3B	100	100
HASPIN	84	77
HCK	96	59
HIPK1	94	53
HIPK2	100	100
HIPK3	100	100
HIPK4	100	43
HPK1	69	94
HUNK	100	100
ICK	74	75
IGF1R	95	100
IKK-alpha	92	90
IKK-beta	100	100
IKK-epsilon	76	100
INSR	68	91
INSRR	88	96
IRAK1	93	99
IRAK3	87	100
IRAK4	100	100
ITK	100	100
JAK1(JH1domain-catalytic)	100	93

Table S4. Results from KINOMEscan™ Profiling Assay with Compound 33 at 1 µM and 10 µM test concentrations **Target Gene Symbol**	**%Control at 1 µM**	**%Control at 10 µM**
JAK1(JH2domain-pseudokinase)	100	100
JAK2(JH1domain-catalytic)	67	69
JAK3(JH1domain-catalytic)	70	67
JNK1	96	89
JNK2	81	72
JNK3	73	69
KIT	96	84
KIT(A829P)	100	100
KIT(D816H)	54	51
KIT(D816V)	100	99
KIT(L576P)	89	83
KIT(V559D)	94	92
KIT(V559D,T670I)	92	98
KIT(V559D,V654A)	98	100
KIT-autoinhibited	100	100
LATS1	100	95
LATS2	100	100
LCK	85	100
LIMK1	100	100
LIMK2	100	100
LKB1	100	100
LOK	100	55
LRRK2	100	100
LRRK2(G2019S)	62	100
LTK	100	96
LYN	71	85
LZK	100	100
MAK	76	58

Table S4. Results from KINOMEscan™ Profiling Assay with Compound 33 at 1 µM and 10 µM test concentrations **Target Gene Symbol**	**%Control at 1 µM**	**%Control at 10 µM**
MAP3K1	80	78
MAP3K15	61	69
MAP3K2	74	61
MAP3K3	81	48
MAP3K4	100	93
MAP4K2	100	100
MAP4K3	98	100
MAP4K4	82	90
MAP4K5	81	100
MAPKAPK2	100	100
MAPKAPK5	66	67
MARK1	89	99
MARK2	77	90
MARK3	100	100
MARK4	94	86
MAST1	100	100
MEK1	94	92
MEK2	93	84
MEK3	77	87
MEK4	94	83
MEK5	79	81
MEK6	100	100
MELK	100	100
MERTK	91	100
MET	100	100
MET(M1250T)	100	100
MET(Y1235D)	100	93
MINK	93	74

Table S4. Results from KINOMEscan™ Profiling Assay with Compound 33 at 1 µM and 10 µM test concentrations **Target Gene Symbol**	**%Control at 1 µM**	**%Control at 10 µM**
MKK7	100	98
MKNK1	88	93
MKNK2	69	65
MLCK	96	95
MLK1	92	100
MLK2	100	100
MLK3	96	100
MRCKA	100	98
MRCKB	93	100
MST1	100	90
MST1R	77	55
MST2	100	100
MST3	100	100
MST4	100	100
MTOR	77	100
MUSK	95	92
MYLK	56	96
MYLK2	86	95
MYLK4	100	100
MYO3A	100	100
MYO3B	100	96
NDR1	88	82
NDR2	76	81
NEK1	100	100
NEK10	100	100
NEK11	64	60
NEK2	94	75
NEK3	82	87

Table S4. Results from KINOMEscan™ Profiling Assay with Compound 33 at 1 µM and 10 µM test concentrations **Target Gene Symbol**	**%Control at 1 µM**	**%Control at 10 µM**
NEK4	75	74
NEK5	94	99
NEK6	85	96
NEK7	100	92
NEK9	98	99
NIK	68	73
NIM1	98	100
NLK	73	100
OSR1	57	59
PAK1	100	100
PAK2	89	100
PAK3	100	100
PAK4	89	100
PAK6	100	100
PAK7	71	88
PCTK1	100	100
PCTK2	87	85
PCTK3	100	100
PDGFRA	75	83
PDGFRB	100	96
PDPK1	69	76
PFCDPK1(P.falciparum)	100	89
PFPK5(P.falciparum)	71	80
PFTAIRE2	100	100
PFTK1	85	100
PHKG1	100	88
PHKG2	100	100
PIK3C2B	94	92

Table S4. Results from KINOMEscan™ Profiling Assay with Compound 33 at 1 µM and 10 µM test concentrations Target Gene Symbol	**%Control at 1 µM**	**%Control at 10 µM**
PIK3C2G	62	82
PIK3CA	90	89
PIK3CA(C420R)	94	98
PIK3CA(E542K)	98	94
PIK3CA(E545A)	100	91
PIK3CA(E545K)	91	93
PIK3CA(H1047L)	81	85
PIK3CA(H1047Y)	100	96
PIK3CA(I800L)	96	99
PIK3CA(M1043I)	79	99
PIK3CA(Q546K)	76	84
PIK3CB	100	100
PIK3CD	100	100
PIK3CG	66	69
PIK4CB	75	79
PIKFYVE	100	100
PIM1	94	100
PIM2	87	96
PIM3	90	100
PIP5K1A	87	87
PIP5K1C	64	77
PIP5K2B	88	98
PIP5K2C	98	92
PKAC-alpha	77	85
PKAC-beta	100	100
PKMYT1	85	100
PKN1	93	100
PKN2	83	99

Table S4. Results from KINOMEscan™ Profiling Assay with Compound 33 at 1 µM and 10 µM test concentrations **Target Gene Symbol**	**%Control at 1 µM**	**%Control at 10 µM**
PKNB(M.tuberculosis)	85	100
PLK1	99	93
PLK2	94	94
PLK3	93	85
PLK4	90	90
PRKCD	96	94
PRKCE	100	100
PRKCH	100	95
PRKCI	92	79
PRKCQ	44	74
PRKD1	100	100
PRKD2	95	90
PRKD3	100	100
PRKG1	76	100
PRKG2	80	84
PRKR	100	100
PRKX	100	90
PRP4	100	100
PYK2	97	97
QSK	70	93
RAF1	85	100
RET	100	100
RET(M918T)	90	100
RET(V804L)	86	100
RET(V804M)	100	100
RIOK1	89	100
RIOK2	100	92
RIOK3	100	100

Table S4. Results from KINOMEscan™ Profiling Assay with Compound 33 at 1 µM and 10 µM test concentrations **Target Gene Symbol**	**%Control at 1 µM**	**%Control at 10 µM**
RIPK1	100	100
RIPK2	100	93
RIPK4	65	69
RIPK5	84	88
ROCK1	94	98
ROCK2	70	68
ROS1	78	100
RPS6KA4(Kin.Dom.1-N-terminal)	97	100
RPS6KA4(Kin.Dom.2-C-terminal)	68	78
RPS6KA5(Kin.Dom.1-N-terminal)	100	94
RPS6KA5(Kin.Dom.2-C-terminal)	100	100
RSK1(Kin.Dom.1-N-terminal)	100	100
RSK1(Kin.Dom.2-C-terminal)	93	100
RSK2(Kin.Dom.1-N-terminal)	78	70
RSK2(Kin.Dom.2-C-terminal)	92	91
RSK3(Kin.Dom.1-N-terminal)	73	95
RSK3(Kin.Dom.2-C-terminal)	95	100
RSK4(Kin.Dom.1-N-terminal)	79	68
RSK4(Kin.Dom.2-C-terminal)	82	100
S6K1	100	100
SBK1	59	52
SGK	83	89
SGK2	100	100
SGK3	100	100
SIK	84	100
SIK2	100	100
SLK	89	100
SNARK	82	65

Table S4. Results from KINOMEscan™ Profiling Assay with Compound 33 at 1 µM and 10 µM test concentrations Target Gene Symbol	**%Control at 1 µM**	**%Control at 10 µM**
SNRK	94	86
SRC	97	100
SRMS	97	100
SRPK1	100	100
SRPK2	100	100
SRPK3	97	69
STK16	100	100
STK33	97	100
STK35	100	100
STK36	86	94
STK39	58	65
SYK	93	100
SgK110	46	43
TAK1	100	100
TAOK1	100	100
TAOK2	100	100
TAOK3	85	100
TBK1	66	90
TEC	99	100
TESK1	100	79
TGFBR1	84	100
TGFBR2	99	100
TIE1	93	100
TIE2	100	95
TLK1	100	100
TLK2	100	100
TNIK	70	100
TNK1	100	100

Table S4. Results from KINOMEscan™ Profiling Assay with Compound 33 at 1 µM and 10 µM test concentrations **Target Gene Symbol**	**%Control at 1 µM**	**%Control at 10 µM**
TNK2	100	100
TNNI3K	95	73
TRKA	78	99
TRKB	70	64
TRKC	100	100
TRPM6	84	84
TSSK1B	100	90
TSSK3	93	75
TTK	99	92
TXK	100	88
TYK2(JH1domain-catalytic)	100	100
TYK2(JH2domain-pseudokinase)	100	100
TYRO3	74	100
ULK1	67	56
ULK2	79	90
ULK3	85	77
VEGFR2	81	70
VPS34	80	89
VRK2	100	100
WEE1	78	100
WEE2	99	100
WNK1	100	100
WNK2	96	86
WNK3	100	100
WNK4	57	51
YANK1	88	88
YANK2	100	100
YANK3	94	100

Table S4. Results from KINOMEscan™ Profiling Assay with Compound 33 at 1 µM and 10 µM test concentrations Target Gene Symbol	**%Control at 1 µM**	**%Control at 10 µM**
YES	92	100
YSK1	100	94
YSK4	61	58
ZAK	100	100
ZAP70	100	100
p38-alpha	100	100
p38-beta	100	88
p38-delta	94	59
p38-gamma	59	100

Eurofins SAFETYscan 47 E/IC50 ELECT panel assay protocols and results.

Compound **33** was tested in this panel of 78 assays to evaluate off-target pharmacological activity against a board range of biological targets that are commonly associated with safety risks. The panel includes 48 functional assays (20 Calcium Flux assays and 28 cAMP assays) against G-protein coupled receptors (GPCR), 13 functional assays against ion channels, 6 functional assays against non-kinase enzymes, 4 assays against nuclear hormone receptor (NHR), 4 binding enzymes against kinase, and 3 functional assays against transporters.

Calcium Mobilization Assay

The calcium mobilization assay evaluates GPCR activity via Gq-mediated signaling using a calcium-sensitive dye. Cells are seeded into 384-well plates and loaded with dye in a specialized buffer. For agonist testing, compounds are added post-dye loading and calcium flux is measured in real-time using a FLIPR Tetra system. For antagonist testing, cells are pre-incubated with the compound, followed by stimulation with an EC80 concentration of a known agonist. Fluorescence changes are recorded over two minutes, and data analysis calculates percent activity or inhibition using area under the curve metrics, with values capped between 0% and 100% for primary screens.

GPCR cAMP Modulation Assay

The cAMP assay protocol involves using DiscoverX's HitHunter cAMP XS+ system to assess GPCR activity via Gs and Gi signaling pathways. Cells are seeded into 384-well plates and treated with test compounds under different formats: Gs agonist, Gi agonist (with forskolin), and antagonist (with EC80 agonist). After incubation, signal detection is performed using a chemiluminescent readout following lysis and enzyme complementation steps. Data analysis calculates percent activity or inhibition based on relative luminescence units (RLU), with responses capped between 0% and 100% for primary screens.

Ion Channel Assays

The ion channel assay protocol involves seeding cells into 384-well plates and loading them with a fluorescent dye in the presence of freshly prepared probenecid. For agonist/opener assays, compounds are added directly to induce ion channel activity, while antagonist/blocker assays involve pre-incubation with the compound followed by stimulation with an EC80 agonist. After incubation, fluorescence changes are measured using a FLIPR Tetra system. Data analysis calculates percent activity or inhibition based on relative luminescence units (RLU), with results capped between 0% and 100% for primary screens.

KINOMEscan Kinase Binding Assays

The binding to 4 target kinases (INSR, LCK, ROCK1, VEGFR2) used KINOMEscan platform to measure compound interactions with kinase active sites via a competition binding format. Kinase-tagged phage or HEK293-expressed kinases are incubated with immobilized ligands and test compounds in 384-well plates. Compounds that bind the kinase prevent its capture on the ligand-coated beads, and the remaining kinase is quantified using qPCR of DNA tags. Binding affinity (Kd) is calculated from dose-response curves using the Hill equation, and percent response is derived from control comparisons, with values capped between 0% and 100% for primary screens.

Nuclear Hormone Receptor Assays

The nuclear hormone receptor (NHR) assay protocol uses PathHunter cell lines to evaluate receptor activation via protein interaction or nuclear translocation. Cells are seeded into 384-well

plates and incubated with test compounds under agonist or antagonist formats. Agonist assays involve direct incubation, while antagonist assays include pre-incubation followed by EC80 agonist challenge. Signal detection is performed using chemiluminescence after adding PathHunter detection reagents. Data analysis calculates percent activity or inhibition, with inverse agonist activity assessed for constitutively active targets. All responses are normalized and capped between 0% and 100% for primary screens.

Transporter Assays

The transporter assay protocol involves seeding cells into 384-well plates and incubating them with test compounds in HBSS/BSA buffer. After a 30-minute incubation at 37 °C, a fluorescent dye is added to assess neurotransmitter uptake inhibition. Cells are further incubated for 30–60 minutes before fluorescence signal detection using a PerkinElmer Envision reader. Data analysis calculates percent inhibition based on relative fluorescence units (RFU), comparing test samples to vehicle and positive controls, with responses capped between 0% and 100% for primary screens.

Non-Kinase Enzymatic Assays

The enzymatic assay protocol involves measuring enzyme activity by tracking substrate consumption or product formation using various detection methods—absorbance, fluorescence, or luminescence. Enzymes such as AChE, COX1/2, MAOA, and PDEs are incubated with test compounds before substrate addition. Specific conditions and reagents are used for each enzyme type, and reactions are terminated appropriately to enable signal detection using a PerkinElmer Envision reader. Data analysis calculates percent inhibition relative to vehicle and positive controls, with results capped between 0% and 100% for primary screens.

Table S5. Results with Compound 33 at up to 10 µM: agonist effect

Target Class	Assay Name	Target	EC_{50} (μM)	Max Response (%)
GPCR	Calcium Flux	ADORA2A	>10	2.87
GPCR	Calcium Flux	ADRA1A	>10	1.15
GPCR	Calcium Flux	AVPR1A	>10	1.32
GPCR	Calcium Flux	CCKAR	>10	0
GPCR	Calcium Flux	CHRM1	>10	1.8
GPCR	Calcium Flux	CHRM3	>10	0
GPCR	Calcium Flux	EDNRA	>10	0
GPCR	Calcium Flux	HRH1	>10	0.79
GPCR	Calcium Flux	HTR2A	>10	0.14
GPCR	Calcium Flux	HTR2B	>10	3.24
GPCR	cAMP	ADRA2A	>10	4.4
GPCR	cAMP	ADRB1	>10	0.92
GPCR	cAMP	ADRB2	>10	1.15
GPCR	cAMP	CHRM2	10	72.09
GPCR	cAMP	CNR1	>10	5.11
GPCR	cAMP	CNR2	>10	8.65
GPCR	cAMP	DRD1	>10	0.21
GPCR	cAMP	DRD2S	>10	14.93
GPCR	cAMP	HRH2	>10	0.05
GPCR	cAMP	HTR1A	>10	13.96
GPCR	cAMP	HTR1B	>10	20.87
GPCR	cAMP	OPRD1	>10	27.15
GPCR	cAMP	OPRK1	>10	19.67
GPCR	cAMP	OPRM1	>10	34.17
Ion Channel	Opener	GABAA	>10	2.5
Ion Channel	Opener	HTR3A	>10	3.93
Ion Channel	Opener	KvLQT1/minK	>10	2.8
Ion Channel	Opener	nAChR(a4/b2)	>10	4.96
Ion Channel	Opener	NMDAR(1A/2B)	>10	2.93

NHR	Translocation	GR	>10	0
NHR	Protein Interaction	AR	>10	0.11

Table S6. Results with Compound 33 at up to 10 µM: antagonist effect

Target Class	Assay Name	Target	EC_{50} (µM)	Max Response (%)
GPCRCalcium FluxADORA2A>102.33GPCRCalcium FluxADRA1A>100GPCR	Calcium Flux	AVPR1A	>10	4.05
GPCR	Calcium Flux	CCKAR	>10	0
GPCR	Calcium Flux	CHRM1	>10	0
GPCR	Calcium Flux	CHRM3	>10	0
GPCR	Calcium Flux	EDNRA	>10	0
GPCR	Calcium Flux	HRH1	>10	0
GPCR	Calcium Flux	HTR2A	>10	0
GPCR	Calcium Flux	HTR2B	>10	0
GPCR	cAMP	ADRA2A	>10	0
GPCR	cAMP	ADRB1	>10	39.4
GPCR	cAMP	ADRB2	>10	49.01
GPCR	cAMP	CHRM2	>10	0
GPCR	cAMP	CNR1	>10	0
GPCR	cAMP	CNR2	>10	0
GPCR	cAMP	DRD1	>10	45.51
GPCR	cAMP	DRD2S	>10	0
GPCR	cAMP	HRH2	>10	34.65
GPCR	cAMP	HTR1A	>10	0
GPCR	cAMP	HTR1B	>10	0
GPCR	cAMP	OPRD1	>10	0
GPCR	cAMP	OPRK1	>10	0
GPCR	cAMP	OPRM1	>10	0
NHR	Translocation	AR	>10	10.72
NHR	Protein Interaction	GR	>10	15.62

Table S7. Results with Compound 33 at up to 10 µM: Ion channel opener and blocker effect

Target Class	Mode	Target	EC_{50} or IC_{50} (μM)	Max Response (%)
Ion Channel	Opener	GABAA	>10	2.5
Ion Channel	Opener	HTR3A	>10	3.93
Ion Channel	Opener	KvLQT1/minK	>10	2.8
Ion Channel	Opener	nAChR(a4/b2)	>10	4.96
Ion Channel	Opener	NMDAR(1A/2B)	>10	2.93
Ion Channel	Blocker	CAV1.2	>10	0
Ion Channel	Blocker	GABAA	>10	7.87
Ion Channel	Blocker	hERG	>10	13.55
Ion Channel	Blocker	HTR3A	>10	0
Ion Channel	Blocker	KvLQT1/minK	>10	18.71
Ion Channel	Blocker	NAV1.5	>10	25.15
Ion Channel	Blocker	NMDAR(1A/2B)	>10	0
Ion Channel	Blocker	nAChR(a4/b2)	>10	0

Table S8. Results with Compound 33 at up to 10 μM: Enzymatic and transporter inhibition effect

Target Class	Assay Name	Target	IC_{50} (μM)	Max Response (%)
Kinase	Binding	INSR	>10	19.04
Kinase	Binding	LCK	>10	21.94
Kinase	Binding	ROCK1	>10	12.14
Kinase	Binding	VEGFR2	>10	0.11
Non-Kinase Enzymes	Enzymatic	AChE	>10	0
Non-Kinase Enzymes	Enzymatic	COX1	>10	0
Non-Kinase Enzymes	Enzymatic	COX2	>10	2.38
Non-Kinase Enzymes	Enzymatic	MAOA	>10	0
Non-Kinase Enzymes	Enzymatic	PDE3A	>10	0
Non-Kinase Enzymes	Enzymatic	PDE4D2	>10	5.43
Transporter	Blocker	DAT	>10	0
Transporter	Blocker	NET	>10	6.01
Transporter	Blocker	SERT	>10	2.41

Table S9: Eurofins SAFETYscan 47 E/IC50 ELECT panel reference controls

Compound Name	Target Class	Mode	Assay Target	Result Type	RC50 (μM)

NECA	GPCR	Agonist	ADORA2A	EC50	0.01714
SCH 442416	GPCR	Antagonist	ADORA2A	IC50	0.07938
A 61603 Hydrobromide	GPCR	Agonist	ADRA1A	EC50	0.00011
Tamsulosin	GPCR	Antagonist	ADRA1A	IC50	0.00117
UK 14304	GPCR	Agonist	ADRA2A	EC50	0.00003
Yohimbine	GPCR	Antagonist	ADRA2A	IC50	0.00447
(−)-Isoproterenol	GPCR	Agonist	ADRB1	EC50	0.00092
Betaxolol	GPCR	Antagonist	ADRB1	IC50	0.00602
(−)-Isoproterenol	GPCR	Agonist	ADRB2	EC50	0.00097
ICI 118,551 hydrochloride	GPCR	Antagonist	ADRB2	IC50	0.0009
[Arg8]-Vasopressin	GPCR	Agonist	AVPR1A	EC50	0.00116
SR 49059	GPCR	Antagonist	AVPR1A	IC50	0.00123
CCK fragment 26-33 Amide	GPCR	Agonist	CCKAR	EC50	0.00006
SR 27897	GPCR	Antagonist	CCKAR	IC50	0.0487
Acetylcholine chloride	GPCR	Agonist	CHRM1	EC50	0.01302
Atropine	GPCR	Antagonist	CHRM1	IC50	0.00904
Acetylcholine chloride	GPCR	Agonist	CHRM2	EC50	0.04167
Atropine	GPCR	Antagonist	CHRM2	IC50	0.00138
Acetylcholine chloride	GPCR	Agonist	CHRM3	EC50	0.01651
Atropine	GPCR	Antagonist	CHRM3	IC50	0.0037
CP 55940	GPCR	Agonist	CNR1	EC50	0.00002
AM 251	GPCR	Antagonist	CNR1	IC50	0.00083
CP 55940	GPCR	Agonist	CNR2	EC50	0.00017
SR 144528	GPCR	Antagonist	CNR2	IC50	0.0455
Dopamine	GPCR	Agonist	DRD1	EC50	0.05179
SCH 39166	GPCR	Antagonist	DRD1	IC50	0.0013
Dopamine	GPCR	Agonist	DRD2S	EC50	0.00192
Risperidone	GPCR	Antagonist	DRD2S	IC50	0.0011
Endothelin 1	GPCR	Agonist	EDNRA	EC50	0.00239
BMS 182874	GPCR	Antagonist	EDNRA	IC50	0.18769
Histamine	GPCR	Agonist	HRH1	EC50	0.01426
Mepyramine	GPCR	Antagonist	HRH1	IC50	0.00849

Histamine	GPCR	Agonist	HRH2	EC50	0.33478
Tiotidine	GPCR	Antagonist	HRH2	IC50	0.08408
Serotonin Hydrochloride	GPCR	Agonist	HTR1A	EC50	0.00311
Spiperone	GPCR	Antagonist	HTR1A	IC50	0.03764
Serotonin Hydrochloride	GPCR	Agonist	HTR1B	EC50	0.00002
SB 224289	GPCR	Antagonist	HTR1B	IC50	0.00883
Serotonin Hydrochloride	GPCR	Agonist	HTR2A	EC50	0.00442
Altanserin	GPCR	Antagonist	HTR2A	IC50	0.01944
Serotonin Hydrochloride	GPCR	Agonist	HTR2B	EC50	0.00193
LY 272015	GPCR	Antagonist	HTR2B	IC50	0.00082
DADLE	GPCR	Agonist	OPRD1	EC50	0.00005
Naltriben	GPCR	Antagonist	OPRD1	IC50	0.00058
Dynorphin A (1-17)	GPCR	Agonist	OPRK1	EC50	0.01118
nor-Binaltorphimine	GPCR	Antagonist	OPRK1	IC50	0.00136
DAMGO	GPCR	Agonist	OPRM1	EC50	0.00086
Naloxone	GPCR	Antagonist	OPRM1	IC50	0.00183
Isradipine	Ion Channel	Blocker	CAV1.2	IC50	0.01404
Picrotoxin	Ion Channel	Blocker	GABAA	IC50	2.67078
GABA	Ion Channel	Opener	GABAA	EC50	5.84033
Astemizole	Ion Channel	Blocker	hERG	IC50	0.23862
Bemesetron	Ion Channel	Blocker	HTR3A	IC50	0.00746
Serotonin Hydrochloride	Ion Channel	Opener	HTR3A	EC50	0.39975
XE 991	Ion Channel	Blocker	KvLQT1/minK	IC50	0.92793
ML-277	Ion Channel	Opener	KvLQT1/minK	EC50	2.65858
Dihydro-β-erythroidine	Ion Channel	Blocker	nAChR(a4/b2)	IC50	0.56808
(−)-Nicotine	Ion Channel	Opener	nAChR(a4/b2)	EC50	1.64972

Lidocaine Hydrochloride	Ion Channel	Blocker	NAV1.5	IC50	38.10624
(+)-MK 801	Ion Channel	Blocker	NMDAR(1A/2B)	IC50	0.08444
L-Glutamic Acid	Ion Channel	Opener	NMDAR(1A/2B)	EC50	0.45497
BMS-754807	Kinases	Inhibitor	INSR	IC50	0.00036
Gleevec	Kinases	Inhibitor	LCK	IC50	0.01403
Staurosporine	Kinases	Inhibitor	ROCK1	IC50	0.00055
SU-11248	Kinases	Inhibitor	VEGFR2	IC50	0.00013
BMS-564929	NHR	Agonist	AR	EC50	0.0012
Geldanamycin	NHR	Antagonist	AR	IC50	0.04035
Dexamethasone	NHR	Agonist	GR	EC50	0.03359
Mifepristone	NHR	Antagonist	GR	IC50	0.06996
Physostigmine	Non-Kinase Enzymes	Inhibitor	AChE	IC50	0.0405
Indomethacin	Non-Kinase Enzymes	Inhibitor	COX1	IC50	0.05316
NS-398	Non-Kinase Enzymes	Inhibitor	COX2	IC50	0.38773
Clorgyline	Non-Kinase Enzymes	Inhibitor	MAOA	IC50	0.00142
Cilostamide	Non-Kinase Enzymes	Inhibitor	PDE3A	IC50	0.02297
Cilomilast	Non-Kinase Enzymes	Inhibitor	PDE4D2	IC50	0.0103
GBR 12909	Transporter	Blocker	DAT	IC50	0.00142
Desipramine	Transporter	Blocker	NET	IC50	0.01395
Clomipramine	Transporter	Blocker	SERT	IC50	0.00145

Pharmaron Cytochrome P450 inhibition assay protocols and results

Cytochrome P450 (CYP) direct and time dependent inhibition (TDI) of Compound 33 was evaluated on seven major CYP enzymes using pooled human liver microsomes. The study included three incubation conditions: no pre-incubation, 30-minute pre-incubation with NADPH, and 30-minute pre-incubation without NADPH, to distinguish between direct and time-dependent inhibition. Each test compound was evaluated across a range of concentrations, and

reactions were initiated by adding NADPH and specific substrates for each CYP isoform. The reactions were terminated with cold methanol containing internal standards, followed by centrifugation and LC-MS/MS analysis. The IC_{50} values were calculated using GraphPad Prism to assess inhibitory potency and potential metabolic liabilities.

The bioanalytical method employed a Shimadzu LC system coupled with AB Sciex QTRAP® 4500 or Triple Quad™ 5500 mass spectrometers using electrospray ionization (ESI) in multiple reaction monitoring (MRM) mode. Chromatographic separation was achieved using an Xselect® HSS T3 column with a gradient of 0.1% formic acid in water and acetonitrile. Specific elution programs were optimized for each metabolite, such as acetaminophen, hydroxybupropion, and dextrorphan. The MS parameters, including ion spray voltage, gas flows, and collision energies, were tailored for each CYP substrate-metabolite pair to ensure sensitive and selective detection. This robust LC-MS/MS method enabled accurate quantification of metabolite formation, which was critical for determining the inhibitory effects of the test compounds.

Table S10: Pharmaron Cytochrome P450 inhibition assay results of Compound 33 at concentration up to 25 µM

CYP Isoform	Substrate	IC_{50} (µM)		
		0-min predicubation	30-minutes pre-incubation with NADPH	30-minutes pre-incubation without NADPH
CYP1A2	Phenacetin	> 25	> 25	> 25
CYP2B6	Bupropion	> 25	> 25	> 25
CYP2C8	Paclitaxel	7.757	13.55	9.419
CYP2C9	Diclofenac	> 25	> 25	> 25
CYP2C19	(S)-Methenytoin	10.96	18.89	13.95
CYP2D6	Dextromethorphan	1.336	2.154	1.322
CYP3A4/5	Midazolam	1.14	0.66	1.10
CYP3A4/5	Testosterone	7.46	2.22	8.58

Table S11: Pharmaron Cytochrome P450 inhibition results with reference compounds

CYP Isoform	Reference Compound	Substrate	IC_{50} (μM)		
			0-min predicubation	30-minutes pre-incubation with NADPH	30-minutes pre-incubation without NADPH
CYP1A2	Furafylline	Phenacetin	2.55	0.42	2.62
CYP2B6	Thiotepa	Bupropion	28.26	3.49	33.62
CYP2C8	Gemfibrozil Glucuronide	Paclitaxel	28.26	3.49	33.62
CYP2C9	Ticrynafen	Diclofenac	1.17	0.19	1.44
CYP2C19	Fluoxetine	(S)-Methenytoin	14.02	1.45	14.28
CYP2D6	Paroxetine	Dextromethorphan	0.99	0.10	1.21
CYP3A4/5	Mifepristone	Midazolam	5.17	0.30	7.11
CYP3A4/5	Mifepristone	Testosterone	6.82	0.36	6.82

References

1. Bockus, A. T.; Leung, S. S. F.; Fraga-Walton, B.; Baldomero, M. P.; Hernandez, L.; Dupper, N. J.; Shapiro, J. A.; Lent, B. M.; Spellmeyer, D. C.; DeMart, M. K.; Luna, J.; Hoang, D.; Chand, M.; Gritsenko, Y.; Ramaseshan, M.; Gleason, C. E.; Hamkins-Indik, F.; Membreno, M. W.; Zheng, J.; Odeh, R.; Nosrati, M.; He, D.; Situ, G.; Bambal, R.; Cremin, P.; Fang, J.; Levin, B.; Wang, E. W.; Evangelista, M.; Earp, D. J.; Kreatsoulas, C.; Singh, R.; Garcia, P. D.; Aggen, J. B. Discovery of Cell-Permeable Macrocyclic Cyclin A/B RxL In-hibitors that Demonstrate Anti-Tumor Activity in E2F-driven Cancers. In Press, Journal of Medicinal Chemistry **2025**.
2. Andrew T. Bockus, Sik Fai Siegfried Leung, David J. Earp, Pablo Santiago Garcia Dominguez, David C. Spellmeyer, Luis Hernandez, Miguel Paolo Baldomero, Catherine E. Gleason, Breena F. Walton, Rajinder Singh, James B. Aggen, Nathan J. Dupper, Justin A. Shapiro, Constantine Kreatsoulas, Ramesh B. Bambal, Chat Cheong Gabriel Fung,

Mahesh Ramaseshan, “Preparation of cyclic peptidic compounds as cyclin inhibitors for treating cancers” US20240218021 (WO2024086814 A2)

3. Andrew T. Bockus, Breena F. Walton, Constantine Kreatsoulas, James B. Aggen, Justin A. Shapiro, Megan DeMart, Nathan J. Dupper, Sik Fai Siegfried Leung, Chinmay Bhatt, Samuel Metobo, Kai Yang, Ming Hsun-Ho, Rajinder Singh, Ramesh Bambal “Cyclin Inhibitors” US2024243010 (WO2024243010 A1)